

Research

**Review of experimental data for modelling
LWR fuel cladding behaviour under loss of
coolant accident conditions**

Ali R. Massih

February 2007

SKI Perspective

Background and purpose of the project

Over the last years the behaviour of nuclear fuel during loss of coolant accidents (LOCA) has been studied to investigate the failure behaviour at high burnup and for modern fuel cladding. The results of recent experimental programmes indicate that the cladding alloy composition and high burnup effects influence LOCA acceptance criteria margins.

SKI has therefore initiated a study to investigate nuclear fuel behaviour during a LOCA. The study is divided in four parts:

- Review of experimental data and models for LWR fuel cladding behaviour under LOCA conditions.
- Critical review of FRAPTRAN-1.3 and its modelling capacity.
- Evaluation of models for cladding oxidation, embrittlement, deformation and burst under LOCA.
- Implementation of alternative models for LOCA in FRAPTRAN-1.3.

The work presented in this report is the first part of the study. In the report a review of experimental data is made and a suggestion for modelling and further evaluation is made.

Results

This project has contributed to the research goal of giving a basis for SKI's supervision by means of evaluating experimental data and modelling the nuclear fuel cladding during a design base accident. The project has also contributed to the research goal to develop the competence about licensing of fuel at high burnup, which is an important safety issue. The results are useful as such, but also are the basis for modifications to FRAPTRAN in a following project.

Responsible for the project at SKI has been Jan In de Betou.
Project Identification Number: 200606025

Research

Review of experimental data for modelling LWR fuel cladding behaviour under loss of coolant accident conditions

Ali R. Massih

Quantum Technologies AB
Uppsala Science Park
SE-751 83 Uppsala, Sweden

28 February 2007

This report concerns a study which has been conducted for the Swedish Nuclear Power Inspectorate (SKI). The conclusions and viewpoints presented in the report are those of the author/authors and do not necessarily coincide with those of the SKI.

List of contents

Abstract	III
Sammanfattning	IV
1 Introduction	1
2 Background to acceptance criteria for LOCA	3
2.1 Fuel clad materials.....	3
2.2 Clad embrittlement phenomenology	4
2.3 Clad embrittlement criteria.....	12
2.4 Bases for clad embrittlement criteria.....	14
2.4.1 Maximum clad oxidation limit	14
2.4.2 Peak cladding temperature limit.....	15
2.4.3 Remarks	17
3 Separate effect tests	21
3.1 Clad oxidation under LOCA conditions.....	21
3.1.1 Transient tests	22
3.1.2 Effects of hydrogen absorption oxidation	25
3.1.3 Cadarache tests	26
3.1.4 Zirconium-niobium alloys	29
3.1.5 Effect of pressure on oxidation.....	34
3.2 Clad deformation and rupture.....	36
3.2.1 Creep deformation	36
3.2.2 Creep Rupture.....	41
3.3 Phase transformation	49
3.4 Modelling	52
4 Integral LOCA tests	55
4.1 Thermal shock tests at JAERI	56
4.2 Thermal shock tests at KAERI	65
4.3 LOCA integral tests at ANL.....	67
4.4 Multi-rod tests at NRU	71
4.5 The PHEBUS-LOCA program.....	71
4.6 LOCA testing at Halden	73
5 Conclusions	75
6 References	77
Appendix A: Clad oxidation rate correlations	89
Notes	95

Abstract

Extensive range of experiments has been conducted in the past to quantitatively identify and understand the behaviour of fuel rod under loss-of-coolant accident (LOCA) conditions in light water reactors (LWRs). The obtained experimental data provide the basis for the current emergency core cooling system acceptance criteria under LOCA conditions for LWRs. The results of recent experiments indicate that the cladding alloy composition and high burnup effects influence LOCA acceptance criteria margins. In this report, we review some past important and recent experimental results. We first discuss the background to acceptance criteria for LOCA, namely, clad embrittlement phenomenology, clad embrittlement criteria (limitations on maximum clad oxidation and peak clad temperature) and the experimental bases for the criteria. Two broad kinds of test have been carried out under LOCA conditions: (i) Separate effect tests to study clad oxidation, clad deformation and rupture, and zirconium alloy allotropic phase transition during LOCA. (ii) Integral LOCA tests, in which the entire LOCA sequence is simulated on a single rod or a multi-rod array in a fuel bundle, in laboratory or in a test reactor, to study the overall behaviour of fuel rod under LOCA. The separate effect tests and results are discussed and empirical correlations deduced from these tests and quantitative models are conferred. In particular, the impact of niobium in zirconium base clad and hydrogen content of the clad on allotropic phase transformation during LOCA and also the burst stress are discussed. We review some recent LOCA integral test results with emphasis on thermal shock tests. Finally, suggestions for modelling and further evaluation of certain experimental results are made.

Sammanfattning

En mängd olika experiment har utförts tidigare för att kvantifiera och förstå bränslestavars beteende under LOCA (olycka orsakad av kylmedelsförlust) förhållanden i lättvattenreaktorer (LWR). Det experimentellt framtagna underlaget utgör basen för nuvarande acceptanskriterier för härdsnödkylsystemet under LOCA förhållanden i LWR. Resultat från experiment under senare tid indikerar att kapslingsrörets legeringssammansättning och förändringar till följd av hög utbränning (högutbränningseffekter) påverkar marginalerna till acceptanskriterierna för LOCA. I denna rapport granskas några äldre viktiga och nyare experimentella resultat. Först diskuteras bakgrunden till acceptanskriterierna för LOCA, nämligen, fenomen som orsakar kapslingsförsprödning, kriterier för kapslingsförsprödning (begränsningar på maximal kapslingsoxidation och maximal kapslingstemperatur) och den experimentella basen för kriterierna. Två typer av omfattande tester har utförts under LOCA förhållanden: (i) Separateffekt tester för undersökning av kapslingsoxidation, kapslingsdeformation och brott, samt zirkoniumlegeringars allotropiska fasövergång under LOCA. (ii) Integrala LOCA tester, i vilka hela LOCA förloppet simuleras (i laboratorium eller i testreaktor) med en enskild stav eller arrangemang med flera stavar i ett bränsleknippe, för att studera det övergripande bränslestavbeteendet under LOCA. Separateffekt tester och resultat diskuteras, samt empiriska korrelationer härledda från dessa tester och kvantitativa modeller visas. Speciellt diskuteras inverkan av niob i zirkonium-bas kapsling och kapslingens väteinnehåll på dess allotropiska fasomvandling under LOCA samt även kapslingens brottspänning. Vidare granskas resultat från några nyare integrala LOCA tester med betoning på termiska chocktester. Avslutningsvis ges förslag på modellering och utvärdering av vissa experimentella resultat.

1 Introduction

A loss of coolant accident (LOCA) in pressurized water reactors (PWRs) and boiling water reactors (BWRs) can be caused by a rupture of the primary coolant line, failure of primary coolant pump seal, inadvertent opening of a pressure relief or safety valve, and so on. It would give rise to increased temperature of fuel cladding (clad) and decreased density of the coolant and possibility of uncovering of the reactor core. Upon rupture of the coolant line, a reactor scram is triggered by the reactor protection system. The negative coolant temperature reactivity coefficient (negative void coefficient) in light water reactors (LWRs) would cause an immediate power reduction thereby an automatic shutdown of reactor. Nevertheless, since the production of decay heat from the fission products continues, a reliable long-term cooling of the reactor core is necessary. Upon decompression and evacuation of the reactor pressure vessel, the emergency core cooling system (ECCS) provides the reactor core with the emergency cooling water, which is kept in the accumulators and the flooding tanks. Nonetheless, the cooling of fuel elements is temporarily deteriorated until the ECCS becomes fully effective. In this time interval, fuel-cladding temperature rises by the decay heat, and when this temperature reaches a certain threshold value, the fuel element can fail.

The temperature transient experienced by the clad depends on a number of parameters, e.g., the magnitude of fuel rod linear heat generation rate (LHGR) just prior to LOCA and the decay heat, the heat transfer coefficient across the pellet-clad gap, and the external heat transfer from clad to emergency core coolant. Figure 1.1, taken from the work of Erbacher et al. (1978), schematically shows the pressure difference across the clad and the clad temperature evolution for two fuel rods with different power densities during a LOCA.

Two types of LOCAs are commonly distinguished: large break (LB) LOCA and small break (SB) LOCA. Exhaustive descriptions of the LOCAs for PWRs and BWRs can be found in the “Compendium” (US NRC, 1988) and in the publication of Rohatgi et al. (1987). Briefly, the LB LOCA is usually considered as having three distinct phases: a *blowdown* phase lasting 12-20 s, a *refill* period lasting 10-20 s, and a *reflooding* period lasting one to two minutes. The blowdown refers to the situation that the primary coolant starts undergoing decompression while it is “blowing down”, meaning that evacuating from the primary circuit. At the end of the blowdown period, the core and part of the lower plenum of reactor pressure vessel are empty. The fuel rods are overheated and are surrounded only by steam. At this time the ECCS must be actuated in order to refill the vessel and reflood the reactor core.

The main concerns in a LB LOCA regarding the zirconium alloy clad failure are:

- 1) Oxidation of the zirconium alloy, which results in embrittlement and fracture of the clad, with the following detrimental consequences:
 - a) Loss of coolable geometry
 - b) Dispersion of fuel and release of fission products
 - c) Generation of hydrogen
 - d) Generation of exothermic heat
- 2) Large plastic deformation of clad causing the restriction of coolant flow in the subchannel between the rods. Rods can swell (inflate) until rupture, releasing fuel pellet bits and fission products to the primary system.

The small break LOCA may occur from a leak in the primary coolant loop or from a problem in the secondary cooling loop of the reactor. Loss of secondary flow implies that heat cannot be removed in the heat exchanger from the primary loop. In such an event, the pressure in the reactor vessel may not be relieved and it may be difficult to establish the flow of replacement water in the complex hydraulic milieu caused by the mixture of steam and water at high pressure. To manage this situation, the ECCS has a high-pressure injection system that provides replacement water to the reactor vessel (Bodansky, 2004).

The past studies have provided the basis of present LOCA acceptance criteria practiced by nuclear industry and authorities. Recent LOCA research, however, has shown strong alloy composition and burnup effects. More specifically, the substitution of traditional Zircaloy-4 clad in PWRs, where most past LOCA tests were made on, with Zr-Nb base alloys, and the effect of high burnup on clad, namely, clad corrosion and in particular hydriding has had an impact on clad embrittlement under LOCA conditions. Hence, the reappraisal of regulatory criteria for LOCA in this situation may be prudent. In this report, we mainly survey the experimental data produced in regards to alloy and burnup effects. The experimental data surveyed provide the basis for the revision of models for clad behaviour under LOCA. In section 2, we discuss the background to the acceptance criteria for LOCA. Section 3 describes experimental results regarding clad oxidation, deformation (ballooning), rupture and the phase transformation of zirconium alloy. In section 4, integral tests performed to determine clad deformation and fracture subject to internal pressure on actual or dummy fuel rods under LOCA conditions are surveyed. The last section provides the concluding summary of our survey.

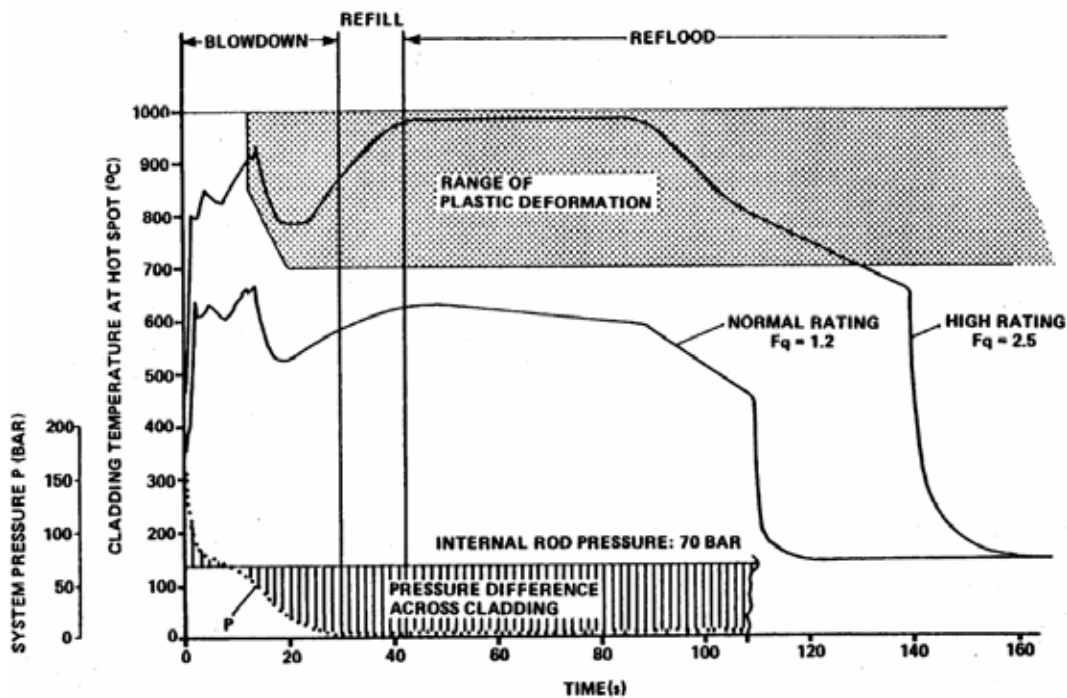


Figure 1.1: Zircaloy-4 clad temperature and pressure load histories in a LOCA at two power ratings (Erbacher et al., 1978). F_q refers to the fuel rod power peaking factor relative to the reactor power.

2 Background to acceptance criteria for LOCA

2.1 Fuel clad materials

Fuel clad materials in LWRs are dilute zirconium base alloys (table 1). Zirconium element due to its low thermal neutron cross section (0.185 barns) makes it the material of choice for LWR applications. Zirconium crystallizes at ambient temperature as a hexagonal closed-packed (hcp) metal, with a c/a ratio of 1.593. It undergoes an allotropic phase transformation from the low temperature hcp α phase to body-centered cubic (bcc) β phase at 1138 K. On cooling, the transformation is either martensitic or bainitic, depending on cooling rate with a strong epitaxy of the α platelets on the former β grains (Douglass, 1971). In BWRs Zircaloy-2 fuel clad has been traditionally used over the years for good corrosion properties with appropriate heat treatments (Massih et al., 2006) while variants of Zircaloy-4 have been and are being used in PWRs. The alloy E110 (Nikulina, 2004) have been used in Russian-built LWRs, while ZIRLO (Comstock et al., 1996) and M5 (Mardon et al., 2000) are two more recent alloys used extensively in PWRs. Table 2.1 lists the main chemical compositions of common zirconium alloys used in nuclear industry.

Zircaloy-2 indicates a sequence of four solid phases (Massih et al., 2004): (i) For temperatures $T > 1250$ K (β -Zr phase), (ii) $1080 \leq T \leq 1150$ K ($\alpha+\beta+\chi$), (iii) $1150 \leq T \leq 1250$ K ($\alpha+\beta$), (iv) $T < 1080$ K ($\alpha+\chi$). χ denotes the precipitate phases, which in Zircaloy-2 are mainly $Zr(Cr,Fe)_2$ and $Zr_2(Ni, Fe)$, while in Zircaloy-4, usually, only $Zr(Cr,Fe)_2$ is found, see also Miquet et al. (1982). The $\alpha \rightarrow \beta$ phase boundary temperatures for common alloys used are summarized in table 2.2.

Major compositions of common fuel clad Zr-base alloys						
Alloy	Sn wt%	Nb wt%	Fe wt%	Cr wt%	Ni wt%	O wt%
Zircaloy-2	1.5	-	0.2	0.1	0.05	0.12
Zircaloy-4	1.3-1.5	-	0.2	0.1	-	0.12
ZIRLO	1	1	0.1	-	-	0.12
M5	-	1	-	-	-	0.12
E110	-	1	0.01	-	-	0.06
Zr-2.5Nb	-	2.5	0.01	-	-	0.12

Table 2.1: Nominal composition of major fuel cladding alloys used in LWRs.

Alloy	T_α (K)	T_β (K)	Source
Zircaloy-2	1073	1253	Bunnell et al., 1983
Zircaloy-2	1095/1053*	1273	Arias & Guerra, 1987
Zircaloy-4	1081	1281	Miquet et al., 1982
Zr-1 wt% Nb	1049	1221	Canay et al., 2000
Zr-2.5 wt% Nb	870	1170	Hunt & Foot, 1977

Table 2.2: Phase boundary temperatures extracted from literature. *Heating/cooling. Here T_α , T_β denote $\alpha \rightarrow (\alpha+\beta)$ and $(\alpha+\beta) \rightarrow \beta$ boundary temperatures, respectively.

Oxygen is an α stabilizer, meaning that, it expands the α region of the phase diagram by formation of interstitial solid solution. Tin, a major element in Zircaloy and ZIRLO is also an α stabilizer. In α and β phases Sn is a substitutional element. On the other hand, niobium is a β stabilizer, which also exists in substitutional solid solution. In the Zr-Nb binary alloy, a monotectoid transformation occurs at ≈ 893 K and ≈ 18.5 at% Nb (Guillermet, 1991), see figure 2.1 for a zirconium-rich portion of the Nb-Zr phase diagram. Phase transition temperatures for a Zr-alloy close to a ZIRLO composition, determined by electric resistivity method, have been reported by Canay et al. (2000). The results for two runs are presented in table 2.3. Note the hysteresis in $(\alpha+\beta)\leftrightarrow\beta$ transitions. Toffolon et al. (2002) have measured the phase transition temperatures for a Zr-alloy close to the M5 composition (figure 2.2), see also (Perez & Massih, 2007).

Run	$\alpha \rightarrow (\alpha+\beta)$	$(\alpha+\beta) \rightarrow \alpha$	$(\alpha+\beta) \rightarrow \beta$	$\beta \rightarrow (\alpha+\beta)$
1	1017	1012	1256	1235
2	1015	1012	1267	1254

Table 2.3: Phase transition temperatures (K) for Zr-1Nb-1Sn-0.1Fe (in wt%) alloy.

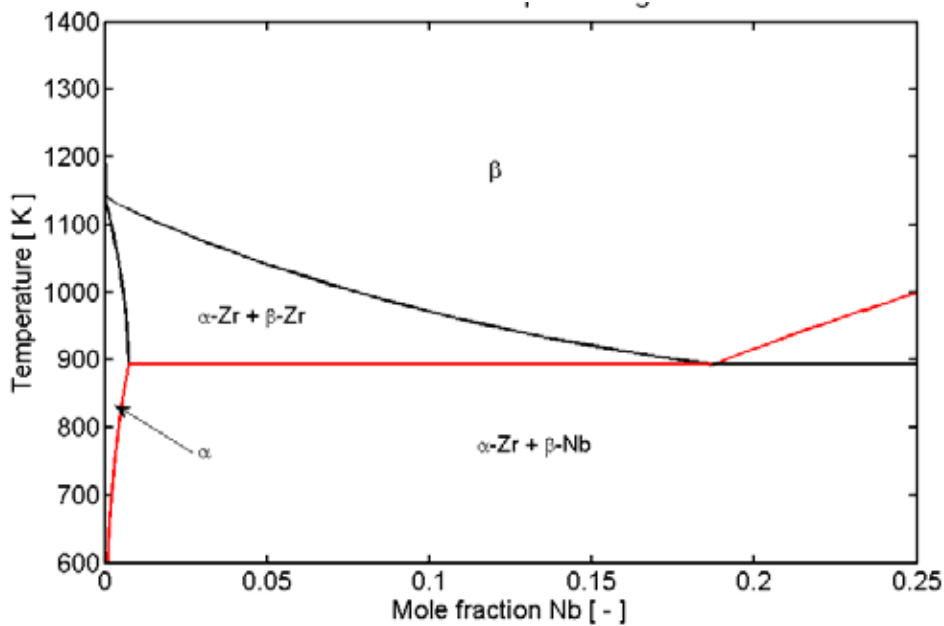


Figure 2.1: Calculated Zr-rich portion of the Nb-Zr binary system phase diagram.

2.2 Clad embrittlement phenomenology

Cladding embrittlement under LOCA is caused by a combination of high temperature oxidation, deformation and cracking. The effect of oxygen on ductility and fracture in Zircaloy-2 has been known since the work of Rubenstein et al. (1961). Extensive cracking of Zircaloy-2 ingots containing 1 wt% O was found after oxidation at 1311 K. Lehr & Debuigne (1963) examined the fracture surfaces of concentrated solid solutions of oxygen in zirconium in the range of 15 to 20 at% O and found that the fracture was completely brittle for both impact and slow strain-rate tests. No evidence of plastic deformation prior to fracture was observed.

Zirconium can dissolve oxygen up to about 29 at% O in solid solution (figure 2.3). During oxidation, oxygen dissolution occurs simultaneously with the growth of oxide, such that an oxygen-rich metal zone beneath the oxide layer is formed. The precise mechanism of oxygen embrittlement in zirconium alloys is not clearly understood. As oxidation proceeds, the increasing extent of oxygen penetration in advance of the metal/oxide interface will lead to an increasing extent of embrittlement of the metal supporting the oxide film. At a certain depth of oxygen infiltration, the metal can no longer support the oxide and cracking in the oxide and embrittled metal zone may follow.

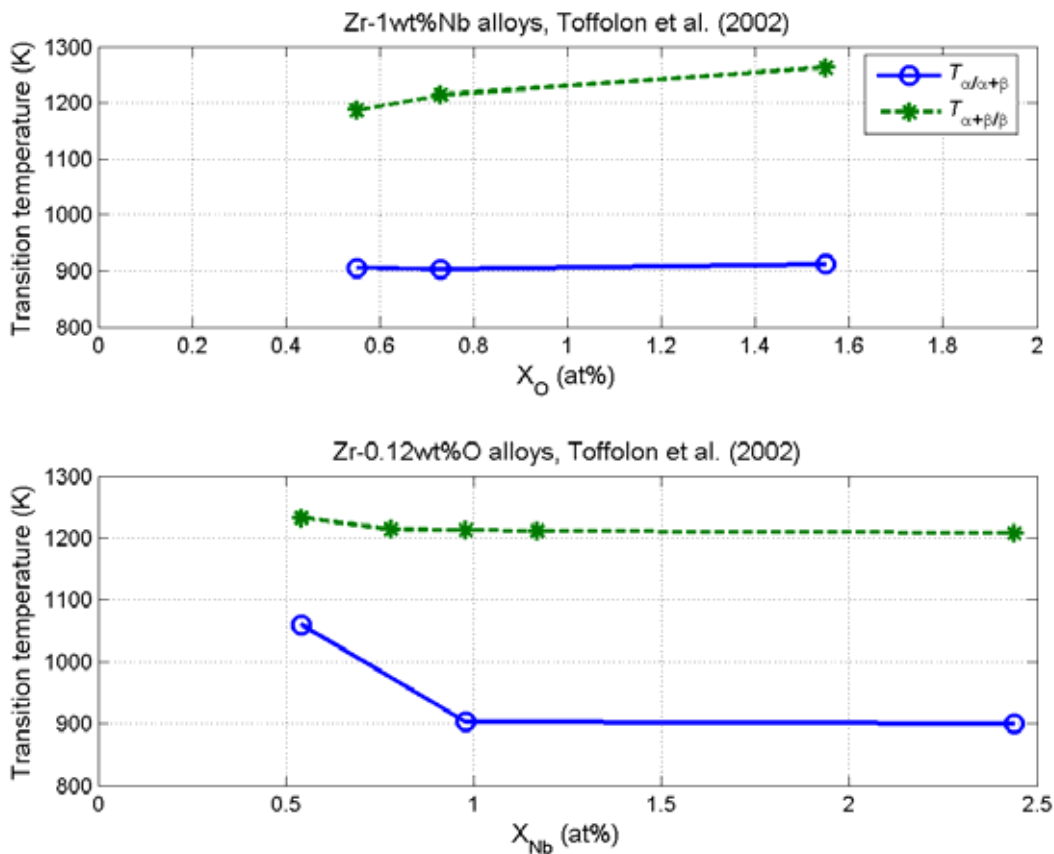


Figure 2.2: The $\alpha \rightarrow (\alpha+\beta)$ and $(\alpha+\beta) \rightarrow \beta$ transition temperatures for a Zr-Nb-O alloy vs. oxygen content (upper panel) and niobium content (lower panel). The symbols are measured values, while the lines are linear interpolations (Toffolon et al., 2002).

For oxidation reactions at temperatures below the $\beta/(\beta+\alpha)$ transformation, the metal at the interface in contact with the growing oxide film will have about 29 at% O in solution, provided equilibrium is maintained. Oxygen will diffuse into α -Zr and its distribution at any time will depend on the oxygen diffusivity, the rate of oxide formation and the geometry of the specimen. At temperatures above 1000 K, oxidation would in general produce four phases (figure 2.3): the outer oxide phase (ZrO_2), an intermediate layer of oxygen stabilized α -Zr, and the inner layers containing $(\beta+\alpha)$ -Zr and β -Zr, respectively. During cooling to room temperature, the β -Zr transforms back to α -Zr, however, the microstructure and the hardness of this new α -Zr is different that of the oxygen stabilized α -Zr. From figure 2.3, we note that the oxygen solubility in the β -Zr is much less than the α -Zr, but it is still sufficiently large to affect hardness and ductility of the material (Douglass, 1971). This implies in mechanical analysis, not only

must the loss of material due to oxide formation be considered, but also property changes in the α -Zr and prior β -Zr as a result of oxygen in solution need to be accounted for. Figure 2.4 provides a conversion curve for mole fraction (atom fraction) to weight fraction in the O-Zr system for reader's convenience.

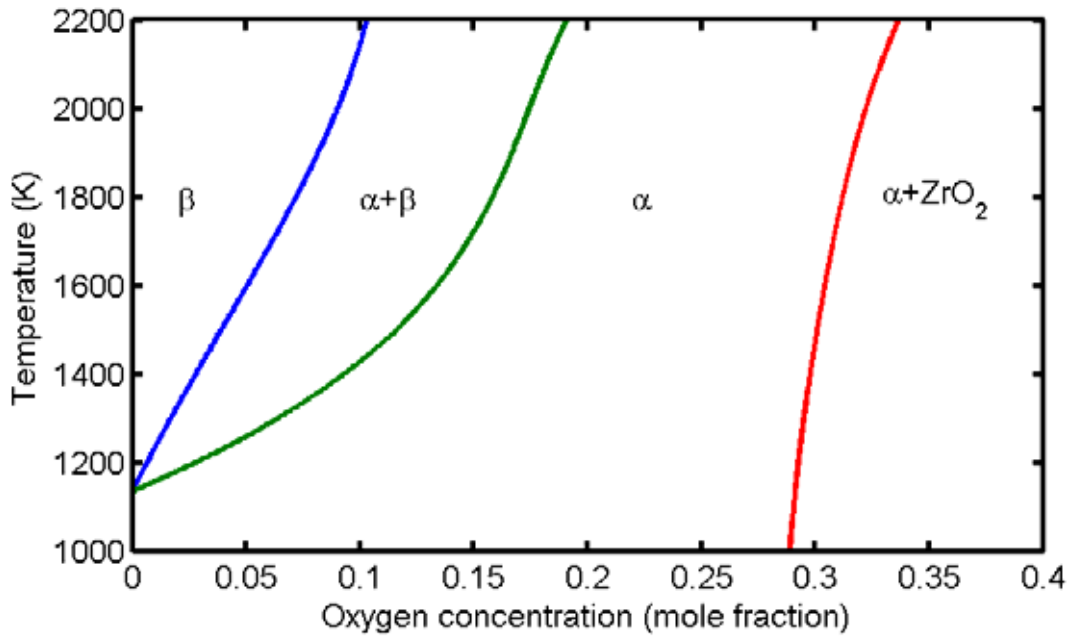


Figure 2.3: Portion of the zirconium-oxygen binary phase diagram based on the assessment of Abriata et al. (1986).

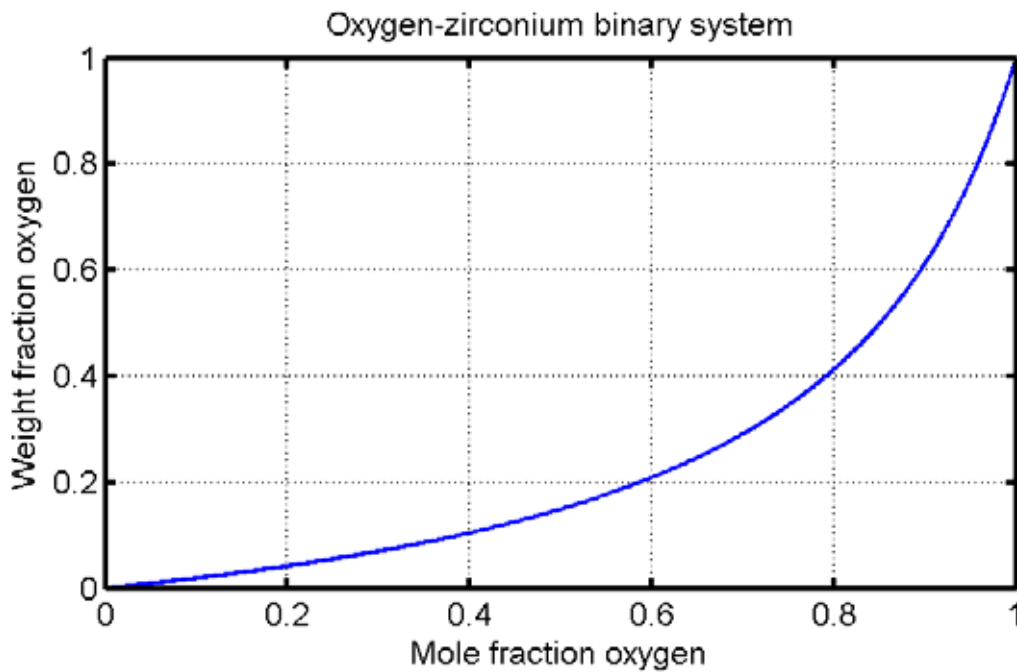


Figure 2.4: Mole fraction vs. weight fraction for the O-Zr binary system.

Chung and Kassner (1979) have made an *isoplethal* study of the Zr-rich portion of the Zircaloy-4/oxygen phase diagram by resistometry measurements and metallographic analysis of equilibrated and quenched specimens. Figure 2.5 shows the outcome of this investigation. Their study indicates that the β -phase boundary for Zircaloy-4/oxygen is virtually the same as that for the zirconium/oxygen system (cf. Abriata et al., 1986) and the Zircaloy-2/oxygen system (cf. Mallett et al., 1959). The α -phase boundary for Zircaloy-4/oxygen solid solution is about 70 K lower than for the Zr/O system.

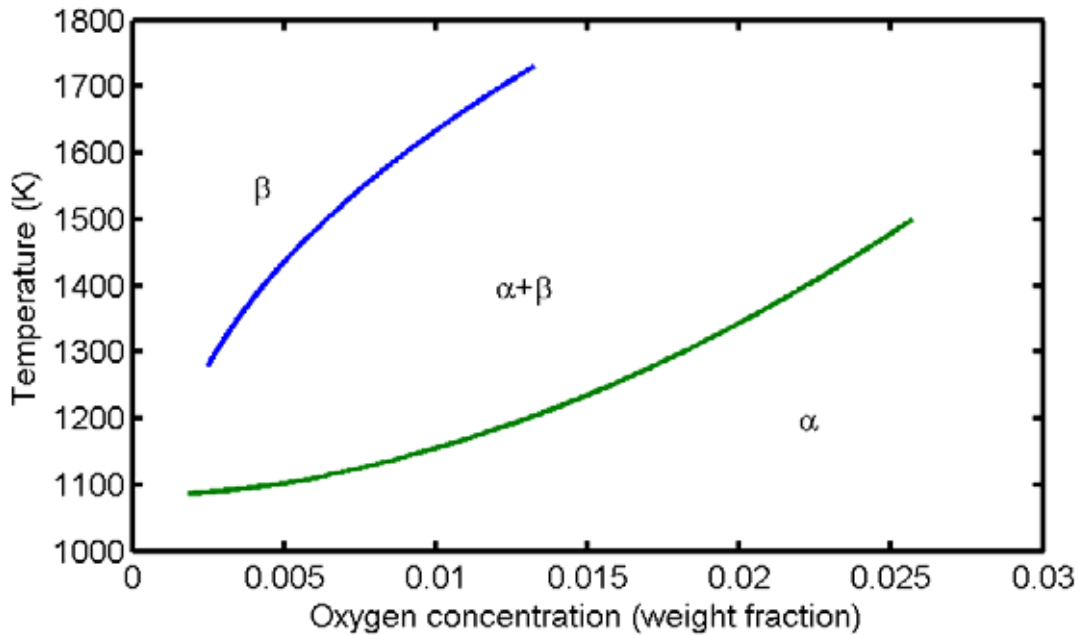


Figure 2.5: An isoplethal section of Zr-rich portion of Zircaloy-4 phase diagram showing the α - and β -phase boundaries, based on metallographic measurements of the equilibrated and quenched specimen (Chung & Kassner, 1979).

The oxygen gradient beneath the ZrO_2 layer in zirconium alloys has been measured and compared with model calculations (Pemsler, 1962, 1965). A typical profile is schematically depicted in figure 2.6. Specific measurements of oxidation in steam at 1023 K are depicted in figure 2.7, which shows the oxygen concentration as a function of distance into the metal below the oxide film. Pemsler's (1962) microscopic examination of certain Zr-base alloys upon corrosion exposure indicated that a nonuniform oxide film can grow, where an "oxide finger" around a crack protrudes into the metal substrate. Figure 2.8 illustrates Pemsler's observation schematically. As can be seen, a relatively thick zone of oxygen-enriched metal surrounds the thicker oxide area, at the left of the diagram. This suggests that the accelerated growth of the oxide layer occurred at an early stage in corrosion and was followed by a period in which the oxide film was protective. On the contrary, the thick oxide bulge in the centre of the diagram is surrounded by a region of small oxygen incursion, indicating that oxide growth was uniform or occurred during the latter stage of corrosion. A very thin oxygen diffusion zones, or no diffusion zones at all, typically surrounded the oxide fingers as illustrated at the right of figure 2.8. Pemsler concluded that the oxide finger is self-perpetuating due to the high local strains in the oxide formed within the finger, which eventually can fracture the specimen. The schematic diagram in figure 2.9, due to Hache

& Chung (2001), shows the microstructure profile and the associating oxygen concentration across a Zircaloy tubing wall after oxidation near 1470 K.

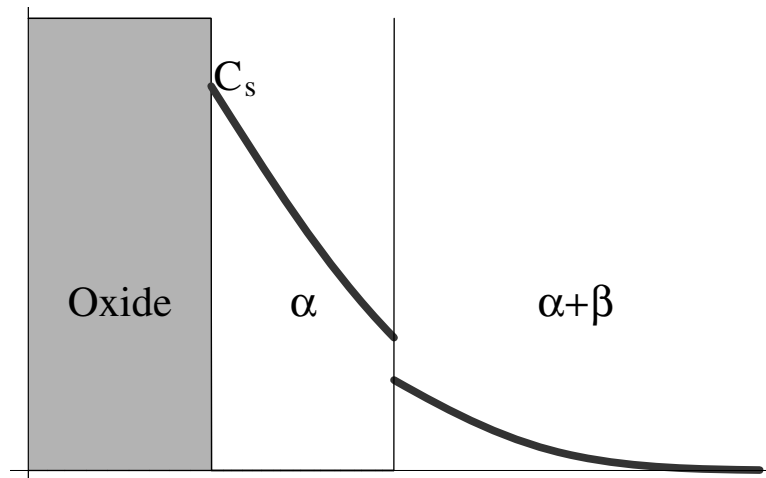


Figure 2.6: Schematic plot of oxygen profile in Zr alloy at temperatures above the $\alpha/(\alpha+\beta)$ transition temperature. Here, oxide is ZrO_2 , C_s stands for the oxygen concentration at the metal oxide interface.

Bradhurst & Heuer (1975) made an experimental study on the effect of oxidation of Zircaloy-2 fuel cladding in flowing steam in the temperature range of 973 to 1573 K with the aim of identifying the embrittlement mechanism of cladding under LOCA condition. They found three concurring effects causing cladding embrittlement, namely, oxidation, deformation and cracking of oxide layer. The embrittlement was related to the rate of deformation. They categorized the rate of deformation under oxidation into two levels, a *fast deformation* and a *slow deformation*. The fast deformation was in the order of a second followed by a period of oxidation of 10 minutes, while the slow deformation was throughout the periods of oxidation, which were mostly about 10 minutes. They made the following observations, based on the metallography of oxidized specimens, regarding the mechanism of the deformation-enhanced oxidation. Tensile deformation during oxidation caused cracking of the growing oxide and local oxidation of the metal at the base of the crack. They also observed that the number of points of local attack was inversely related to the temperature of oxidation. Slow deformation initially caused cracking of oxide layer (figure 2.10a). Further deformation resulted in continual disruption of the oxide formed at the base of each crack. They noted that any plasticity of the oxide would reduce the number of cracks initially formed. The effective rate of oxygen transport was increased, being limited by the rate at which oxygen can diffuse down the cracks in the oxide and by the diffusion rate through the oxide film, which continually reformed at the base of the crack. The steeper oxygen concentration gradient in the thin oxide near the crack tip caused more rapid oxygen diffusion into the metal in these positions. In the case of fast deformation (figure 2.10b) similar behavior was observed, except that the cracks in the oxide layer were wider when the deformation occurred within a relatively short time (about 1 s). Further oxidation then ensued by the typical process of inward oxygen diffusion. Table 2.4 lists oxidation data for rapid and slow modes of deformation at 1333 K /10 min. Figure 2.11 shows the calculated increase in maximum oxygen penetration into the clad under slow deformation as a function of time at 1333 K. The oxygen penetration δ is the sum of the oxide thickness w and the oxygen stabilized layer of α -Zr.

Set conditions		Calculated parameters		Measured data		Calculated data	
Time, t	T	D	$L = \sqrt{Dt}$	δ	δ_{\max}	δ	δ_{\max}
s	K	m ² /s	m	μm	μm	μm	μm
Fast							
600	1333	2.43E-12	3.82E-05	78.5	91.5		
600	1333	2.43E-12	3.82E-05	82.8	91.5		
Slow							
600	1333	2.43E-12	3.82E-05	68.9	128	79	175
600	1333	2.43E-12	3.82E-05	68.9	123	79	175

Table 2.4: Oxidation data for slow and rapid deformations of Zircaloy-2 clad specimens during corrosion in steam, after Bradhurst & Heuer (1975). Here, D is the oxygen diffusivity and δ is the sum of the oxide thickness and the oxygen stabilized layer α -Zr.

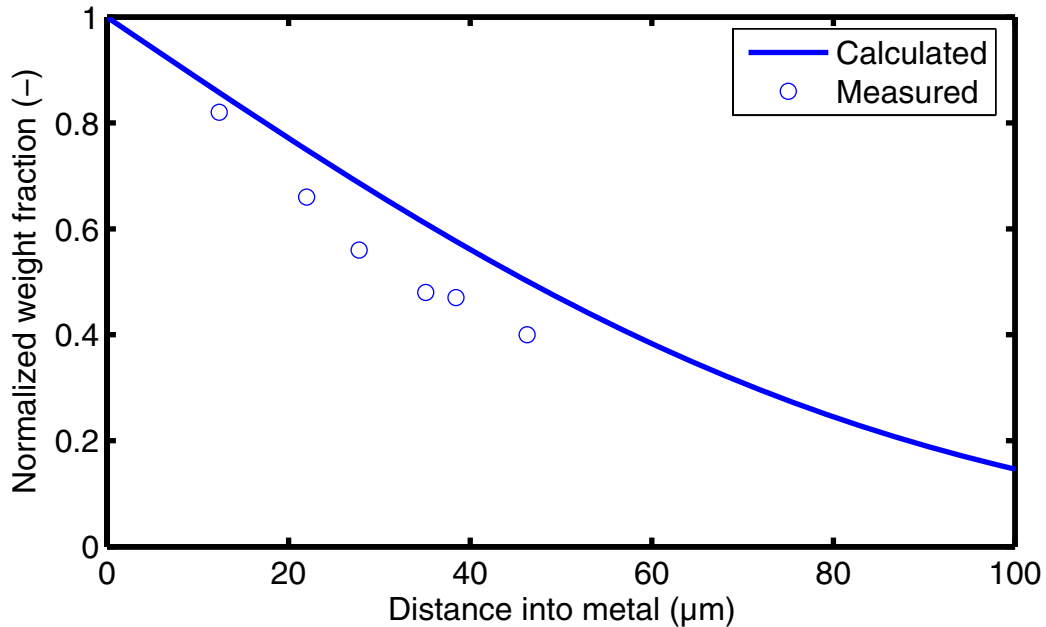


Figure 2.7: Oxygen concentration gradient in corroded zirconium alloy specimen in steam at 1023 K to a weight gain of 470 mg/dm² (normalized with 0.067 wt. fraction), after Pemsler (1962).

The experiments of Bradhurst & Heuer (1975) indicated that deformation, imposed during the high temperature steam oxidation of Zircaloy-2 clad, causes a significant increase in the amount of oxidation. This increase takes the form of augmented local oxygen penetration of the metal beneath cracks in the oxide layer. The maximum oxygen penetration in the clad was about twice that of the undeformed specimens. Fast deformation was less effective than slow deformation in disrupting the oxide film during the high-temperature excursions for LWR clad. The results suggest that the strain rate and the amount of pre-oxidation are important parameters affecting the embrittlement process of clad during LOCA. Therefore, the effect of deformation-enhanced oxidation of fuel clad should be included in LOCA modeling analysis.

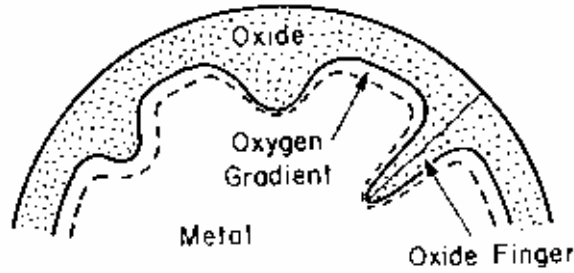


Figure 2.8: Schematic picture of oxygen profile around a thick oxide layer of zirconium alloy cladding, after Pemsler (1962).

Chung et al. (1977) investigated the rupture characteristics of Zircaloy-4 clad (outer diameter of 10.9 mm, wall thickness 0.635 mm) in a vacuum environment (2.6 Pa) over a wide range of internal pressures (0.35 to 15 MPa) at several heating rates.ⁱ Moreover, they examined the impact of axial constraint (gap between pellet column and end plug) by using an alumina (Al_2O_3) mandrel that simulated pellets in a fuel rod. In particular, they investigated the relationships between the effective rupture stress and temperature and the maximum circumferential strain and the burst temperature. Their aim was to understand the deformation process near the onset of plastic instability, i.e., the transition from uniform tube expansion to localized ballooning (inflation) which is important to the development of a failure criterion for an internally pressurized fuel rod during LOCA.

Chung et al. (1977) defined an instability criterion according to

$$\frac{d \ln \dot{\epsilon}_d}{dt} \leq 2 \frac{d \ln \epsilon_d}{dt}, \text{ (plastic stability)} \quad (2.1)$$

where $\epsilon_d = D/D_0$, $\dot{\epsilon}_d = d\epsilon_d/dt$, and D and D_0 are the initial and current tube outer diameters at time t , respectively.

Figure 2.12 shows the effective stressⁱⁱ at the onset of plastic instability as a function of temperature for axially constrained tube specimens at two different strain rates. The rapid decrease in strength at 1120 to 1250 K is caused by $\alpha \rightarrow \beta$ phase transition.

The results of Chung et al. on the circumferential strain at failure are depicted in figures 2.13a-b, where an oscillatory behaviour is observed. It is seen that there are two superplastic strain maxima at about 1100 and 1350 K, and a third maximum at about 1500 K. The strain at failure in steam is lower than in vacuum at temperatures beyond 1300 K in these experiments, seemingly due to the oxidation effect. Chung et al. (1976) based on their observations, envisioned a sequence of events for deformation and rupture of cladding under LOCA conditions (at temperatures >1270 K), shown in figure 2.14. Cracks initiate in the thin oxide layer, and then penetrate through the α -stabilized layer causing an intergranular fracture, and afterward extending to the β -phase region similar to observation by Bradhurst & Heuer (1975), cf. figure 2.10a. Chung et al. also attempted to construct an engineering clad failure criterion based on rupture strain of as-received Zircaloy-4 clad in terms of the initial pressure and heating rate. An example of

such a measure is shown in figure 2.15 (cf. figure 2.13a). Although the general trend in clad behaviour seen in figure 2.15 is credible, the actual values of strains can vary from test to test due to slight variations in the initial conditions or material microstructure.

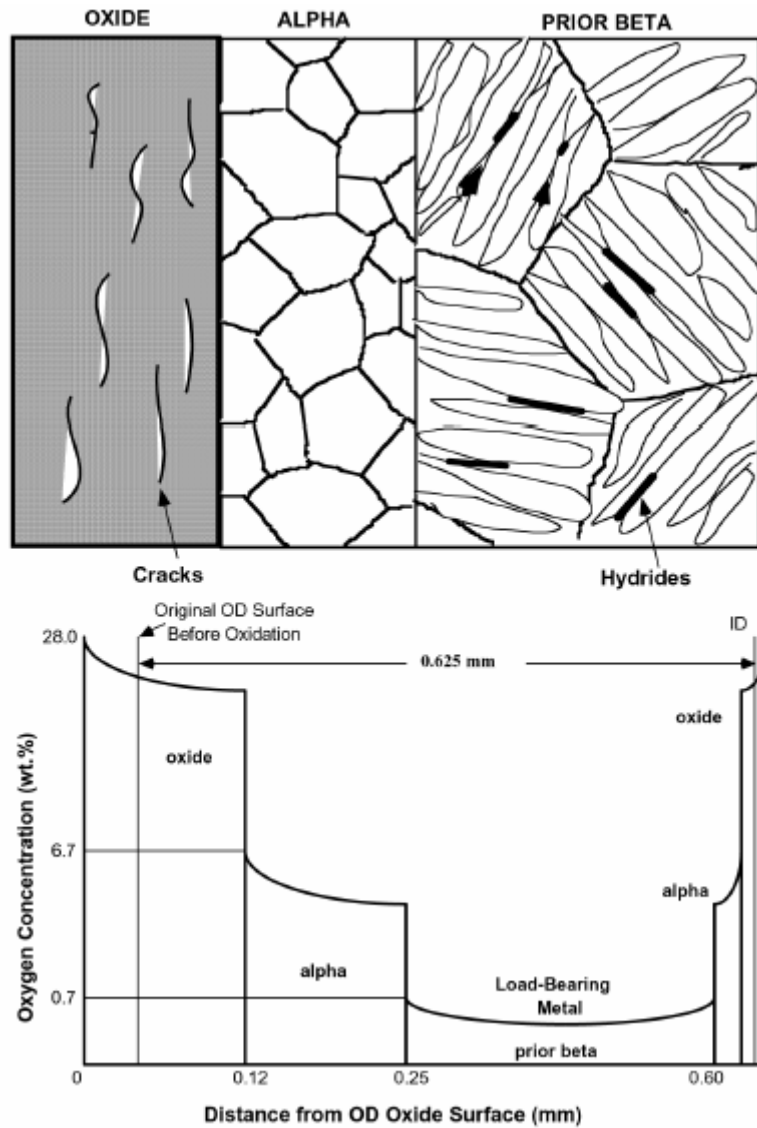


Figure 2.9: Schematic picture of microstructure of Zircaloy cladding subjected to high temperature oxidation (top) and the associated diagram of oxygen distribution (bottom); illustration is from Hache & Chung (2001).

Another stage in a postulated LOCA event that has an impact on clad embrittlement behaviour is the action of ECCS water, which entails the collapse of vapour film that covers the clad outer diameter surface prior to subsequent transition boiling, see e.g. (IAEA, 2001). It is believed that this event occurs at a constant temperature, the so-called *Leidenfrost temperature* of the liquid at the surface (Chung & Kassner, 1980).ⁱⁱⁱ For oxidized Zircaloy clad rewetted by bottom flooding water, rewetting occurs in the temperature range of 748-873 K (Chung & Kassner, 1980). If the clad is sufficiently embrittled by oxidation, the abrupt change in the heat transfer conditions induces large thermal stresses in the clad, which can fracture it. Hache & Chung (2001) point out that there are two main factors that worsen the situation, that is, make oxidized clad susceptible to post-quench embrittlement in comparison with clad fragmentation during

quenching, namely (i) a more pronounced effect of oxygen dissolved in the β -Zr and later, after phase transition, in former β phase at lower temperatures, (ii) the effect of hydrogen uptake and hydride precipitation at lower temperatures.

The phase diagram of the hydrogen-zirconium system indicates that below 823 K (550°C) hydride particles (δ phase) coexist with α -Zr over a wide range of hydrogen compositions (figure 2.16). Above 823 K, at hydrogen concentrations between 37.5 (0.66) and 56.7 (1.43) at% H (wt% H), hydride precipitates coexist with β -Zr (Zuzek et al., 2000). The presence of oxygen perturbs the hydrogen solubility limits. The experimental work of Singh & Parr (1963) shows that the hydrogen-rich boundaries between $\beta/(\beta+\delta)$ and $(\beta+\delta)/\delta$ domains decrease as oxygen concentration is increased in the temperature range of 973-1123 K. Figure 2.17 shows their results for temperatures 973 and 1073 K. Setoyama & Yamanaka (2003) assessed the phase diagram for Zr-O-H ternary system and showed that the $\alpha/(\alpha+\beta)$ and $(\alpha+\beta)/\beta$ phase boundaries in the Zr-O binary system shift to lower temperatures with addition of H; and the dissolved H increases the oxygen content of β phase, hence enhancing clad embrittlement in the former β phase upon quenching. The eutectoid temperature for hydride precipitation in Zr-1wt%Nb alloy is a bit higher (about 863 K) and the kinetics could be different than Zircaloy (section 3.3). The effect of oxygen on phase transition of Zr-Nb-O system has recently been evaluated (Perez & Massih, 2007), however no corresponding assessment of ternary phase diagram Zr-Nb-H to our knowledge is published.

2.3 Clad embrittlement criteria

During a postulated LOCA, a combination of thermal-mechanical loads (see section 1) may fracture the fuel clad if it is sufficiently oxidized and embrittled, causing loss of fuel rod geometry and even disrupting the reactor core coolability. The aim of the reactor emergency cooling system design (acceptance) criteria is to avoid such a situation. These criteria were established following the 1972-1973 hearings in the United States, and are described in US government documents (AEC, 1973) and (US Code of Federal Regulations, 1981). In relation to fracture of fuel clad during a postulated LOCA, the criteria comprise the following requirements:

1. *Peak clad temperature* (PCT). The calculated maximum fuel element clad temperature shall not exceed 1477 K (1204°C).
2. *Maximum clad oxidation* (MCO). The calculated *equivalent clad reacted* (ECR) must not exceed 0.17 times the clad wall thickness.
3. The *Baker-Just correlation* (Baker & Just, 1962) must be used to calculate Zircaloy-steam oxidation rates for LOCA conditions.

ECR is defined as the ratio of the converted metal thickness to initial clad wall thickness. Converted metal thickness is the equivalent metal thickness that would be converted to oxide if all the oxygen absorbed by, and reacted with, the clad locally converted to stoichiometric zirconium dioxide (AEC, 1973). The Baker-Just correlation is used to calculate ECR.

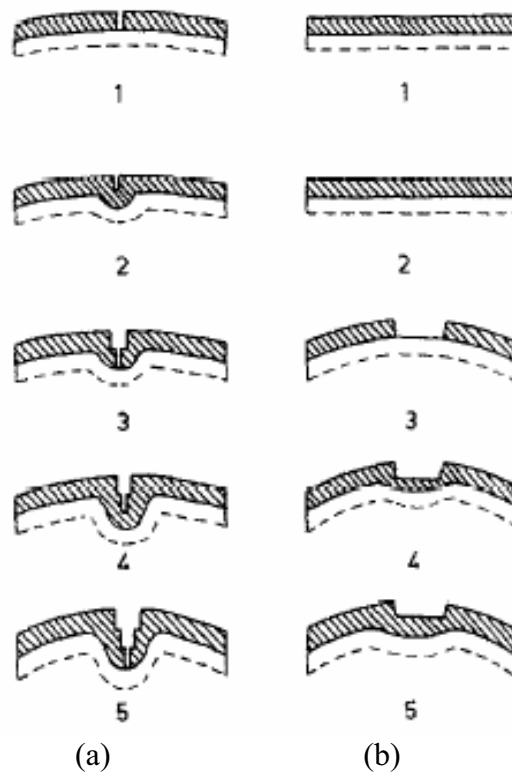


Figure 2.10: Schematic representation of the process of deformation-enhanced oxygen incursion in Zircaloy during high temperature oxidation in steam; for slow deformation (a) and fast deformation (b); after Bradhurst & Heuer (1975).

The PCT and ECR limits define the boundaries of a region of acceptable reactor core conditions during a postulated LOCA, within which the clad is expected to remain intact. The third criterion above quantifies how fast the Zircaloy clad would approach the boundaries at a given oxidation temperature.

In addition to the aforementioned acceptance criteria for clad embrittlement, there are three additional rules for maintaining the LWR core integrity and coolability, described in (US Code of Federal Regulations, 1981), namely:

- *Maximum hydrogen generation.* The calculated total amount of hydrogen generated from the chemical reaction of the clad with water or steam shall not exceed 0.01 times the hypothetical amount that would be generated if all of the metal in the clad tubes surrounding the fuel, excluding the clad surrounding the plenum volume, were to react.
- *Coolable geometry.* Calculated changes in core geometry shall be such that the core remains amenable to cooling.
- *Long-term cooling.* After any calculated successful initial operation of the ECCS, the calculated core temperature shall be maintained at an acceptably low value and decay heat shall be removed for the extended period of time required by the long-lived radioactivity remaining in the core.

Appendix K of *ibid.* describes various models that must be used for calculating these limits or requirements. The appendix specifies which models should be employed for calculation of in-reactor processes, e.g., initial stored energy in fuel, radioactive decay heat, metal-water reaction, reactor internal heat transfer, clad ballooning and rupture, other relevant models related to blowdown phase of LOCA.

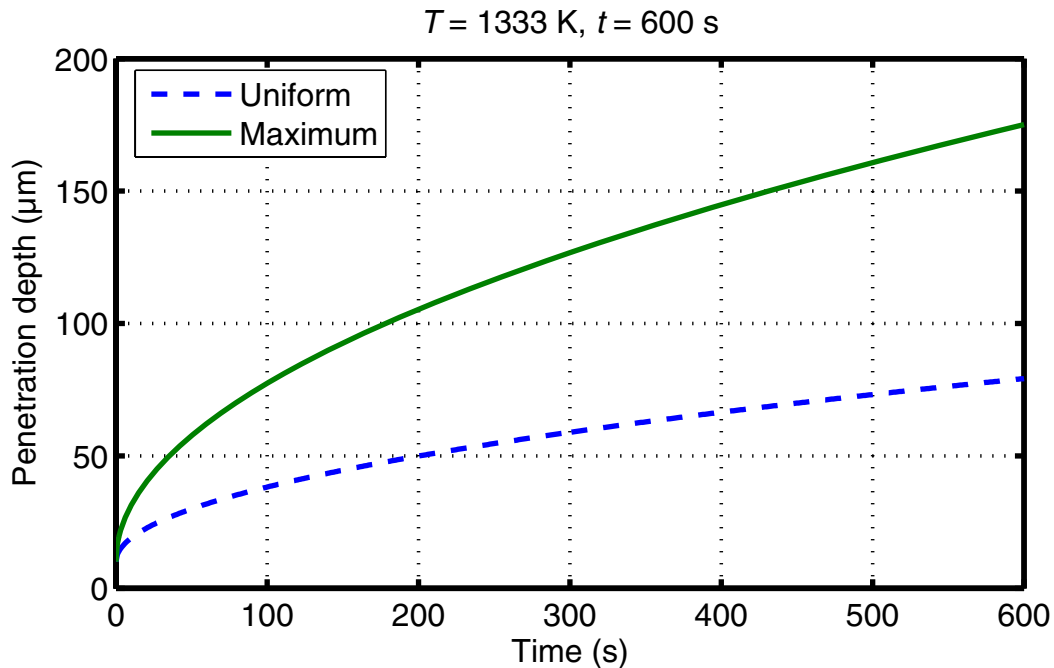


Figure 2.11: Calculated Oxygen incursion in Zircaloy-2 under slow deformation during oxidation in steam, based on data of Bradhurst & Heuer (1975).

2.4 Bases for clad embrittlement criteria

Recently Chung (2005) has discussed the rationale for establishment of the two criteria (PCT and MCO) in detail and thus here we only summarize the main deliberations of the design basis.

2.4.1 Maximum clad oxidation limit

The 17% ECR limit (also the 1477 K PCT limit) is primarily based on the results of post-quench ductility tests made by Hobson & Rittenhouse (1972). In these tests Zircaloy-4 cladding tubes (nominally 0.686 mm wall thickness \times 10.72 mm outer diameter) were oxidized in steam followed by direct quenching from high temperatures (1200-1588 K) to room temperature in water. Ring tube specimens from the pre-oxidized tubes were subjected to total elongation or impact loading tests. Hobson and company suggested a nil ductility temperature (NDT^{iv}) no higher than the saturation temperature during reflood (about 408 K). The NDT at this temperature was equivalent to a β -Zr layer fraction of combined oxide layer of about 0.58 or a fraction of combined oxide layer plus α -Zr layer thickness of 0.42. This latter value corresponds to 0.44 if it would be calculated based on the as-fabricated cladding wall. If ξ_T denotes the total oxide layer and α -Zr layer thickness, and h stands for the original specimen

thickness, $\xi_T/h = 0.44$, which corresponds to the NDT of 408 K and ECR=0.17 per calculated by the Baker & Just (1962) correlation. Indeed, from the plots of ECR versus oxidation time at different temperatures and ξ_T/h , it was observed that the $\xi_T/h = 0.44$ lines evaluated by different workers lie above ECR=0.17 (Chung, 2005). To conclude, the ECR=0.17 is tied to the Baker & Just oxidation correlation and the tests performed by Hobson & Rittenhouse (1972, 1973) on Zircaloy-4 cladding tubes with a wall thickness of 0.686 mm.

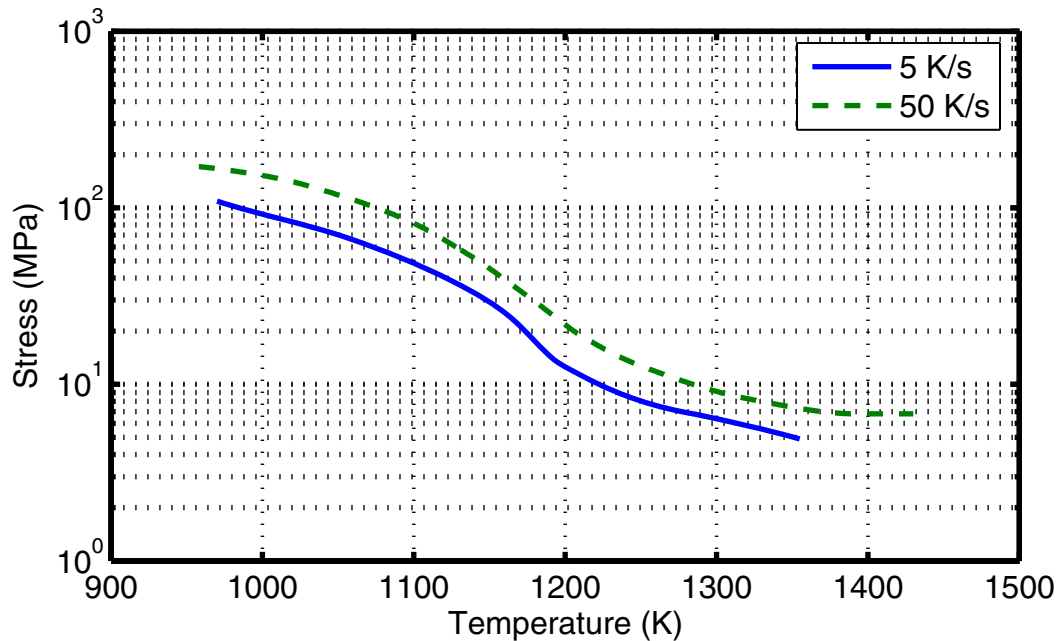
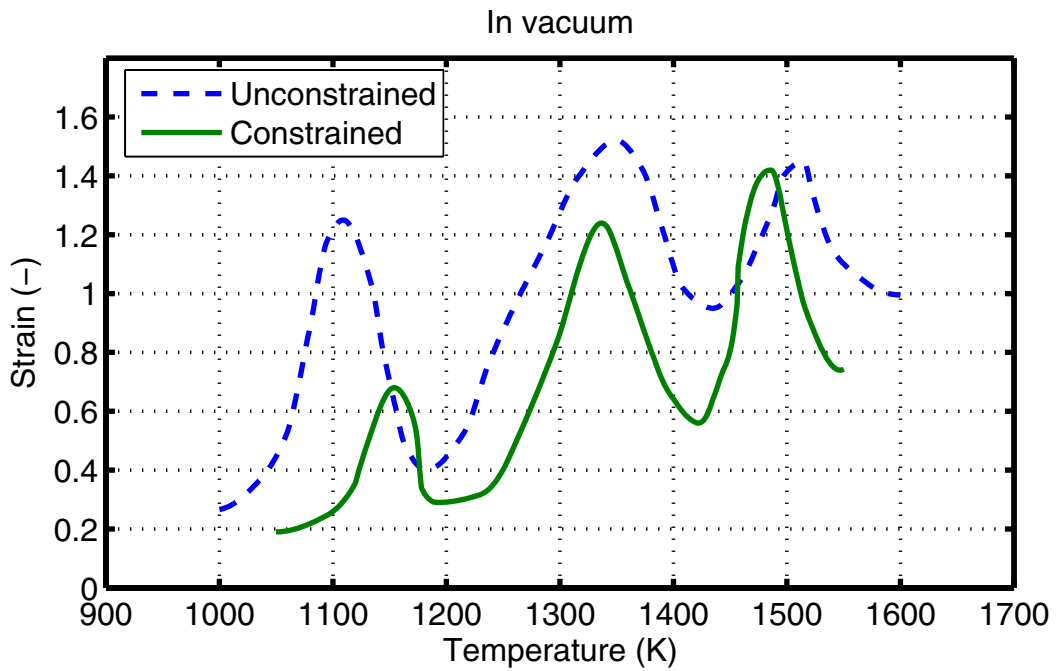


Figure 2.12: Effective stress at instability versus temperature for Zircaloy-4 cladding subjected to an axial constraint and deformed at two heating rates in vacuum, after Chung et al. (1977).

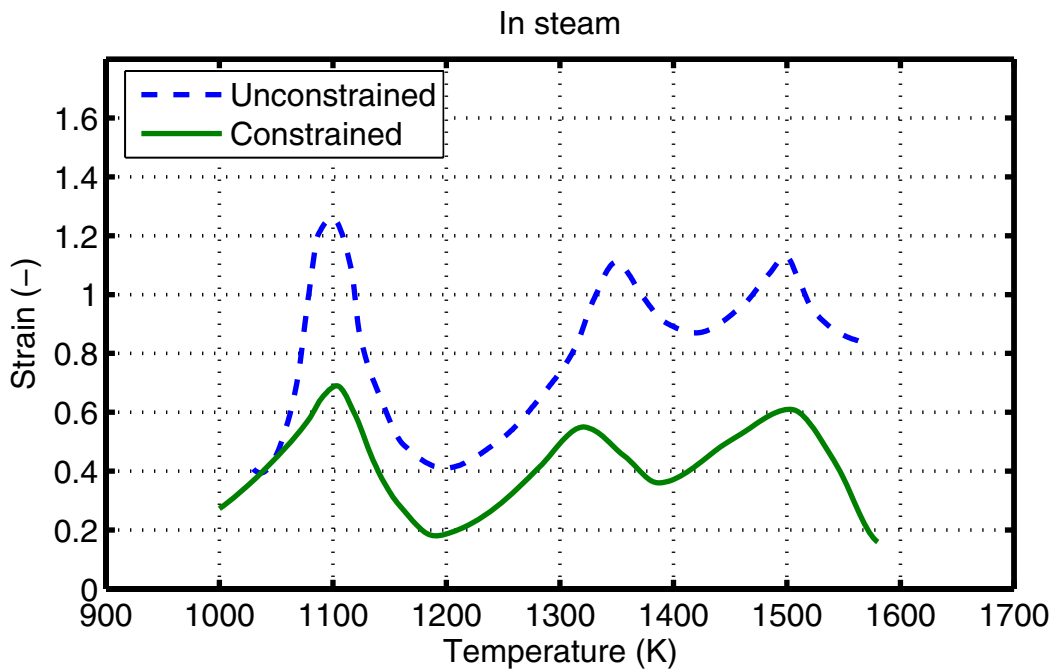
2.4.2 Peak cladding temperature limit

Hobson's metallographic examination (1973) of tested Zircaloy-4 specimens exhibited a good correlation between NDT and the fractional thickness of β -Zr layer, denoted by $F_w = 1 - \xi_T/h$, so long as the specimen was oxidized at temperatures ≤ 1477 K.^v The specimens oxidized above 1477 K, e.g. at 1588 K, were more brittle than the ones oxidized at temperatures ≤ 1477 K.

Pawel's evaluation of Hobson's data (Pawel, 1974) indicated that the onset of room-temperature brittleness in Zircaloy-4 occurs when the average oxygen concentration in the transformed β -Zr reaches 0.7 wt% O (≈ 49 at% O). Moreover, he showed that this concentration cannot be reached at 1477 K (1204°C) but can be attained at 1588 K. This is the origin of the 1477 K (1204°C) PCT limit. In fact, it has been argued that the average 0.7 wt% O limit, which can be calculated by a suitable model, may be a more appropriate limit for cladding ductility than PCT (Pawel, 1974). However, It should be mentioned that the oxygen solubility in β -Zr is much affected by the presence of hydrogen. The hydrogen effect was not considered in the 1974 *Journal of Nuclear Materials* publication (Pawel, 1974).



(a)



(b)

Figure 2.13: Maximum circumferential strain at rupture versus burst temperature for axially constrained and unconstrained Zircaloy-4 cladding at a heating rate of 115 K/s: (a) in vacuum, (Chung et al., 1977), (b) in steam (Chung et al., 1976).

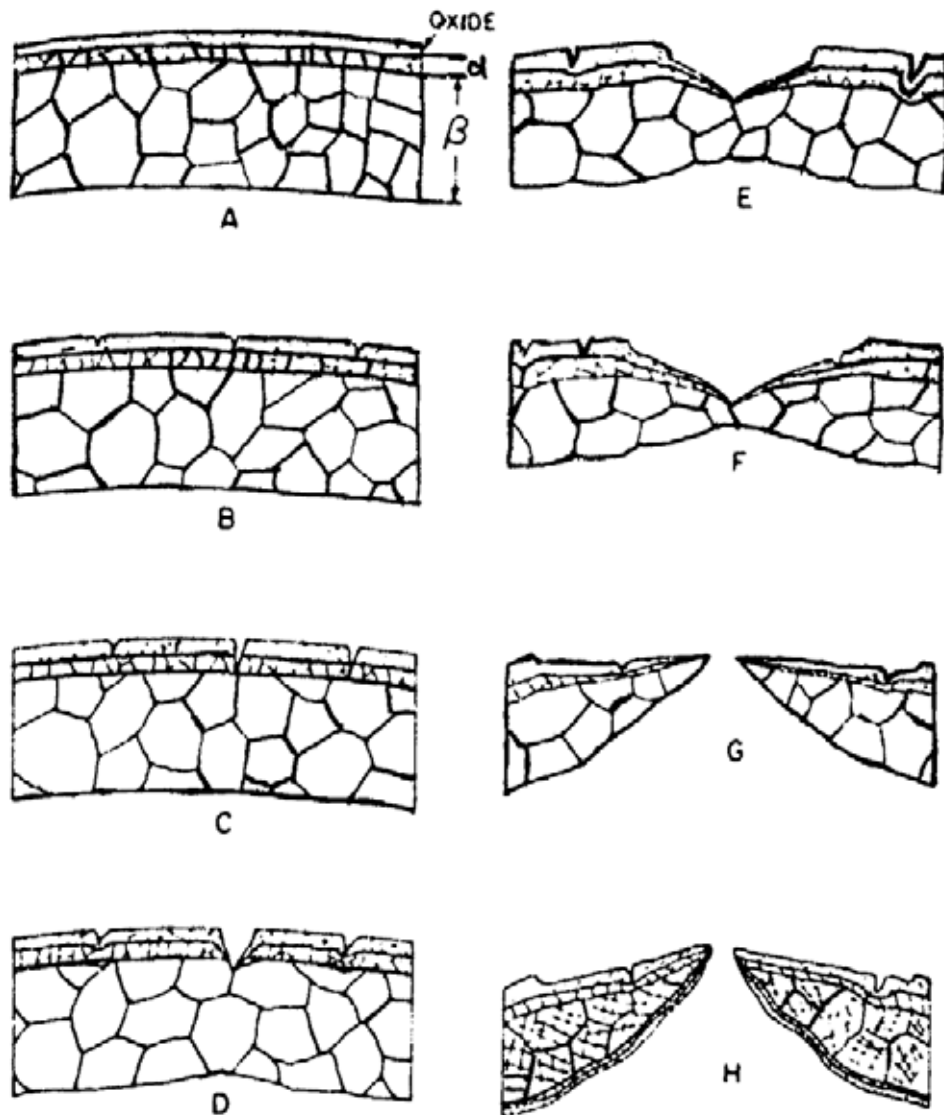


Figure 2.14: Cartoon of the deformation and rupture sequence for clad in a steam environment as envisioned by Chung et al. (1976).

2.4.3 Remarks

As can be understood from the preceding subsections the aforementioned acceptance criteria for cladding embrittlement under LOCA are appropriate (conservative) for (i) Zircaloy materials, (ii) certain clad designs (wall thickness, diameter), (iii) the Baker-Just oxidation data and correlation, (iv) unirradiated claddings, i.e., fresh fuel rods. Since 1973, when these rules were made, considerable changes have occurred in LWR fuel evolution, regarding clad materials in PWRs, design and in-reactor exposure levels. Moreover, an appreciable number of tests have been conducted and analyses made on LOCA conditions, which made a reappraisal of these criteria advisable. Appendix A outlines the basis to the Baker & Just oxidation correlation and compares it with the other empirical correlations developed subsequently. A good assessment of safety margin and embrittlement criteria for ECCS acceptance in light of the available database up to 1986 can be found in (Williford, 1986).

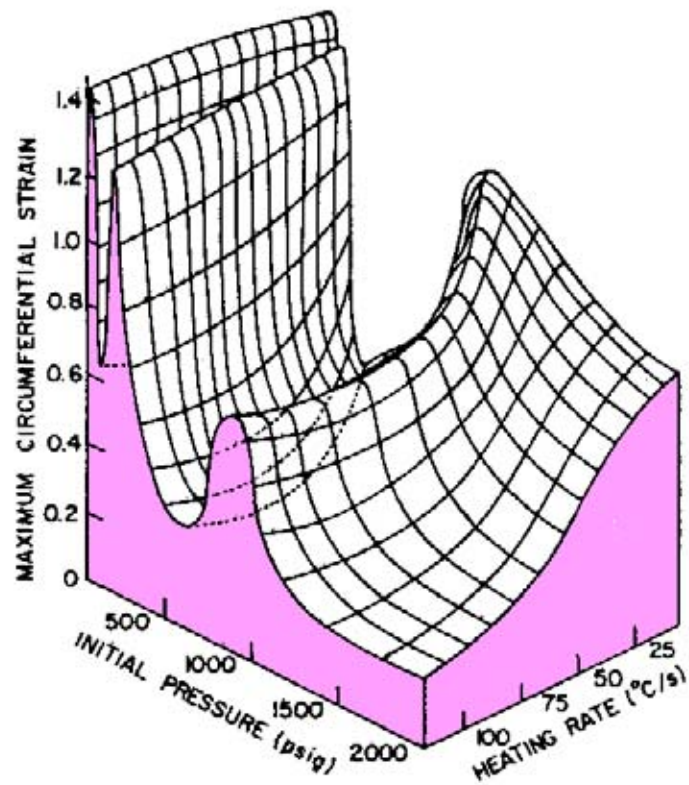


Figure 2.15: Impact of the initial internal pressure (1 psi = 6984 Pa) and heating rate on the maximum circumferential strain for axially constrained Zircaloy-4 clad burst tested in vacuum (Chung et al., 1976).

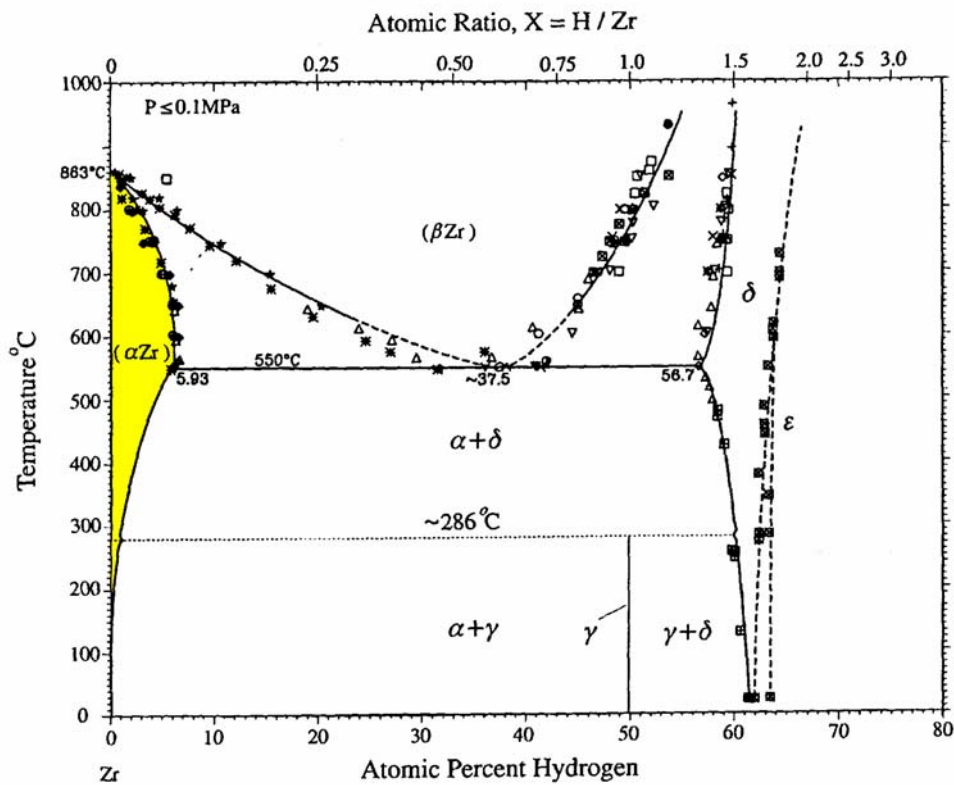


Figure 2.16: Phase diagram of the hydrogen-zirconium system assessed by Zuzek et al. The symbols denote various experimental data evaluated (Zuzek et al., 2000).

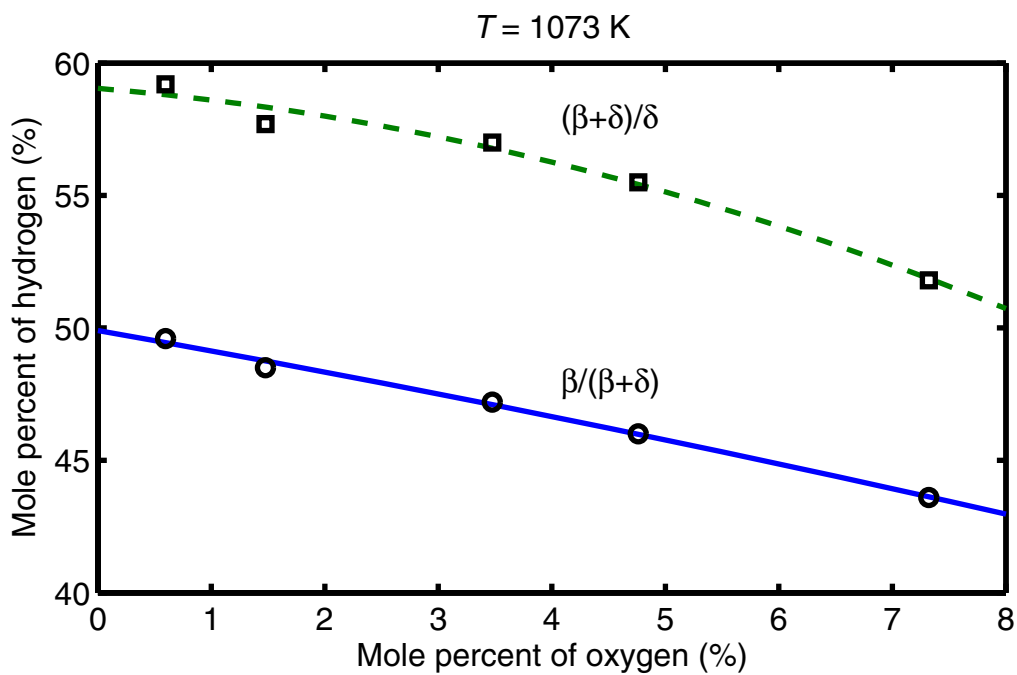
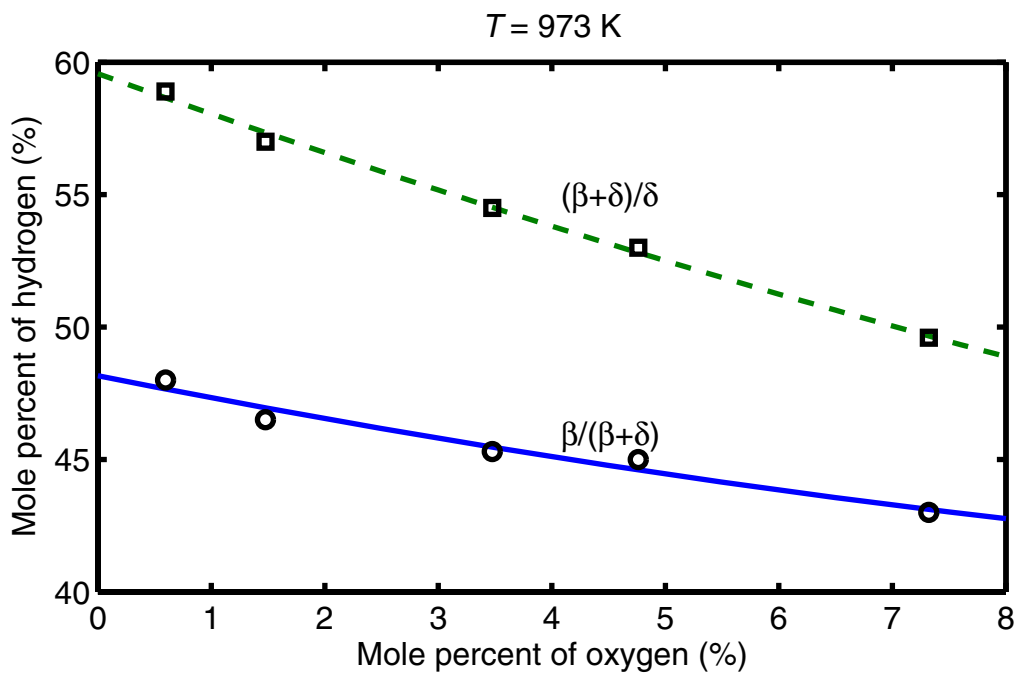


Figure 2.17: Isothermal portions of Zr-O-H alloys showing the hydrogen rich phase transition boundaries (Singh & Parr, 1963).

3 Separate effect tests

In this section, we review the main experimental results on cladding behaviour under LOCA conditions. Namely, clad oxidation, deformation (ballooning), rupture and the overall phase transformation of zirconium alloy. The results were obtained from separate effect tests in various laboratories simulating the LOCA conditions for each of the aforementioned effects. Relationships obtained from these tests (correlations) and simple models used to describe the effects are delineated.

3.1 Clad oxidation under LOCA conditions

During a LOCA, the zirconium alloy is oxidized in steam at high temperatures. Steam oxidation is chiefly a reaction of the outer surface of the fuel rod clad. Under LOCA conditions, however, clad rupture may occur, letting steam into the fuel rod thereby causing inner surface oxidation of the clad. Hence, double-sided steam exposure of clad has been a common test approach for examining the oxidation behaviour of Zircaloy tubing. Zircaloy steam oxidation occurs according to the reaction:



where $Q = -586 \text{ kJ/mol}$ is the released heat. The tests are commonly performed at temperatures between 900 and 1900 K under isothermal and LOCA-type temperature transient conditions.

We only present a brief survey of exemplars of the extensive number of publications on the oxidation of zirconium and its alloys under LOCA conditions. Oxidation of Zircaloy in high temperature steam, results in oxygen-containing layers: ZrO_2 , $\alpha\text{-Zr (O)}$ and $\beta\text{-Zr (O)}$. Baker and Just (1962) from their experiments obtained a reaction rate relation of the Arrhenius type, which as discussed in the foregoing section, is the backbone of the LOCA acceptance criteria. Later, Cathcart et al.'s (1977) experiments lead to similar correlations for integral mass increase, the combined growth of the $\text{ZrO}_2 + \alpha\text{-Zr (O)}$ layers, and diffusion of oxygen in $\beta\text{-Zr}$ (Pawel et al., 1977) in the temperature range of 1273-1773 K. Similar studies of the oxidation kinetics were made by Ballinger et al. (1976), Kawasaki et al. (1978), Urbanic & Heidrick (1978) and Brown & Healey (1980). These investigations were mainly conducted under isothermal conditions in furnace by direct electric heating of specimens or induction heating (Urbanic & Heidrick, 1978), where radiation heating in furnaces is considered to provide the most reliable temperature control. The resulting correlations for the oxidation rate obtained from these experiments are outlined in appendix A. A critical review of Zircaloy oxidation data prior to 1980 has been duly made by Ocken (1980).

Moalem & Olander (1991) studied steam oxidation of as-received Zircaloy-4 specimens in pure steam at atmospheric pressure in the temperature range from 1373 to 1773 K. They found that the parabolic portion of oxidation by pure steam is characterized by rate constants that were 20-40% higher than most the others reported in literature, with the exception of the Baker-Just results.

Nagase et al. (2003) have performed isothermal oxidation tests in flowing steam on low-Sn Zircaloy-4 clad in the temperature range from 773 to 1573 K for the duration between 30 and 2.16×10^6 s. The specimens tested (10 mm long rings) were taken from as-received stress relieved Zircaloy-4 tubing containing 1.3 wt% Sn. The outer and inner diameters of the tube were 9.50 and 8.26 mm, respectively. Nagase and company found that the oxidation kinetics for oxygen mass gain of specimens follow a parabolic rate law for the examined exposure times at temperatures between 1273 and 1573 K, and for the short time range up to 900 s at 773 to 1253 K. The Arrhenius-type rate relations for the parabolic oxidation are listed in appendix A and are also compared with that of the Baker-Just and the Cathcart-Pawel correlations. The comparison of the temperature dependences (figure A.2) shows that the Baker-Just and Cathcart-Pawel correlations overestimate the oxidation above 1073 K, hence are proper for use in safety calculations. But, this is not true for temperatures below 1073 K. The long-term oxidation at temperatures from 773 to 1253 K obeyed a cubic law with Arrhenius-type rate relations (Nagase et al., 2003).

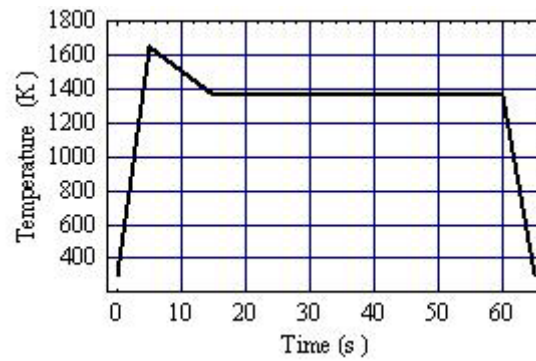
Nagase and co-workers suggest that the change of oxidation kinetics from the cubic to the parabolic law and the discontinuities observed in the temperature dependence of the rate constants are due to the monoclinic/tetragonal phase transformation of ZrO_2 which occurs below 1273 K in the oxide layer according to Nagase et al. and is consonant with the Zr-O phase diagram shown by Schanz (2003).^{vi} The slight decrease of Sn content in Zircaloy-4 from 1.5 wt% to 1.3 wt% showed a negligible effect on the high temperature oxidation kinetics of the material.

The chemical interaction between clad and fuel has been investigated by Hofmann et al. (1979, 1984), who quantified the kinetics of the chemical reactions and described the sequence of transformed layers in the clad. Nevertheless, without fuel-clad contact or the presence of oxide scale on the clad inner surface, the chemical interaction is thwarted. Hence during a LOCA, fuel-clad interaction is not so important, since clad lift-off under internal rod pressure reduces the fuel-clad contact area.

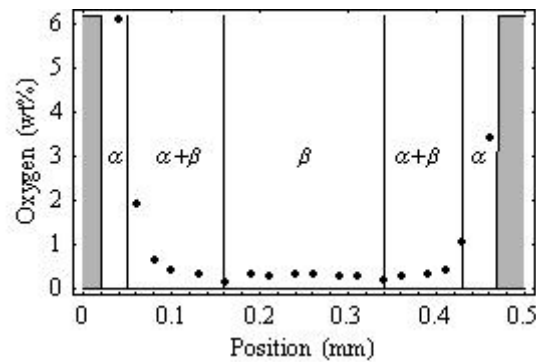
3.1.1 Transient tests

Non-isothermal oxidation, simulating the LOCA temperature transient, has also been studied by many investigators. In a classical experiment, Sawatzky et al. (1977), studied the oxidation under rapid heating/cooling, by placing Zircaloy-4 tube specimens (wall thickness of about 0.5 mm) in an induction furnace and exposed them to steam under the temperature history shown in figure 3.1a. Figure 3.1b shows the oxygen distribution in a specimen from this test. The positions of the ZrO_2/α -Zr and $\alpha/(\alpha+\beta)$ -Zr were determined by metallographic examination. For more details see (Sawatzky et al., 1977, FIG. 5).

Sawatzky et al. (1977) found that, when Zircaloy-4 was cooled during oxidation from above the α/β transus, the $\alpha/(\alpha+\beta)$ interface moved more rapidly at the given temperature and interface position than it did under the same conditions during isothermal oxidation. In the case when the specimen was cooled slowly (2 K/s) from above the α/β transus during oxidation, oxygen diffused back from the β phase to the β/α interface, resulting in a thicker β phase layer and depletion of β phase region (figure 2.3). On the other hand, when the specimen was cooled rapidly (say 100 K/s) an $(\alpha+\beta)$ -Zr region was formed next to the α -Zr layer.



(a)



(b)

Figure 3.1: Sawatzky et al. (1977) transient oxidation experiment of Zircaloy-4 tube specimen in steam: (a) Temperature history; (b) oxygen distribution across tube wall, where points are measurements, the shaded region marks the ZrO_2 layers.

Pawel et al. (1980) reported results of a series of transient oxidation tests on Zircaloy-4 PWR clad specimens in steam under several types of transient temperature histories. More specifically, their test series included two-peak temperature transients illustrated in figure 3.2. The outcome was that the measured values for oxide layer thickness after these transients were 47.5 and 40.2 μm for case (1) and case (2), respectively. This, prima facie, was surprising, since case (2) after the first temperature excursion had the same temperature history as case (1). The explanation for this anomaly was provided by the structural phase transition behaviour (hysteresis) of ZrO_2 crystal (Baun, 1963). The argument goes as follows: It is noted that the oxide formed during heating to the first peak is largely tetragonal. On cooling to the first pit, if the temperature is lower than about 1170 K, the oxide transforms from tetragonal to the monoclinic structure. Then during the second heating, because of the existence of monoclinic oxide, oxidation proceeds more slowly than would have been predicted on the basis of the high temperature isothermal data. This condition will continue until temperature reaches to 1470 K, when the monoclinic oxide is transformed back to the tetragonal phase. This phenomenon is not currently modelled in oxidation of Zircaloy.

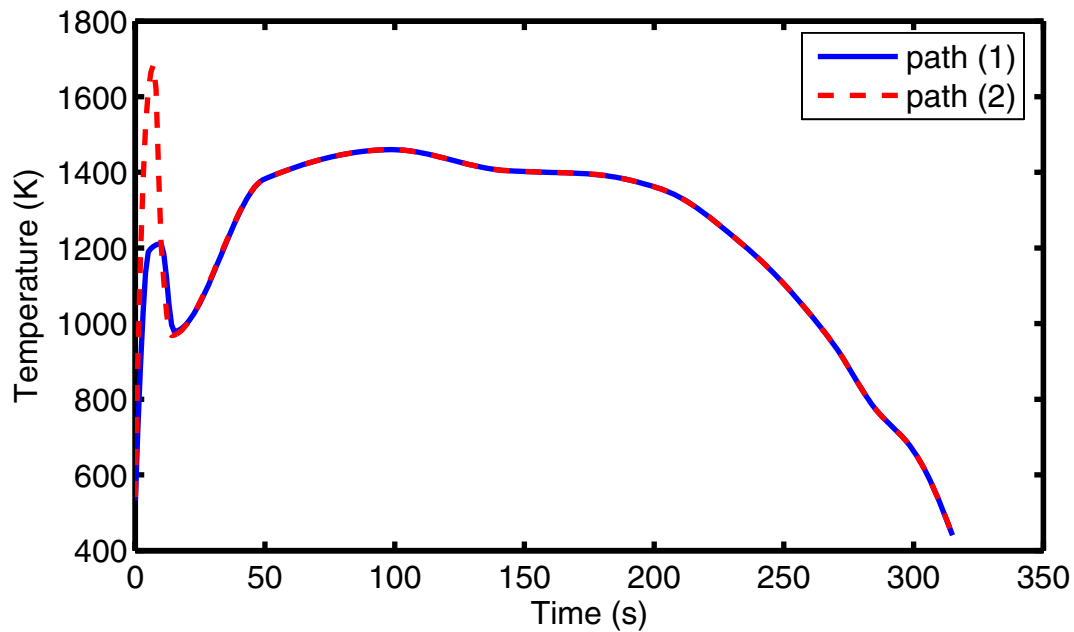


Figure 3.2: Schematic temperature-time histories used in one of the steam oxidation tests on Zircaloy-4 PWR clad performed by Pawel et al. (1980). The measured values for oxide layer thickness after these transients were 47.5 and 40.2 μm for path (1) and path (2), respectively.

Leistikow et al. (1979) have systematically studied Zircaloy-4 oxidation under LOCA type transients. Zircaloy-4 tubing tested had an outer diameter of 10.75 mm and wall thickness of 0.725 mm. The tests were performed at atmospheric pressure in laboratory steam loops with induction heating devices; see also (Leistikow & Schanz, 1987; Erbacher & Leistikow, 1987). Examples from these tests are illustrated in figure 3.3, where both the temperature transients and measured oxygen mass gains are indicated. The associating isothermal tests performed at peak temperatures, indicated in figure 3.3, after about 180 s of exposure time showed oxygen mass gains of 3, 4.8 and 7.8 mg/cm^2 compared with transient values: 2, 3.26 and 5.38 mg/cm^2 , respectively. These tests provide valuable transient oxidation data for modelling of oxidation of Zircaloy.

Moalem & Olander (1991) studied as-received Zircaloy-4 oxidation rates in pure steam at 1 atmosphere (0.1 MPa) at flow rates 200-600 cc (STP)/min at temperatures greater than 1873 K (1600°C). At about 1773 K, the stable oxide of zirconium converts from tetragonal ZrO_2 to cubic ZrO_2 : It is discussed that oxygen diffusivity in cubic ZrO_2 is larger than in tetragonal ZrO_2 resulting in a higher oxygen uptake at temperatures above 1873 K. The transient oxidation test made by Moalem & Olander (1991) from 1873 K to a peak temperature of 2075 K (melting point of oxygen free Zircaloy) in 5 s then cooled down slowly back to 1873 K, indicated a linear oxygen mass gain followed by a weak parabolic solid-state diffusion controlled mass gain. Moalem & Olander's conclusion was that above 1773 K, parabolic oxidation law cannot be observed; and thus the only reliable way of analyzing oxygen uptake at high temperature is by a fundamental oxygen diffusion model, which accounts for initial steam starvation and non-isothermal behaviour.

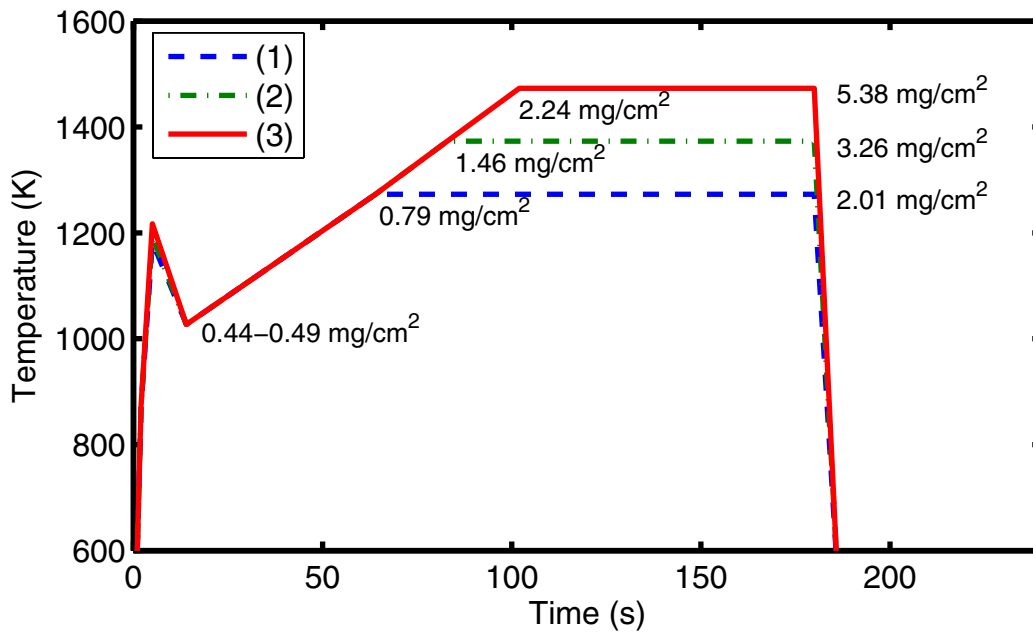


Figure 3.3: Schematic temperature-time histories, applicable to LOCA condition, used in steam oxidation tests on Zircaloy-4 PWR clad conducted by Leistikow et al. (1979). The measured oxygen mass gain values at different stages of transients are also indicated. It is noted that 1 mg/cm² mass gain corresponds to about 6.7 μm ZrO₂.

3.1.2 Effects of hydrogen absorption on oxidation

During oxidation of the clad, hydrogen is continuously generated at the surfaces of the clad, according to relation (3.1). The hydrogen generated at the outer surface of the clad is mostly removed by the steam flow, and thus is not absorbed by the clad appreciably. Whereas, during the clad inner surface oxidation (by penetration of steam into the fuel rod caused by clad rupture), hydrogen absorption can be significant due to the absence of flow, i.e., stagnant steam. Uetsuka et al. (1981) have measured hydrogen contents in the clad up to 1500 wppm at temperature of 1440 K after an exposure time of 240 s caused by clad inner surface oxidation. This level of hydrogen absorption in the clad severely reduces the ductility of Zircaloy (Furuta et al., 1981).

Oxidation of Zircaloy in steam, diluted with hydrogen has been investigated by Moalem & Olander (1991). More specifically, steam containing H₂ at mole fractions of 0.5, 0.73 and 0.91 at 1573 K were exposed to as-received Zircaloy-4 specimens. The oxidation results of the tests employing 0.5 and 0.73 mole fractions hydrogen were almost the same as those tested in pure steam at the same temperature. In contrast, the 0.91 mole fraction, exhibited a relatively long (≈ 100 s) non-parabolic stage followed by a parabolic stage. In the non-parabolic stage, the rate of oxygen mass gain in the 91 mol% H₂ environment is greater than in pure steam, i.e., the presence of hydrogen accelerates oxidation. Moalem & Olander (1991) noted that, the initial rapid absorption of hydrogen, prior to formation of the oxide film, produces a heat source, which heightens the initial temperature excursion, due to oxidation. The high initial temperature accelerates the oxidation rate, thus yielding larger hydrogen uptake than in pure steam.

Moalem & Olander (1991), also examined the effect of hydrogen containing Zircaloy-4 specimens on their oxidation behaviour. In two experiments, specimens were charged to high concentrations of hydrogen, namely, 29 at% (4500 wppm) and 20 at% (2755

wppm) prior to exposure to pure steam (for ≈ 600 s). The temperatures were 1368 and 1488 K, respectively. The tests showed that the oxidation behaviour was parabolic and the rate constants did not differ from that of hydrogen free Zircaloy-4 specimens.

3.1.3 Cadarache tests

A series of LOCA separate effects tests were performed in Cadarache, France starting in 1991 and continued through 2001 to assess LOCA safety margins relative to the acceptance criteria practiced at the time. All the tests entailed double-sided oxidation and thermal shock tests made on empty 17×17 Zircaloy clad samples in a steam environment (Grandjean et al., 1996). The TAGCIS series, completed in 1993, tested unirradiated tube specimens, both in as-fabricated conditions and also pre-corroded specimens simulating the end-of-life state of the clad after reactor irradiation. In another series, the TAGCIR program, completed in June 1993, clad samples irradiated to over 5 reactor cycles in a commercial EDF PWR corresponding to a fuel rod burnup of about 60 MWd/kgU were subjected to the aforementioned tests.

More specifically, the TAGCIS tests were made on different series of unirradiated Zircaloy-4 cladding tube samples with the following characteristics:

- As-received tube with a wall thickness of 0.57 mm (reference sample);
- As-received tubes thinned down to 0.525, 0.370 or 0.270 mm;
- Tube pre-corroded in a pressurized loop containing LiOH;
- Tube samples, 0.525 mm thick with hydrogen contents of 500 or 1000 wppm.

The TAGCIR tests were made on irradiated clad samples that were cut from selected high burn up rods at different axial levels with the following characteristics:

- About 80% of the samples had uniform outer tube oxide layers between 50-70 μm thick;
- About 20% of the samples had oxide layers with thicknesses varying between 60-120 μm .

The tests, simulating LOCA conditions, consisted of oxidation of tubes in steam at isothermal conditions (between 1273 and 1573 K) followed by quenching them in water at ambient temperature. After testing, the samples were sectioned in the vicinity of pyrometric measurement positions and subjected to metallographic examinations using optical microscopy. The oxide layer width, the α -Zr and prior β -Zr layers were determined. Details of the experimental procedure are presented in (Grandjean et al., 1996). The results of the tests were quantified in terms of three parameters: (i) The thickness of remaining β -Zr layer, (ii) the volume fraction of remaining β -Zr and (iii) the equivalent clad reacted (ECR). The ECR vs. temperature for the TAGCIS tests showed that in the considered temperature range, $\text{ECR} \approx 20\%$ can be chosen as the failure limit for all the unirradiated samples that were tested.

For the TAGCIR samples the ECR vs. temperature map showed that failure $\text{ECR} \approx 26\%$ for two-sided oxidation, while for one-sided oxidation failure $\text{ECR} \approx 17\%$, i.e., just the value of the acceptance criterion. No failure was observed below this value in these tests. It should be pointed out that these values correspond to transient oxidation alone, i.e., the contribution from initial oxidation had not been taken into account, which

would have increased these values. These failure ECR values were changed later, i.e. increased to higher values, after reinterpretation of the data in a presentation (Grandjean et al., 1998), however, the justification for this is not fully convincing to us. None of these works (Grandjean et al., 1996, 1998) were published in peer-reviewed journals for rigorous independent scrutiny.

The β -Zr layer thickness versus temperature data indicate that the one-sided and two-sided failure limits are 300 μm and 180 μm , respectively. The one-sided layer thickness failure level was close to the unirradiated specimens tested ($\approx 260 \mu\text{m}$). Neither the difference between one- and two-sided oxidation behaviour nor the relative behaviour between irradiated vs. unirradiated samples was explained, i.e., only speculative explanations were given (Grandjean et al., 1996).

In addition to the TAGCIR program, a specific test series called CODAZIR program were performed in the same facility. These tests involved isothermal oxidation runs without water quenching on short clad ring specimens that were initially stripped off the in-reactor waterside corrosion oxide layer by mechanical attrition (Grandjean et al., 1996). In these tests, the temperature was raised at 50 K/s up to different target values, then kept at each temperature for 470 s before switching off the inductive heating (figure 3.4). The characteristics of samples were as follows:

- As-received samples;
- As-received samples charged to around 500 wppm hydrogen;
- Irradiated samples with removed waterside oxide layer.

Figure 3.4 shows the oxygen mass gain as a function of clad surface temperatures obtained from these tests. It is seen that the hydrogen charged samples exhibited higher oxygen mass gains than the as-received ones (with hydrogen contents usually below 10 wppm), whereas for the irradiated samples, the oxygen mass gains were intermediate. It is argued by Grandjean et al. (1996) that the preparation of the irradiated samples (removal of oxide layer) affected their high temperature oxidation behaviour. In particular, the removal of the oxide layer included a sublayer of (Zr + hydride) at the clad rim that could have affected the subsequent oxidation kinetics of the sample. This implies that without the removal of oxide layers from the irradiated samples, the oxygen mass gain of these samples during the LOCA oxidation test would have been higher than that shown in figure 3.4. The figure also displays the results of calculations made by the correlations of Baker-Just and Cathcart-Pawel (appendix A) and relation (A.2). It is seen that both correlations bound the data.

Since the hydrogen content was identified as the main cause of oxidation enhancement during a LOCA, a separate test program called HYDRAZIR was launched to study this phenomenon (Grandjean et al., 1998). This program consisted of a series of oxidation and quenching tests on unirradiated hydrogen-charged Zircaloy-4 specimens. The hydrogen content varied between 500 to 5000 wppm, thus including the contents of high burnup fuel claddings during in-reactor conditions (<1000 wppm) and also the hydrogen uptake during a LOCA transient condition (>1000 wppm).

Results of the HYDRAZIR isothermal oxidation tests indicate that the specimens with 500 wppm hydrogen experience a larger oxygen gain mass relative to the as-received specimens depending on temperature. At 1323 and 1523 K, the increase in the oxidation

rate relative to the as-received specimens was about 9% and 23%, respectively. However, this enhancement in mass gain disappeared for hydrogen contents larger than 1000 wppm, which is consistent with the aforementioned findings of Moalem & Olander (1991). The measured data, oxide mass gain vs. time, in the reported temperature range of 1323-1523 K were covered by the Baker-Just correlation.

Nevertheless, for high hydrogen content specimens (>2000 wppm) direct water quenching at the end of isothermal oxidation period caused severe embrittlement relative to specimens with lower range of hydrogen contents. This degradation was attributed to the increase in oxygen solubility in the β -Zr due to the presence of high hydrogen concentration, thereby making the material more brittle. This embrittlement effect apparently was cooling rate dependent. In the case of slow cooling to 973 K prior to quenching this severe embrittlement was not observed, i.e., the degree of degradation was similar to “hydrogen free” material according to Grandjean et al. (1998). Unfortunately, the authors do not provide sufficient data and details, nor provide physically-based explanations for their observation, and as such their work, as presented in (Grandjean et al., 1998), can be considered at best as tentative.

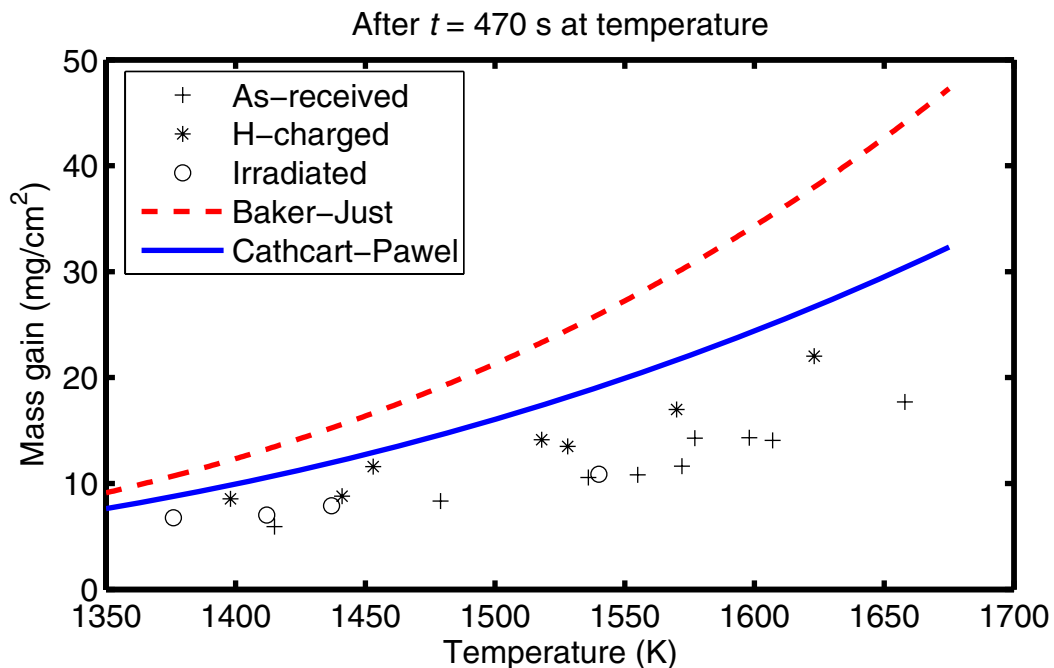


Figure 3.4: Oxygen mass gain of Zircaloy-4 samples tested vs. surface temperature in the CODAZIR program (Grandjean et al., 1998). Oxidation time was 470 s. The symbols denote measured values, while the curves are calculations according to the standard correlations outlined in appendix A.

We should note that Zircaloy-4 clad samples from fuel rods irradiated to 49 MWd/kgU in a Japanese PWR, then subjected to post-irradiation high temperature oxidation tests showed that oxide mass gain for irradiated clad was similar to that for unirradiated clad, and no effect of hydrogen absorption on clad oxidation could be observed (Ozawa et al., 2000).

3.1.4 Zirconium-niobium alloys

LOCA-type oxidation data reported in literature are mostly on Zircaloy materials. In this section, we briefly survey oxidation of other Zr-based alloys, in particular and Zr 1 wt% Nb alloys used increasingly in PWRs. High temperature isothermal tests have been performed on Zr-1Nb (Zr-1Nb-0.06O, by wt%), known also as E110 alloy (table 2.1), and standard Zircaloy-4 (as reference) tube specimens in a flowing steam environment in the temperature range of 973 to 1373 K for durations between 10 and 30 min. (Böhmert et al., 1993). The specimens were taken from typical PWR claddings. Experiments by Böhmert and colleagues showed that the oxidation behaviour of the two alloys was quite similar, which both could be described well by a parabolic growth law with the mass gain according to an Arrhenius relation: $K = 0.4873\sqrt{t} \exp(-10261/T)$, where K is the mass gain per unit area in the units [gcm^{-2}], the exposure time t in [s] and the temperature T in [K], see figure 3.5.

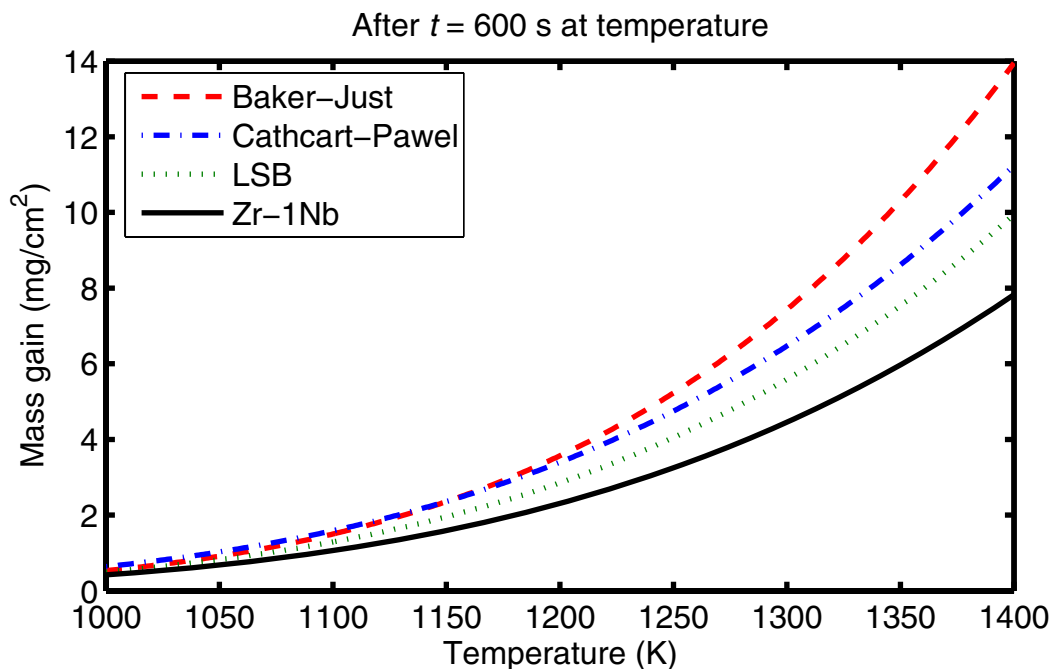


Figure 3.5: Oxygen mass gain vs. temperature for Zr-1Nb according to a correlation obtained by Böhmert et al. (1993) (solid line) and comparison with other standard correlations for Zircaloy, outlined in appendix A.

Böhmert et al. (1993), however, observed that the oxygen stabilized α -Zr layer was wider for Zr-1Nb than for Zircaloy-4 in temperatures above 1273 K. The ratio between the oxide scale and the α -Zr layer amounted to 0.72 ± 0.1 for Zircaloy-4 and 0.48 ± 0.091 for Zr-1Nb. The prior β -Zr structure was similar for both alloys. They both had a basket weave *Widmanstätten structure*; however, in the case of Zr-1Nb alloy, the needle-like grains were usually finer.

The hydrogen uptake during oxidation was much higher in Zr-1Nb than in Zircaloy-4. For example at 1273 K, the hydrogen uptakes were 600 and 80 wppm for Zr-1Nb and Zircaloy-4, respectively, after 10 min. in steam.

Böhmert et al. (1993) observed that in the Zr-1Nb specimens, the oxide scales were very heterogeneous. Usually, a white or relatively transparent outer oxide layer and a dark inner layer were observed. The two layers were separated by cracks and locally the outer layer could extend in a lenticular form into the metal interface. In contrast, Zircaloy-4 had a glossy black firmly adhered oxide, which formed as a single layer and relatively free from cracks.

Ring compression tests were made on Zr-1Nb and Zircaloy-4 specimens, after oxidation experiments, to determine their ductility as a function of the relative equivalent oxide layer thickness, h_{eq} , defined as (Böhmert, 1992)

$$h_{eq} = \frac{A(Zr)}{M(O_2)\rho(Zr)h_0} K . \quad (3.2)$$

Here $A(Zr)$ is the atomic weight of Zr, K the oxygen mass gain per unit area, $M(O_2)$ the molecular weight of O_2 , $\rho(Zr)$ the density of Zr and h_0 the initial wall thickness of the tube. Böhmert (1992) observed that while for Zircaloy-4 the ductility drops gradually as a function of oxide layer thickness and total embrittlement reached at $h_{eq} \approx 18\%$, the ductility for Zr-1Nb alloy is reduced drastically with oxide layer, for which the embrittlement limit was attained at $h_{eq} \approx 5\%$.

The oxidation behaviour of as-received and pre-hydrided clad (unirradiated) samples have been studied by Portier et al. (2005). The materials used in their study were SRA low-Sn Zircaloy-4 (Zr-1.3Sn-0.21Fe-0.1Cr-0.12O by wt%) and M5 (Zr-1Nb-0.026Fe-0.13O by wt%). The hydrogenated samples were obtained by gaseous charging, such that the Zircaloy-4 specimens had hydrogen contents in the range of 150-600 wppm, while the M5 hydrogen content level varied from 50 to 300 wppm. The authors selected these ranges based on end-of-life expectations of hydrogen pickup for these alloys in PWRs. The cladding tube wall thickness for high temperature tests was 0.572 mm for Zircaloy-4, while for M5 was either 0.572 mm or 0.609 mm.

The oxidation test temperatures were made at 1273, 1373, and 1473 K and the test durations covered 1800 s, which is typical for LOCA condition. The oxidation kinetics for the Zircaloy-4 and M5 samples were similar. They both obeyed a parabolic time evolution behaviour bounded by the Cathcart-Pawel correlation (appendix A). In the tests no “breakaway” of oxidation reaction was detected in the studied temperature/time range. Moreover, no effect of hydrogen on the oxidation kinetics was noticed at 1573 K, for H concentrations of up to 600 wppm for Zircaloy-4 and 300 wppm for M5 alloy.

After the oxidation tests, some samples (Zircaloy-4, M5) were quenched in water and subsequently subjected to metallurgical examination. Both as received samples and hydrogenated specimens were tested. Portier et al. focused their analysis on the ductility/toughness of the material with prior β phase layer, which is believed to govern the ductile failure mode of the zirconium alloys. It is supposed that the important parameter governing the residual ductility of the tubes is the oxygen content of the prior β -Zr. Portier and company also performed complementary microhardness and oxygen content measurements of the prior β -Zr layer for various oxidizing temperatures and times. The results of the microhardness measurements of the prior β phase layer for Zircaloy-4 and M5 are shown in figure 3.6. It is seen that the correlation between hardness and oxygen content is compelling and Zircaloy-4 is slightly more brittle than

M5, while hydrogenated samples (≈ 320 wppm) are more brittle than the as-received samples.

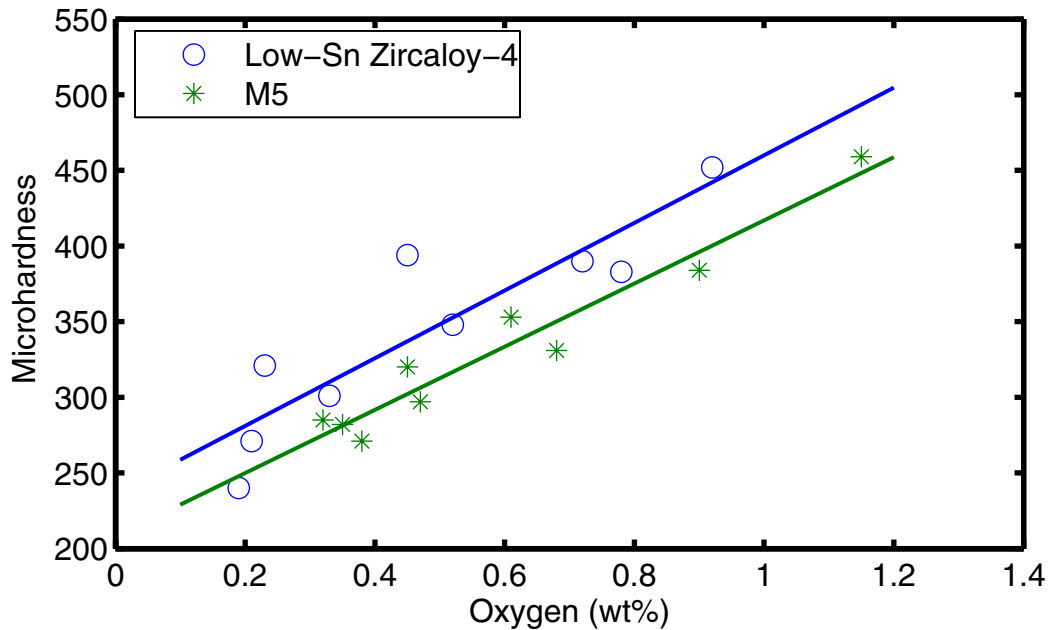


Figure 3.6: Microhardness (Vickers, 100 g) vs. oxygen content of prior β phase layer of clad samples. The lines are linear fits to the respective data (Portier et al., 2005). The two data points above the upper line represent pre-hydrogenated samples (≈ 320 wppm) and oxidized at 1473 K, cf. figure 3.7.

We have plotted the mass gain of the samples due to oxidation as a function of time in figures 3.7a-b for Zircaloy-4 and M5 clads, respectively. Along the data points, we have also shown the predictions of the Cathcart-Pawel correlation (appendix A). It is seen that the correlation captures the data quite well at the three examined temperatures. The high temperature oxygen uptake of Zircaloy-4 and M5 are quite similar. In these tests, one sample for each alloy was pre-hydrogenated to about 320 wppm with no impact on the oxidation kinetics results.

Very little data have been reported regarding the oxidation and post-quench ductility behaviour of ZIRLO clad and performance comparison with the standard or low-Sn Zircaloy-4 clads in open literature. Billone et al. (2004a, 2004b) have briefly reported steam oxidation tests performed on samples that comprised as-received low-Sn Zircaloy-4, ZIRLO, and M5 tubes (table 2.1). The tube wall thickness for the samples was 0.57, 0.57, 0.61 mm, respectively. The oxygen mass gains of the samples were measured at temperature/time (K/s): 1273/3400, 1373/1100, 1473/400. The tests at 1273K/3400s indicated that the oxygen mass gain of M5 and ZIRLO were about 36% and 20% less than that of Zircaloy-4. Moreover, for shorter test durations, the M5 mass gain was consistently lower than for Zircaloy-4, while the mass gains of ZIRLO and Zircaloy-4 were about the same. The details of the investigations are documented in a number of unpublished reports available from the NRC on site data base ADAMS (Yan et al., 2004a) and the references therein. Figures 3.8a-b present the results of measured ECR for the three clad types at 1273 and 1373 K as a function of the *equivalent oxidation time*, calculated from two-sided oxidation using the Cathcart-Pawel relation (appendix A). For the measured oxygen mass gain values, see the last cited references.

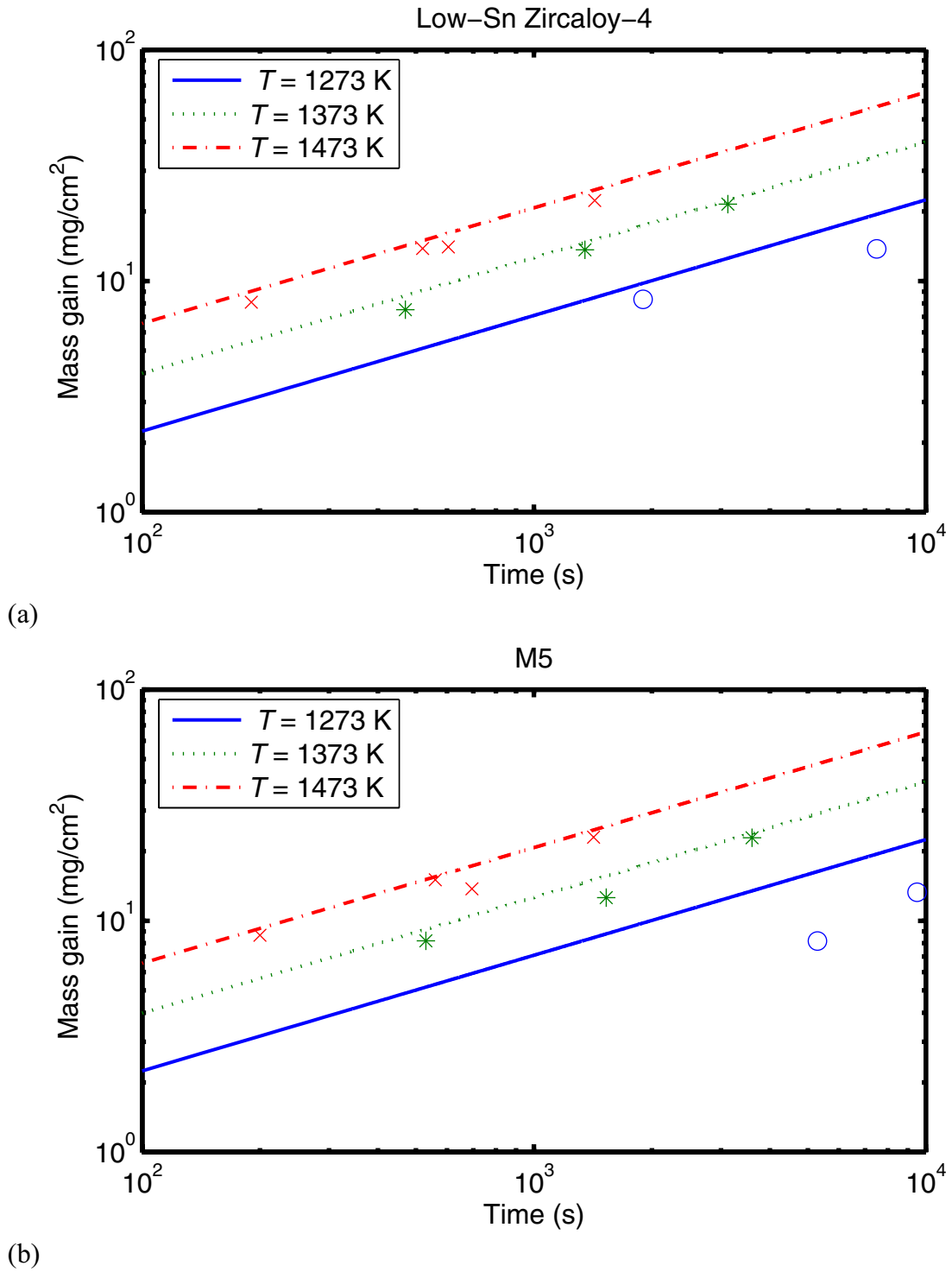
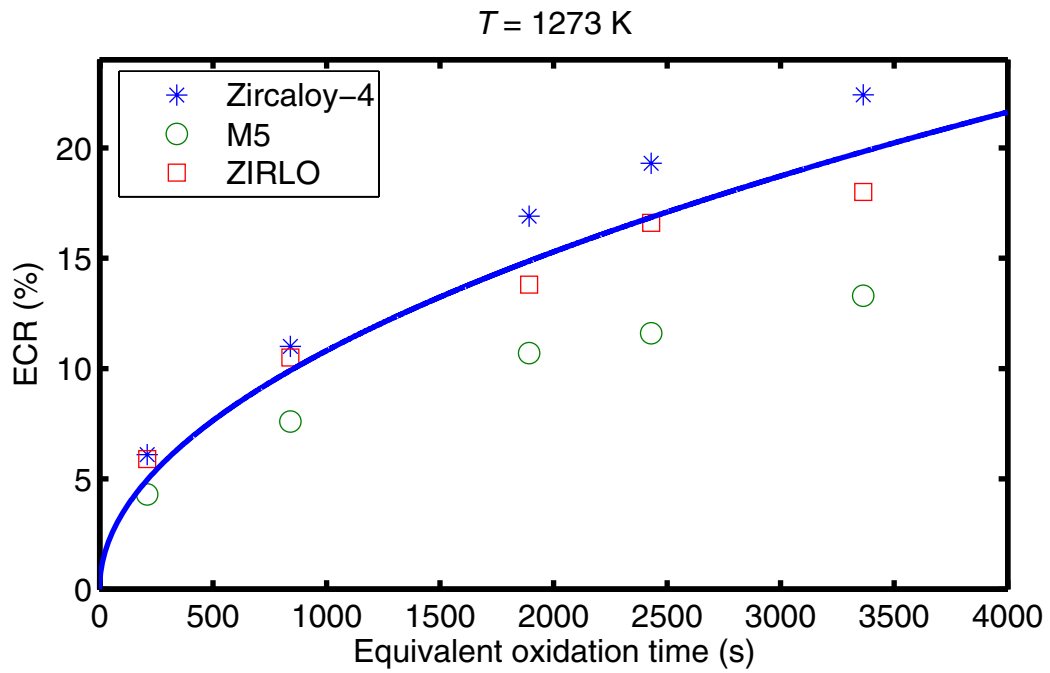
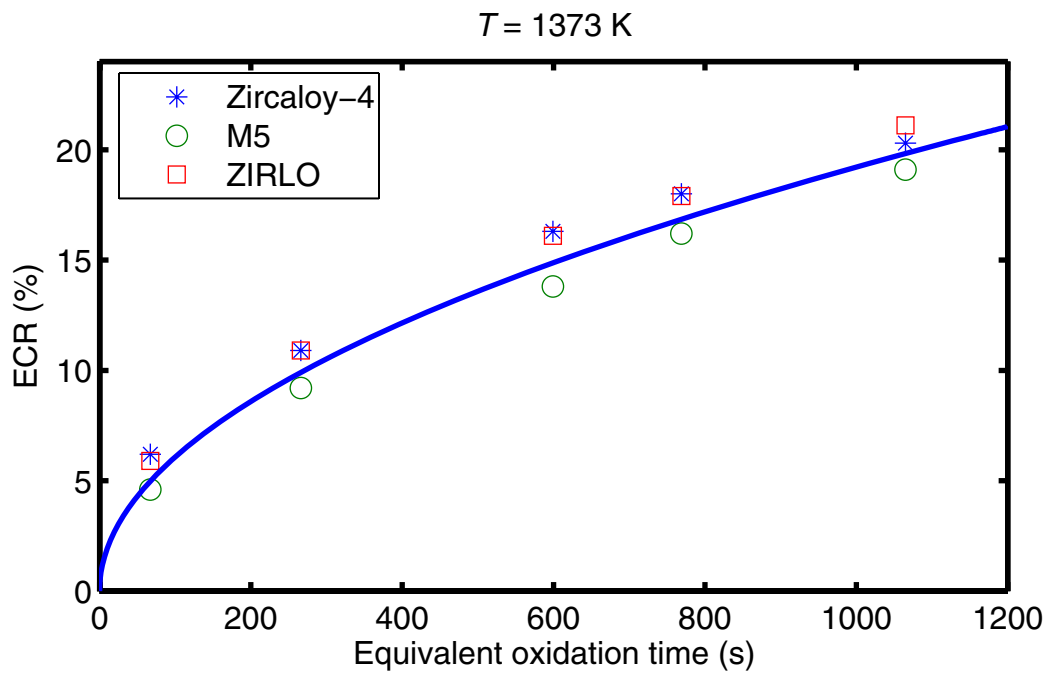


Figure 3.7: Mass gain due to oxidation of tube samples for (a) low-Sn Zircaloy-4, (b) M5 (Portier et al., 2005). The data (symbols) are from the prior β phase layer measurements. The lines are the predictions of the Cathcart-Pawel correlation (appendix A). The pre-hydrated samples (320 wppm), oxidized at 1473 K had a mass gain of 14 mg/cm² after 605 s and 695 s for Zircaloy-4 and M5, respectively.



(a)



(b)

Figure 3.8: The symbols denote measured two-sided ECR values vs. the equivalent oxidation time (Yan et al., 2004a) for three different clad materials. The curves are the predictions of the Cathcart-Pawel correlation (appendix A) for the clad wall thickness of 0.57mm. (a) $T=1273 \text{ K}$, (b) $T=1373 \text{ K}$.

3.1.5 Effect of pressure on oxidation

The majority of the steam oxidation tests reported in literature are carried out at atmospheric pressure (0.1 MPa). Since the clad under LOCA conditions is also subject to pressure, a number of workers have studied the influence of pressure on high temperature oxidation.

Bramwell et al. (1994) investigated the oxidation of Zircaloy-4 at elevated pressures in the temperature range of 1023 to 1273 K exposed to flowing steam at pressures up to 18.6 MPa for durations up to 2500 s. They observed that the oxidation is enhanced due to high pressure steam. In particular, they found that the pressure-induced enhancement saturated around 15.2 MPa at 1073 K. At 1273 K, the pressure effect was less pronounced than at 1173 K, with maximum enhancement factors of about two.

In a more recent paper, Park et al. (2000) studied the effects of steam pressure on Zircaloy-4 clad oxidation. The experimental temperature range was from 973 to 1173 K and the pressures in the range of 0.1 to 15 MPa. The specimens tested were Zircaloy-4 clads used in the Kori power plant (PWR) in South Korea (No details regarding clad diameter, wall thickness, alloy chemical composition are provided). Experiments showed that the partial pressures of steam were important in controlling the oxide growth process. The higher the applied pressure, the thicker became the oxide layer.

Park et al. (2000), by fitting of their measured data, have developed a simple correlation between the oxide layer thickness and the exposure time, pressure and temperature. The correlation is very nonlinear and hence applicable only in the range of experimental data. We have illustrated the results of the correlation, oxide layer thickness vs. pressure at different temperatures after 1500 s of exposure time in a log-log plot (figure 3.9). Similarly, figure 3.10 illustrates the dependence of oxide layer, as a function of inverse temperature, on applied pressure. In this figure, we have also plotted the predictions of the Baker-Just relation (appendix A) as a function of temperature after 1500 s of oxidation reaction. It is seen that the BJ relation underestimates the oxide layer thickness growth for pressures of 5 MPa and higher. We should note that, in the application of the BJ relation we have used $K = \delta_{\tau} \sqrt{t/2}$ instead of $K = \delta_{\tau} \sqrt{t}$ (see appendix A for notation) in order to be compatible with Park et al.'s evaluation.

Park et al. (2000) suggest that this pressure-induced accelerated oxidation in high-temperature steam emanates from the formation of microcracks produced during the transformation of tetragonal phase of ZrO_2 to monoclinic phase.

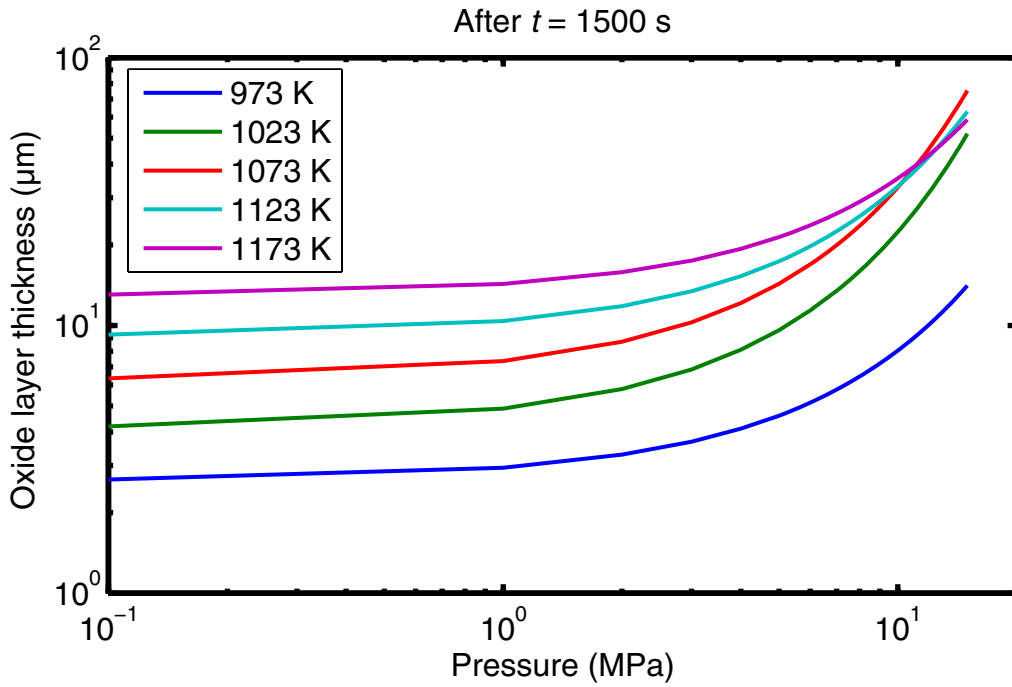


Figure 3.9: Oxide layer thickness after 1200 s oxidation in steam as a function of steam pressure ($P = 0.1-15$ MPa) according to the empirical correlation of Park et al. (2000).

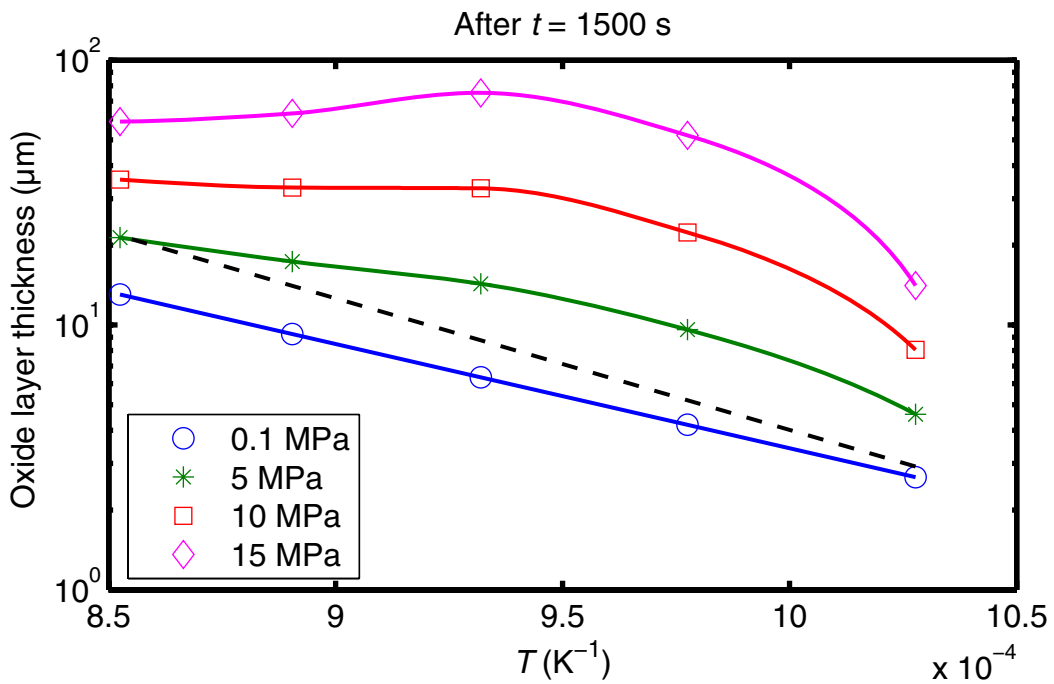


Figure 3.10: Oxide layer thickness after 1200 s oxidation in steam as a function of temperature ($T = 973-1173$ K) at different pressures according to the empirical correlation of Park et al. (2000). The broken line is the Baker-Just correlation, where we have used (appendix A) $K = \delta_{\tau} \sqrt{t/2}$ in table A.2 to be compatible with Park et al.

3.2 Clad deformation and rupture

In the event of LOCA, the depressurization of the primary circuit may cause the fuel cladding to inflate as a result of the rod internal pressure. If clad ballooning were to continue without rupturing, the flow of emergency core cooling (ECC) water would be restricted because of mechanical contact between adjacent fuel rods, causing blocking of sub-channels.

The deformation of zirconium alloy clad has been studied extensively, albeit mainly unirradiated as-received clad materials. The deformation and rupture behaviour of clad during a LOCA has been reviewed in the past (Parsons et al., 1986; Shewfelt, 1988). Our description will be more focused on the recent advances regarding long exposure reactor effects and new alloys used in PWRs.

The basic parameters controlling clad deformation are stress, temperature and creep strength; the latter being affected by oxidation, grain size, chemical composition, the anisotropy and the structural phase of the material. The presence of oxide layer imposes an additional stress on the tube, which can cause diameter increase of up to 1% at 1113 K in 500 s (Donaldson & Evans, 1981). In addition, the oxidation also affects the ductility and lowers the total hoop rupture strain (Parsons et al., 1986).

When the temperature is uniformly distributed in the clad under stress, deformation can become unstable, meaning that, if the diameter of the tube increases at any axial position, the stress is increased due to the larger diameter and reduced wall thickness, provided that the rod internal pressure does not reduce significantly. This positive feedback enhances the creep rate leading to a runaway deformation before clad rupture (figure 3.11). But under LOCA conditions, fuel pellets assume an asymmetric position within the fuel rod (figure 3.12). As has been discussed by Erbacher & Leistikow (1987), small hoop temperature gradients on the clad cause a relatively homogeneous decrease of the wall thickness around the circumference and thereby lead to relatively large strains. On the other hand, large hoop temperature variations occurring during the course of deformation, lead to a localized reduction in wall thickness on the hot part of the tube circumference and so give rise to relatively low burst strains. Erbacher & Leistikow assert that the magnitude of hoop temperature gradients around the tube's circumference is one of the most decisive parameters affecting clad strain, thereby flow blockage and coolability in a LOCA. There are a number of investigations that provide a reasonable explanation for this effect, among these are (Ferner & Rosinger 1983; Jones et al., 1984; Ferner & Rosinger, 1985; Shewfelt & Godin, 1986; Parsons et al., 1986; Shewfelt, 1988) and references therein.

3.2.1 Creep deformation

Detailed knowledge of the dependence of creep rates on stress and temperature is fundamental for analysis of clad deformation during LOCA. For example, for PWR Zircaloy-4 clad in the cold-worked and stress-relieved condition, the material structure recrystallizes above 1000 K in the order of a few seconds. Therefore, following a LOCA, the irradiation-induced defects would be removed as the recrystallizing front is swept through the lattice. The migrating boundaries would also prevent the build-up stresses during deformation, suppressing crack formation (Parsons et al., 1986). This

effect combined with the observation that textures opposes wall thinning could cause necking, resulting in large clad hoop strains during deformation in the temperature range of about 1000 to 1100 K. Above about 1100 K, the β -Zr phase transformation begins. The presence of β -Zr in the α -Zr matrix reduces the strength of the component appreciably, whilst the amount of β phase is time/temperature dependent. The ductility remains high, but large strains do not occur unless strain rates are low (or else rupture would occur).

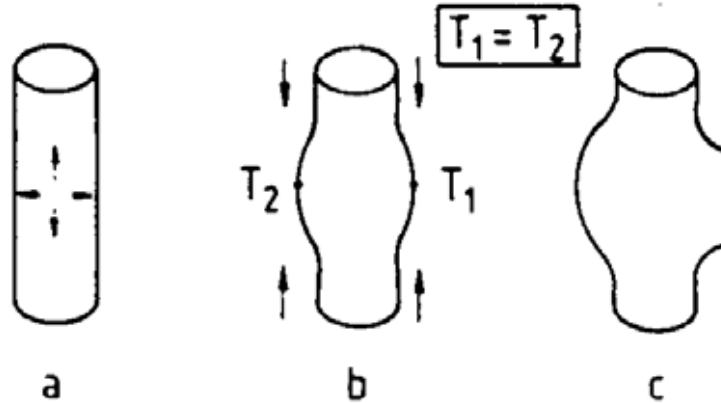


Figure 3.11: Schematic picture of symmetric deformation with large burst hoop strain. (a) Tube under biaxial stress due to internal gas pressure. (b) Ballooning and tube shortening. (c) Tube burst, after Erbacher & Leistikow (1987).

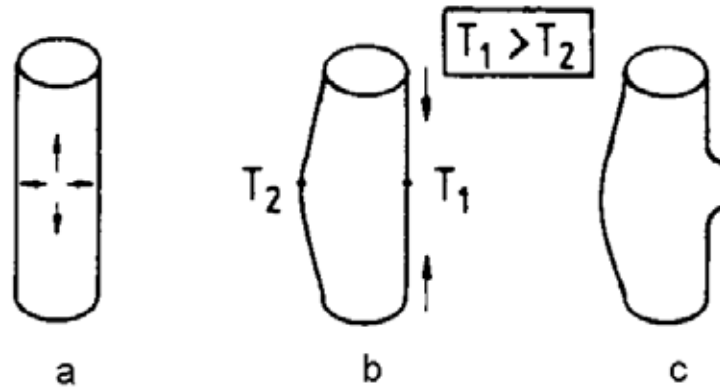


Figure 3.12: Schematic picture of asymmetric deformation with small burst hoop strain. (a) Tube under biaxial stress due to internal gas pressure. (b) One sided ballooning and tube bending. (c) Tube burst, after Erbacher & Leistikow (1987).

The phenomenological equation describing creep strain rate can be expressed as

$$\frac{d\varepsilon}{dt} = \dot{\varepsilon}_s = A\sigma^n \exp(-Q/kT), \quad (3.3)$$

where A , n , Q are material-structure dependent parameters determined by measurements and k is the Boltzmann constant. The high temperature creep rates of zirconium, Zircaloy-2 and Zircaloy-4 have been studied by many workers experimentally in the past, through which the parameters A, n, Q were determined.

Rosinger et al. (1978, 1979) provide a summary of these data and hence we shall not repeat those details here. Rosinger et al. (1978, 1979) reported also own investigations on creep behaviour of Zircaloy-4 clad in the temperature range of 940 to 1873 K. Uniaxial creep testing was carried out in an inert atmosphere to obtain a base-line of Zircaloy-4 deformation data, which are unaltered by strengthening mechanisms such as those due to oxygen. The strain rates between 10^{-6} to 10^{-2} s^{-1} were obtained. For both α -Zr and β -Zr phases, the activation energies for creep rates (Q) were in agreement with those for the self-diffusion of Zr. Hence, in the considered temperature range, creep is controlled by a mechanism in which diffusion plays a central role, possibly by dislocation climbing or dislocation gliding or both (Rosinger et al., 1979). For the ($\alpha+\beta$) phase region, when the creep rates were below 0.003 s^{-1} , Rosinger et al. obtained a separate creep rate correlation. The low creep rate region was identified as being due to grain boundary sliding.

Rosinger et al. (1979) evaluated their measurements and also all the other published data on Zircaloy then available. Empirical correlations of the form (3.3) for the α -Zr, ($\alpha+\beta$)-Zr, and β -Zr were obtained (table 3.1). Because Rosinger et al.'s correlations describe similar behaviour observed in tests done by using different test rigs, they are not biased by being associated with only a particular experimental procedure and are consequently believed to be applicable for use in safety analysis, for any type of Zircaloy-4 clad. Rosinger et al.'s correlations were also in good agreement with Zircaloy-2 data. Figures 3.13 and 3.14 show the plots of creep rate versus stress at various temperatures (973-1473 K) using Rosinger et al.'s correlations.

The creep of Zircaloy-4 was also studied within the EDGAR experiments, which were separate effect tests on clad mechanical behaviour in the stress-temperature domain of large break LOCA conditions (Réocreux & Scott de Martinville, 1990). In addition, the experiments intended to supply data for construction of models for clad deformation and burst for French nuclear reactor safety programs. Moreover, the tests were to study the influence of irradiation on the mechanical behaviour of clad under LOCA conditions. In the cited paper, very little background information is provided to confirm the authors' claims. For example, in their plot of creep rate versus temperature, Réocreux et al. do not supply the values for the stress levels which are necessary for interpreting and validating the data. Their presented creep data apparently fit the correlation (3.3), however, some of the values for the parameters are not given (table 3.1). These data are simply missing from this peer-reviewed paper!

Correlation	A	n	Q kJ/mol	Source
α	2000	5.32	284.6	Rosinger et al., 1979
($\alpha+\beta$)	0.0068	1.8	56.6	
β	8.1	3.79	142.3	
α	NG	5.65	246	Réocreux et al., 1990
($\alpha+\beta$)	NG	2.97	20	
β	NG	NG	NG	

Table 3.1: Creep rate parameters for Zircaloy-4 according to relation: $\dot{\epsilon} = A\sigma^n \exp(-Q/RT)$ in s^{-1} , σ is the stress in MPa and RT has its usual meaning. NG≡not given.

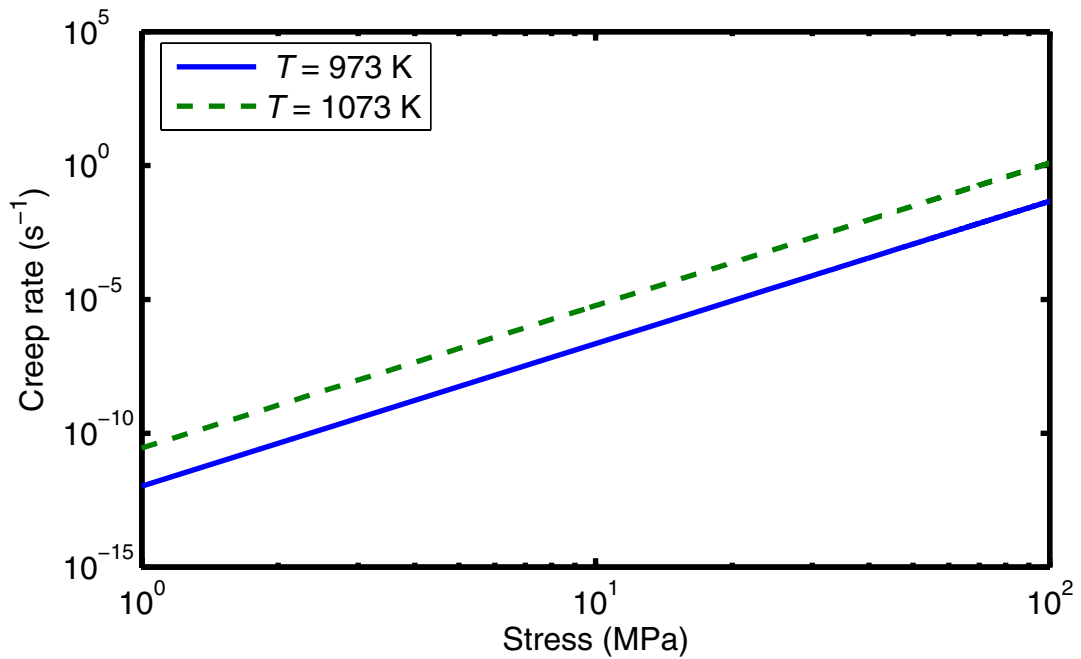


Figure 3.13: Strain rate of steady-state creep deformation for Zircaloy clad under stress in a log-log plot calculated using the empirical correlations (best estimate fit to measured data) of Rosinger et al. (1979). The lines are for α -Zr.

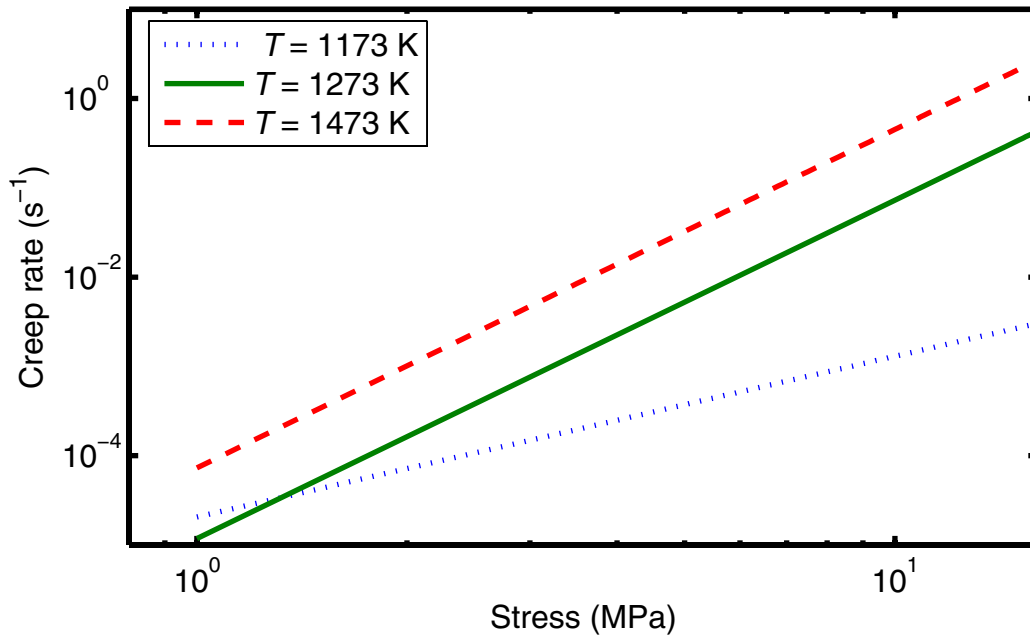


Figure 3.14: Strain rate of steady-state creep deformation for Zircaloy clad under stress in a log-log plot calculated using the empirical correlations (best estimate fit to measured data) of Rosinger et al. (1979). The solid and dashed lines are for β -Zr, while the blue dotted line is for ($\alpha+\beta$)-Zr.

The clad rupture was also determined in the early EDGAR tests, however since Réocreux et al. do not present enough background information on their data and model (burst stress vs. temperature) it is very difficult to evaluate or judge their results (see next section for discussion on this topic).

The influence of long reactor service exposure on transient creep properties of low thin Zircaloy-4 (1.3 wt% Sn) and M5 alloys under LOCA conditions has been investigated by Portier et al. (2005). PWR clad samples, 9 cm long, both in as-received condition and irradiated up to 6 annual reactor cycles (rod burnup of 66 MWd/kgU), were subjected by Portier and colleagues to thermal ramps under uniaxial loading. The thermal ramp rates used were 35 and 100 K/s with stress loadings of 40 and 50 MPa. The unirradiated samples comprised hydrogen charged materials to 150 and 450 wppm for Zircaloy-4 tubes (wall thickness of 0.57 mm), and 100 and 200 wppm hydrogen for M5 tubes (wall thickness of 0.61 mm). These values were considered to be representative of end-of-service hydrogen pick-up values in the respective clad types. The temperatures at which axial creep strains were measured varied from about 800 to 1150 K, i.e., in the α to $(\alpha+\beta)$ phase region of the Zr matrix. The tests showed that for Zircaloy-4, hydrogen reduces the creep resistance appreciably and the effect is being greater for the higher hydrogen content. For example, for Zircaloy-4 under uniaxial loading of 80 MPa and heating rate of 100 K/s to about 1000 K, the axial strains recorded were 5, 15, 25% for the as-received, hydrogenated 150 and 450 wppm samples, respectively.

For M5 samples, the creep rate increased with the increase in hydrogen content, but the effect for hydrogen contents of 100 and 200 wppm was small relative to those of Zircaloy-4's. For example, for M5 under uniaxial loading of 80 MPa and heating rate of 100 K/s to about 1000 K, the axial strains recorded were around 2.5, 6, 8% for the as-received, hydrogenated 100 and 200 wppm samples, respectively.

The effect of irradiation was insignificant for the creep deformation of Zircaloy-4, however, the creep rate was observed to be lower at the very beginning of heating ramp, and then faster near the end just before the rupture. The results for M5 were quite different according to Portier et al. (2005). For example, for a stress level of 80 MPa and heating rate of 100 K/s, the creep rates of all the irradiated samples were appreciably lower than those of the unirradiated samples up to a temperature of around 1020 K. That is, the creep rate remained nearly the same up to 1020 K for samples irradiated to 34 (48), 44 (37) and 66 (63) MWd/kgU (wppm H). For temperatures greater than 1020 K, the creep rate of the irradiated samples accelerated just before the rupture. The temperature-to-rupture was the same as for the as-received samples for 80 MPa and 100 K/s and even slightly higher at 80 MPa, 25 K/s. On the other hand, for all the tests done at 40 MPa, the irradiated samples behaved similar to the as-received materials for the heating rate of 25 K/s.

In conclusion, Portier and company's investigation shows that hydrogen decreases the creep strength of Zircaloy-4 clad under uniaxial loading and that the effect is enhanced with the increase in hydrogen content. The effect of hydrogen on creep rate of M5 clad, however, remained within the scatter of experimental data, at least up to a hydrogen content of 100 wppm. The impact of irradiation and hydrogen on ductility and rupture is discussed in the next section.

3.2.2 Creep Rupture

Creep rupture mechanism of zirconium alloy clad tube under LOCA is believed to be due to the progressive loss of cross-sectional area by material flow, rather than caused by nucleation, growth and coalescence of cavities on grain boundaries (Burton, 1983). That is, when a tube is subjected to a constant load, it gets longer and thinner. The stress in the tube increases as the cross-sectional area decreases and the creep accelerates, leading finally to rupture. Burton (1983) found a simple relationship between the creep rate and time-to-rupture, viz.

$$\dot{\epsilon}_0 = \frac{1}{nt_f}, \quad (3.4)$$

where $\dot{\epsilon}_0$ is the initial creep rate, n is the stress exponent of the creep rate and t_f is the failure time. This failure criterion is for the case of uniaxial creep under constant load. For the case of a tube creeping under constant pressure (biaxial loading), the criterion becomes $2nt_f\dot{\epsilon}_0 = 1$.

To get a feeling for the order of magnitude, we have re-plotted the data presented in Burton's figure 5 for Zircaloy-2 specimens in our figure 3.15. It is not clear that if these data are from tubular specimens under biaxial loading or otherwise. Relation (3.4) fits the data very well with $n = 4$ and $n = 10$ for α -Zr and β -Zr, respectively. If equation (3.4) is an appropriate relationship for describing the data, the selected stress exponents seem to be too large (typically they are between 3 and 5 for diffusion controlled creep).

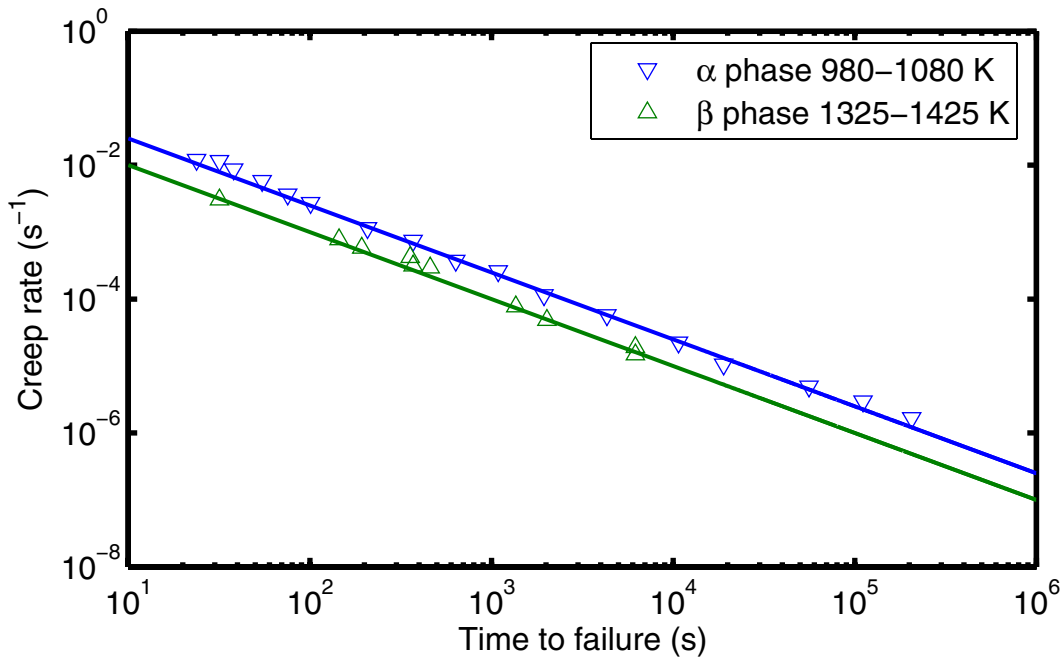


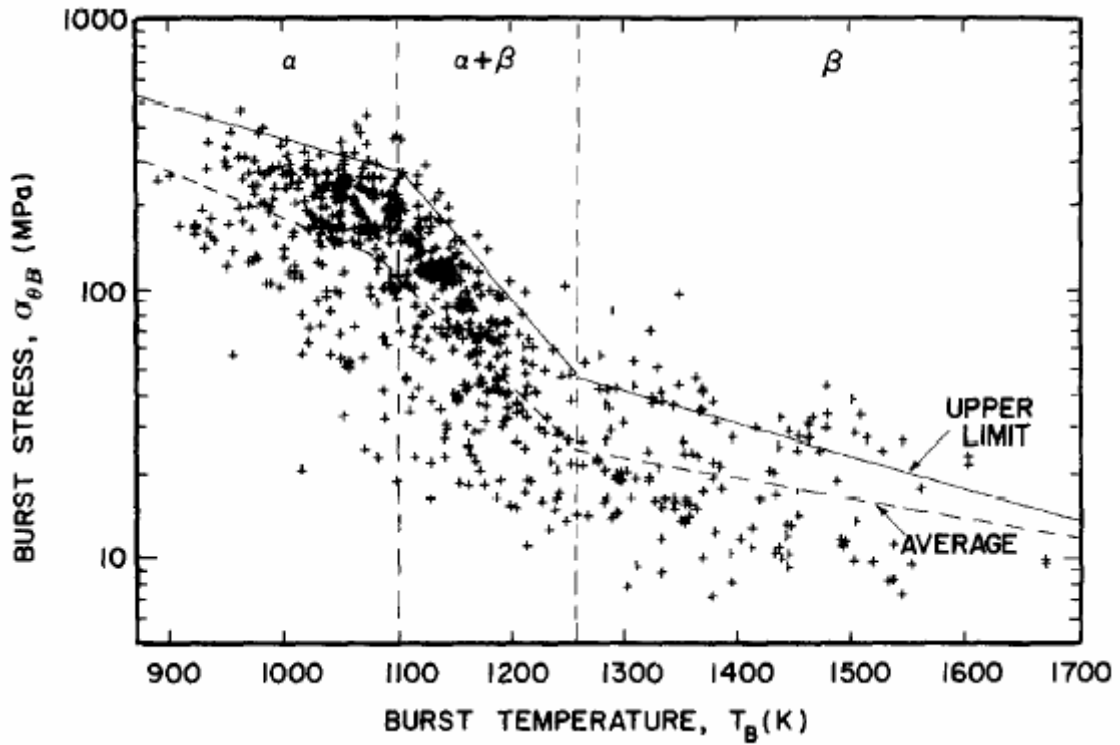
Figure 3.15: Creep rate versus time to failure for Zircaloy-2 material (Burton, 1983), where the lines are fits according to relation (3.4) with $n = 4$ and $n = 10$ for α -Zr and β -Zr, respectively.

There is a large published database on Zircaloy clad materials that were obtained from temperature ramps and differential pressures until failures occurred. The data generated prior 1983 have been reviewed by Rosinger and co-workers (Neitzel & Rosinger, 1980, Varty & Rosinger, 1982; Ferner & Rosinger, 1983), Erbacher & colleagues (Erbacher, 1981; Erbacher & Leistikow, 1987) and Parsons et al. (1986). Rosinger (1984) has assessed the clad burst data, and has provided a model for prediction of clad failure during a LOCA. The data consisted of about 700 points and comprised a wide range of test conditions: constant pressure or closed-tube tests in an inert gas or a vacuum and constant pressure or closed-tube tests in steam or oxygen atmosphere. Some of the burst data were generated for irradiated fuel clads. These data for burst stress and burst strain versus burst temperature are shown in figures 3.16a-b, respectively. Varty and Rosinger (1982) provide the sources for these experimental data. From figure 3.16, we see that despite a large scatter in data, a general trend emerges, i.e., a Z-form behaviour for the burst stress vs. temperature and a double-hump shape for burst strain vs. temperature. The burst stress displays a substantial decrease with temperature as phase transition occurs, while the burst strain shows maxima in the α and β phases and exhibits a minimum in the ($\alpha+\beta$) domain.

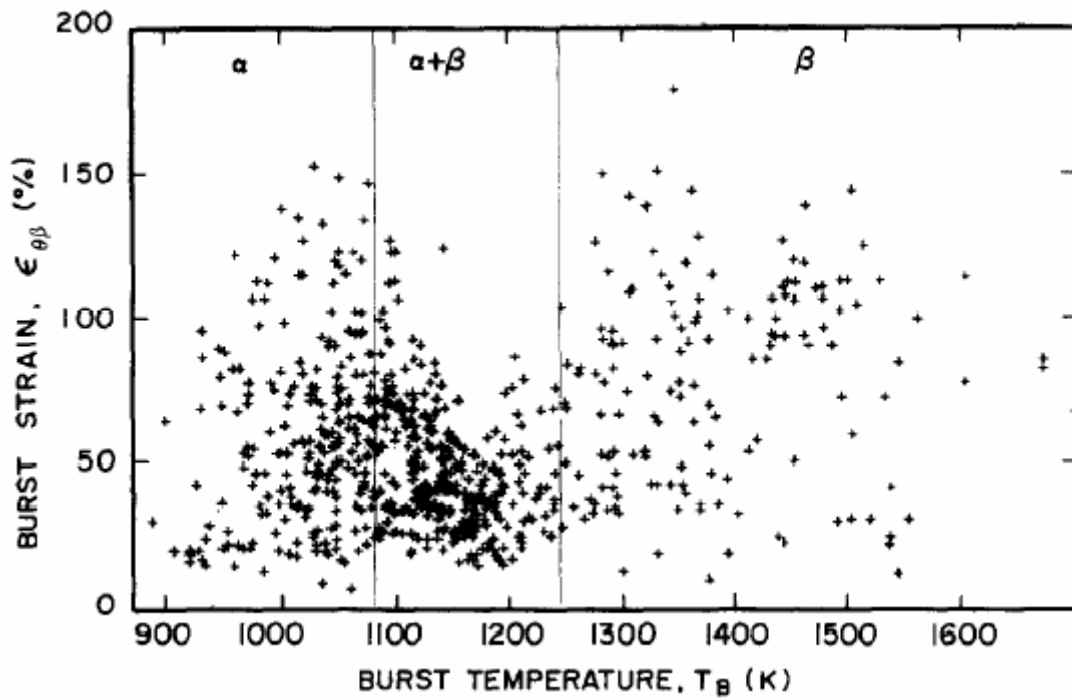
Notable among these experiments were the single-rod transient tests in steam that were performed within the REBEKA program in Karlsruhe, Germany (Erbacher et al., 1982). In this program, the investigators used fuel rod simulators with indirect electric heating of 325 mm heating length, which provided well-defined boundary conditions. The internal overpressure and heating rates were kept constant during the deformation. The measurements provided fairly accurate data for modelling burst and developing a burst criterion. A further outcome of these tests was the quantification of the effect of oxidation on burst stress (Ferner & Rosinger, 1983). A burst criterion, i.e., burst stress vs. burst temperature as a function of oxygen mass gain during LOCA was developed. This empirical correlation is depicted in figures 3.17 and 3.18. Figure 3.17 shows the upper-limit curve, while figure 3.18 shows the reduction of burst stress as a function of oxygen mass gain. The burst temperature and burst strain depend on heating rate. Increasing the heating rate for the same initial stress, say from 1 to 100 K/s, increases the burst temperature from about 910 K to 1050 K for 150 MPa initial stress (Rosinger, 1984). Also, the burst strain is inversely proportional to heating rate. For example, at 1100 K, the burst strain is reduced from 150% to 70%, when the heating rate is increased from 1 to 100 K/s (Rosinger, 1984).

Anisotropy or texture of zirconium has also an affect on creep and thereby on burst temperature and strain. Increasing the degree of anisotropy from isotropic case increases the burst temperature. For example, at an initial stress of 100 MPa, the calculated burst temperature can vary within a 60 K band, depending on the assumed anisotropy. Moreover, the burst strain is inversely proportional to the degree of anisotropy. For example at 1100 K, the burst strain is reduced from 121% for the isotropic case to 77% for the most severe anisotropy (Rosinger, 1984).

More recent data on deformation vs. burst time and initial pressure, under isothermal conditions; and rupture temperature vs. total deformation under ramps in the temperature range of 953-1473 K were generated for Zircaloy-4 clad by Kim et al. (2004), which can readily be used to check the validity of model calculations.



(a)



(b)

Figure 3.16: Experimental data on Zircaloy clad burst stress (a) and burst strain (b) versus burst temperature under LOCA conditions, from (Varty & Rosinger, 1982).

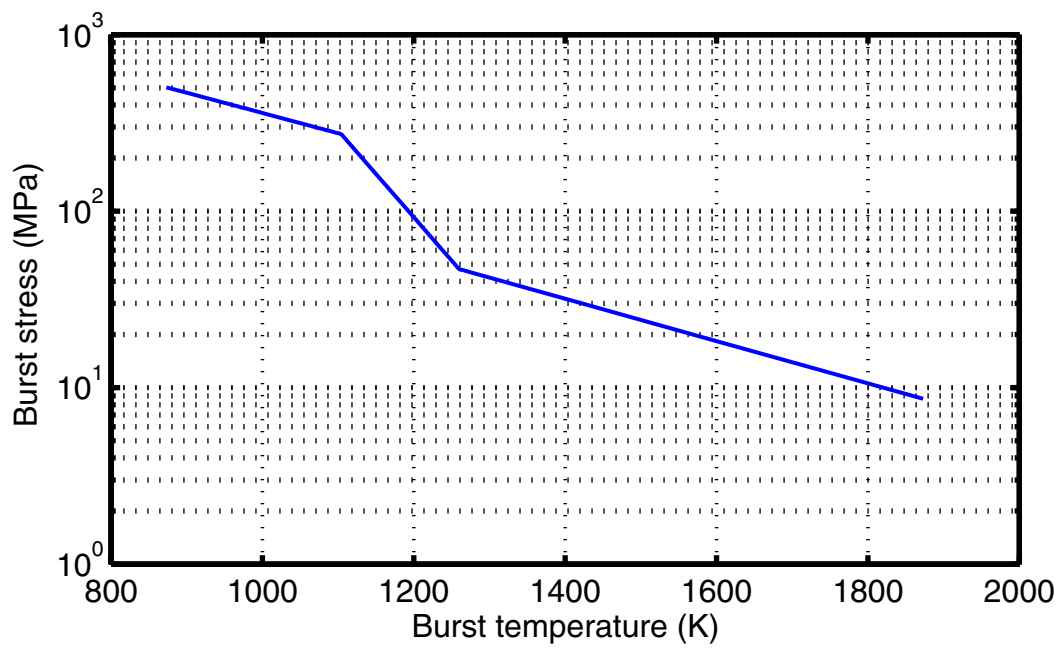


Figure 3.17: The upper-limit curve for burst-stress vs. burst temperature for Zircaloy clad calculated by the empirical correlation of Varty & Rosinger (1982), cf. figure 3.16.

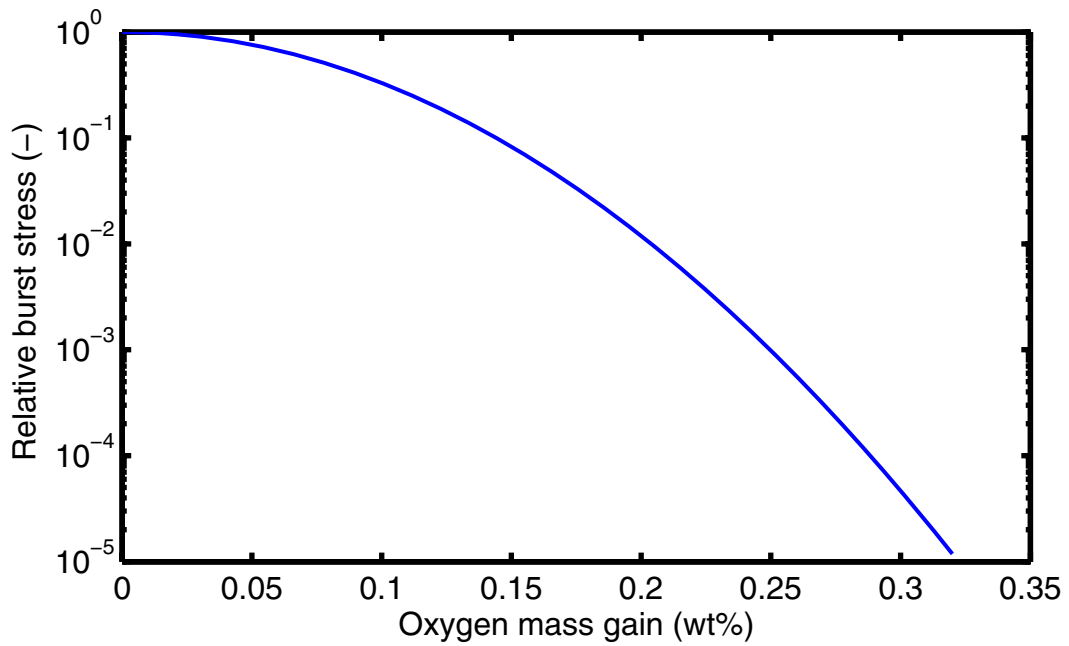


Figure 3.18: Reduction in burst-stress vs. oxygen content (mass gain) of Zircaloy clad calculated by the empirical correlation of Varty & Rosinger (1982).

The creep burst behaviour of M5 alloy and Zircaloy-4 (standard and 1.3 wt%Sn) claddings were examined and compared within the French EDGAR program (Forgeron et al., 2000) under both isothermal and temperature transient conditions. In these tests, the time to rupture versus test temperature and burst temperature; and burst stress versus burst temperature (burst criterion) were determined for unirradiated as-received specimens. The tests covered temperatures between 873 and 1273 K. The time to rupture of M5 alloy was slightly longer than the Zircaloy-4's for the same initial pressure at 1173 K (figure 3.19). Similarly, the total elongation (ductility) versus burst temperature data indicated clearly a rapid decrease in the two-phase ($\alpha+\beta$) temperature domain. The maximum elongations for Zircaloy-4 and M5 were around 175% and 170%, which occurred at temperatures 1123 K and 1098 K, respectively. The decrease of ductility in the M5 alloy began earlier due to its lower phase transition temperature relative to that of Zircaloy-4.

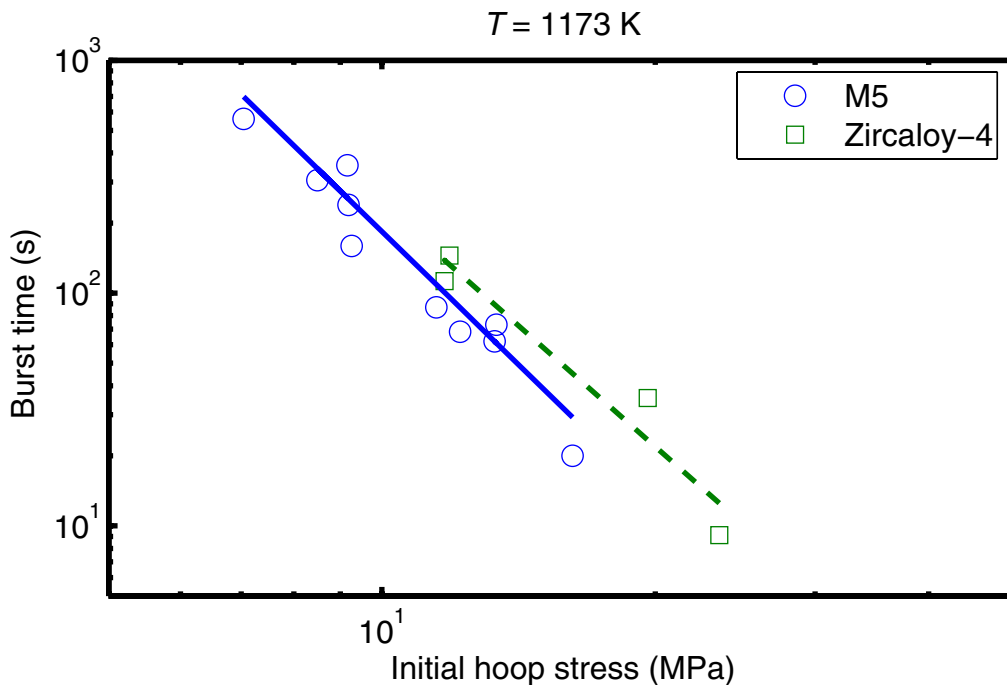


Figure 3.19: Time to rupture versus stress from EDGAR creep tests on PWR clad materials (Forgeron et al., 2000).

Thermal ramp tests were conducted within the EDGAR program to obtain ductility limit curves and also to study and model the mechanical behaviour of clad under transient conditions. These tests were performed under constant heating rates between 653 K and the burst temperature. The heating rates ranged from 2 to 100 K/s. Burst stress versus burst temperature data, obtained from creep tests and thermal ramp tests, were used to develop burst criteria. Figure 3.20 shows the burst criterion for M5 clad and comparison with the associating one for Zircaloy-4 clad as provided by a later publication from the same laboratory (Brachet et al., 2002). These curves are considered to be best-estimate curves, rather than bounding ones as those depicted in figures 3.16 and 3.17. The burst stress of M5 came a bit earlier due to a lower allotropic phase transition temperature of that alloy relative to Zircaloy-4. Moreover, from figure 3.20, it is seen that in the ($\alpha+\beta$) temperature domain, the burst stress of M5 is lower than in Zircaloy-4.

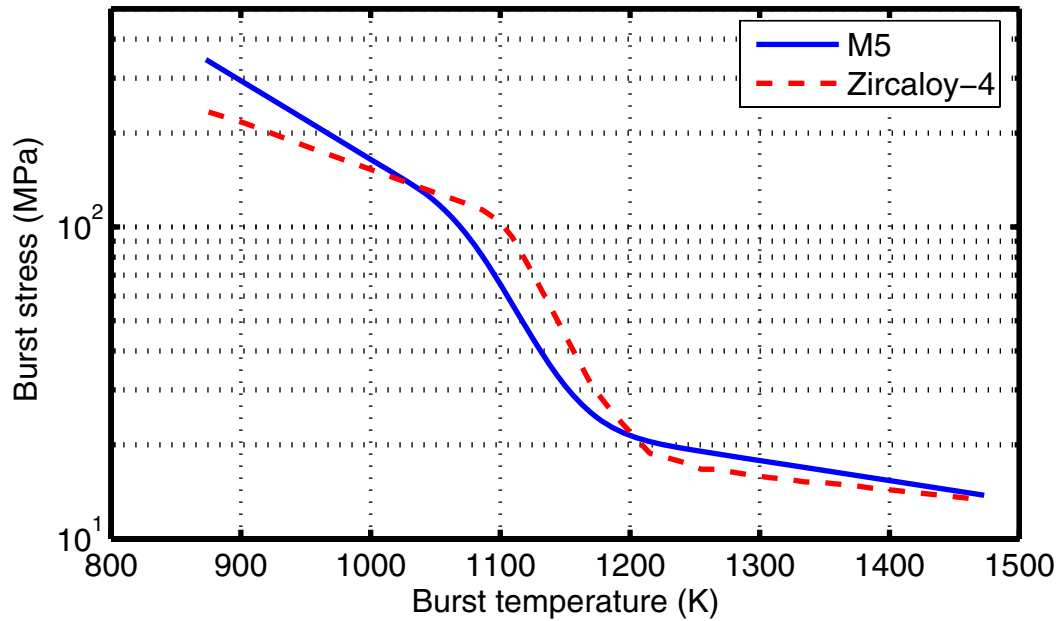


Figure 3.20: Burst criteria for clad materials deduced from the EDGAR tests: for M5 alloy (Forgeron et al., 2000) and Zircaloy-4 (Brachet et al., 2002).

Another important parameter is the effect of hydrogen on mechanical properties of Zr alloys, in particular the burst criterion. It is well known that hydrogen in excessive concentrations (e.g. beyond 500 wppm H) reduces the ductility of Zircaloy drastically (Bai et al., 1994). In Zircaloy-4 irradiated to high exposures such concentrations are anticipated (Mardon et al., 2004). As mentioned in the foregoing section, hydrogen content of clad (C_H) reduces the creep resistance of Zr alloys. The question that arises is how hydrogen would affect the LOCA clad burst criterion.

Brachet et al. (2002) studied the effect of $C_H = 600$ wppm on the clad burst criterion. Figure 3.21 shows burst stress versus burst temperature data obtained by creep and thermal ramp tests for Zircaloy-4 specimens with $C_H = 600$ wppm. In the same figure the best-estimate burst criterion for the as-received Zircaloy-4 is depicted. It is seen that most of the measured data fall below the best-estimate curve. Hence, a C_H dependent burst criterion is needed, when evaluating the rupture properties of long service high-exposure clad tubes that contain appreciable amount of hydrogen atoms.

As mentioned in the previous subsection, the CEA-Saclay group in a later publication (Portier et al., 2005) quantified the impact of hydrogen and long service exposure on clad burst for M5 and Zircaloy-4 alloys. More specifically, Portier et al. presented data regarding burst temperature versus hydrogen content obtained by uniaxial loading, 40 or 80 MPa, and heating rates of 25 and 100 K/s. The burst temperature depreciated with hydrogen content; however the hydrogen contents of the M5 specimens were much lower than the Zircaloy-4 specimens, as experienced from post irradiation examination. The specimens loaded with 80 MPa/100 K/s had a lower burst temperature than those tested at 40 MPa/25 K/s. In figure 3.22, we have plotted the lower-bound trend lines for the decline of the burst temperature with hydrogen content of M5 versus Zircaloy-4 for the 80 MPa/100 K/s tests.

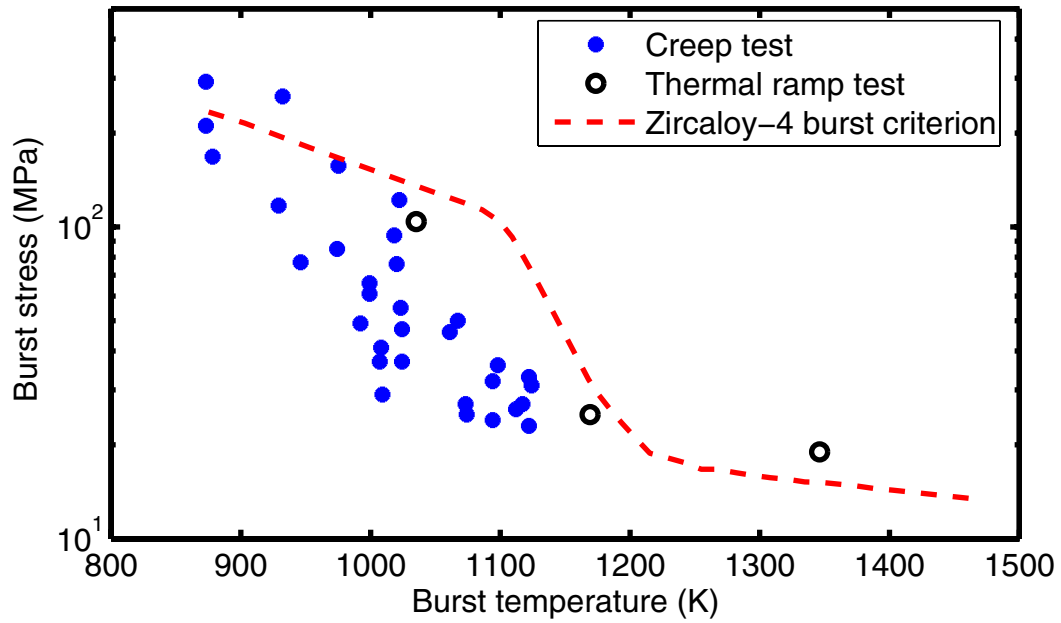


Figure 3.21: Burst data obtained in the EDGAR tests for Zircaloy-4 specimens with hydrogen content of 600 wppm (Brachet et al., 2002). The dashed curve shows a best-estimate burst criterion for the as-received Zircaloy-4 tubes.

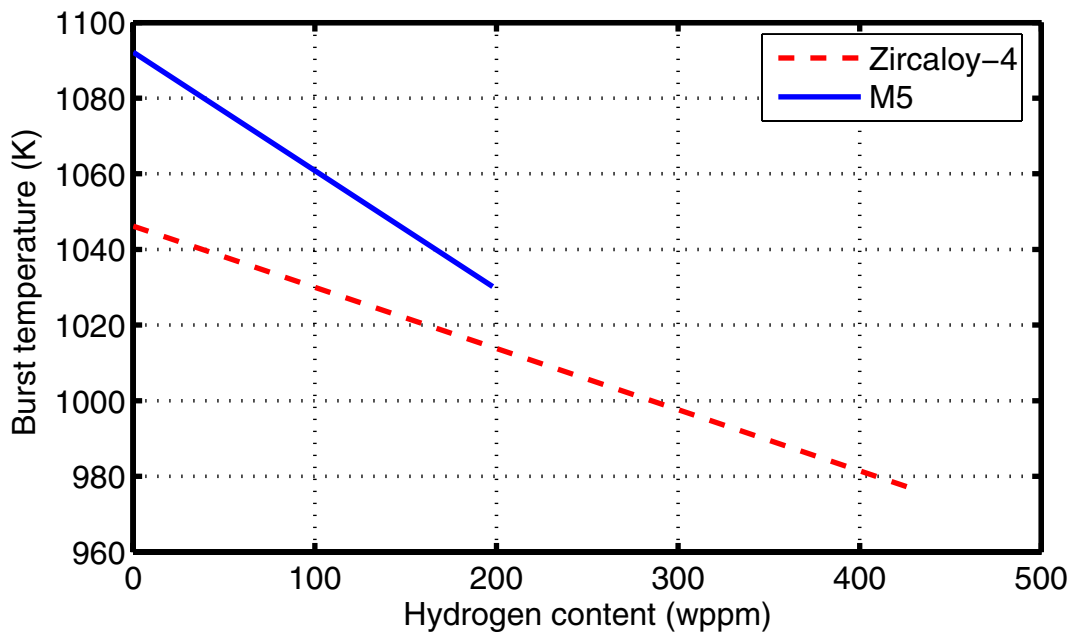


Figure 3.22: Lower-bound trend lines for burst temperature vs. hydrogen content from test data obtained for M5 and Zircaloy-4 clad samples by uniaxial loading under 80 MPa at 100 K/s (Portier et al., 2005). The data included both hydrogen charged as-received samples and clads irradiated in power plants subject to corrosion.

Effects of oxide layer thickness and high hydrogen on the ballooning and rupture properties of Zircaloy-4 clad have recently been reported by Kim et al. (2006). More specifically, low-tin Zircaloy-4 (1.3 wt% Sn) PWR clad tube specimens with diameter of 9.5 mm and wall thickness of 0.57 mm were tested. The as-received specimens were oxidized to oxide layer thicknesses of 20 and 50 μm or hydrogenated to contents of 300 and 1000 wppm H. The objective was to simulate the conditions of in-reactor corroded clads and for determining their impact on ballooning and rupture during LOCA.

Kim and company conducted high temperature ballooning tests in which the pressurized clad specimens were heated until rupture occurred. Thermal ramp rates for the pre-oxidized and hydrogenated samples were chosen to be 10 and 100 K/s. All the pre-oxidized samples ruptured below 1273 K and their elongations were appreciably less than those of the as-received samples. The hydrogen charged samples had lower burst ductility (e_f elongation) than the as-received ones for temperatures below 1073 K and higher values beyond this temperature (see Kim et al., 2006, figure 4).

Clad ductility in the as-received samples exhibited a minimum at around 1148 K ($e_f = 35\%$), after which the ductility increased and reached its maximum at around 1372 K ($e_f = 113\%$). The corresponding minima for specimens charged with 1000 wppm hydrogen were 1073 K ($e_f = 41\%$) and 1223 K ($e_f = 107\%$), respectively. Kim and co-workers' results showed that the oxide layer reduces the minimum ductility of the specimen under ballooning relative to the as-received one from about $e_f = 35\%$ to $e_f = 27\%$, whereas hydrogen stabilized the β phase increasing ductility, but it also caused hydrogen embrittlement leading to earlier (lower temperature) failure compared to as-received Zircaloy-4. As an example, the rupture temperatures measured by Kim et al. (2006) for tube specimens with an internal pressure of 40 MPa are listed in table 3.2. For burst temperature data at 20 and 60 MPa, see Kim et al. (2006). In section 4.2, we shall further discuss the results of some integral LOCA tests, conducted by Kim and co-workers, concerning embrittlement behaviour of Zircaloy-4 during oxidation and water quenching.

Samples	Burst temperature, K	
	10 K/s	100 K/s
As-received	1034	1178
Pre-oxide, 20 μm	1093	1073
Pre-oxide, 50 μm	1164	a
Hydrogenated 300 wppm	1022	1057
Hydrogenated 1000 wppm	992	a

^a Early clad failure.

Table 3.2: Burst temperature data of Zircaloy-4 claddings with an initial internal pressure of 40 MPa (Kim et al., 2006, table 2).

3.3 Phase transformation

Understanding the global (over all) rate of phase transformation in zirconium alloys utilized in light water reactors is important for prediction of mechanical behaviour of the alloy during a postulated LOCA. More specifically, the kinetics of α -Zr to β -Zr phase transition, i.e., the time evolution of the amount (volume fraction) β -Zr phase as a function of temperature and heat rate needs to be quantified. In the past years, there has been a number of investigations for quantifying the kinetics of phase transition during heating ($\alpha \rightarrow \beta$) and cooling ($\beta \rightarrow \alpha$). A summary of the transition temperatures extracted from literature was presented in section 2.1. Among the early works, we should mention the papers by Higgins & Banks (1966) and Hehemann (1972), who reported the time-temperature-transformation (TTT) diagrams for certain zirconium-niobium alloys. Chung et al. (1976) reported measurements of $\alpha \leftrightarrow \beta$ transformations in Zircaloy-2/4 obtained by an electric resistivity technique at different cooling rates. They also provided a method for calculating TTT diagrams from resistivity data. Yoo & Kim (1991) evaluated the $\alpha \rightarrow \beta$ phase transition kinetics, i.e., the volume fraction of β -Zr under isothermal conditions (1163 and 1223 K) in Zircaloy-4 by means of metallography.

A more comprehensive study of the $\alpha \rightarrow \beta$ phase transition kinetics on Zircaloy-4 and M5 alloy was recently made by Forgeron et al. (2000). We have reviewed this work and a few highlights of it are presented here. Forgeron and colleagues within the EDGAR program in CEA-Saclay investigated $\alpha \leftrightarrow \beta$ transformations both under equilibrium and temperature transient conditions. They employed high-temperature/high sensitivity calorimeter and dilatometer to measure on-heating $\alpha \rightarrow \beta$ and on-cooling $\beta \rightarrow \alpha$ phase transitions from near thermodynamic equilibrium up to LOCA conditions, with thermal rates up to 100 K/s. Figure 3.23 shows the near equilibrium data on the fraction of β -Zr as a function of temperature for Zircaloy-4 versus M5 alloy. It is seen that the phase transition in M5 starts and ends at lower temperatures compared to Zircaloy-4. Evidently this difference results in different mechanical behaviour during the course of transition for the two alloys. Hence the models for Zircaloy-4 must be modified for M5 or zirconium-niobium base alloys. The kinetics of phase transition depends on the applied rate of heating and cooling. Figure 3.24 displays the data of Forgeron et al. (2000) for the case of Zircaloy-4 at ± 10 K/s. It is seen that increasing the rate of heating retards the $\alpha \rightarrow \beta$ phase transition, while the cooling rate does the opposite. Hence, the effect of heating/cooling rate on the kinetics of phase transition needs to be accounted for in fuel rod LOCA modelling.

In a subsequent paper, the Saclay group (Brachet et al., 2002) extended Forgeron et al.'s work in order to investigate the influence of hydrogen content on the kinetics of $\alpha \leftrightarrow \beta$ transformation. We have plotted in figure 3.25 the equilibrium curves for the fraction of β -Zr in Zircaloy-4 as a function of temperature at three different hydrogen contents: $C_H \approx 0$, $C_H \approx 500$ and $C_H \approx 1000$ wppm. These curves are generated using empirical correlations fit to the data presented by Brachet et al. (2002). The results clearly show that hydrogen expedites the phase transition, i.e., the transition to the $(\alpha+\beta)$ -domain starts at lower temperature with increasing hydrogen content. Hence, the hydrogen effect needs to be modelled in LOCA analysis.

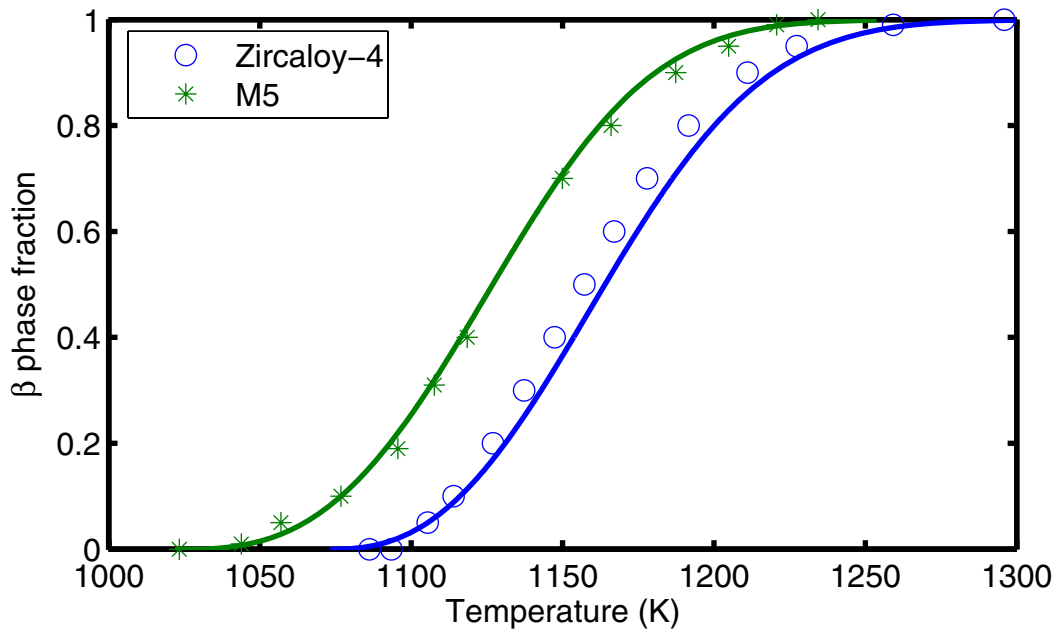


Figure 3.23: Fraction of β -Zr phase as a function of temperature in near-equilibrium condition (Forgeron et al., 2000).

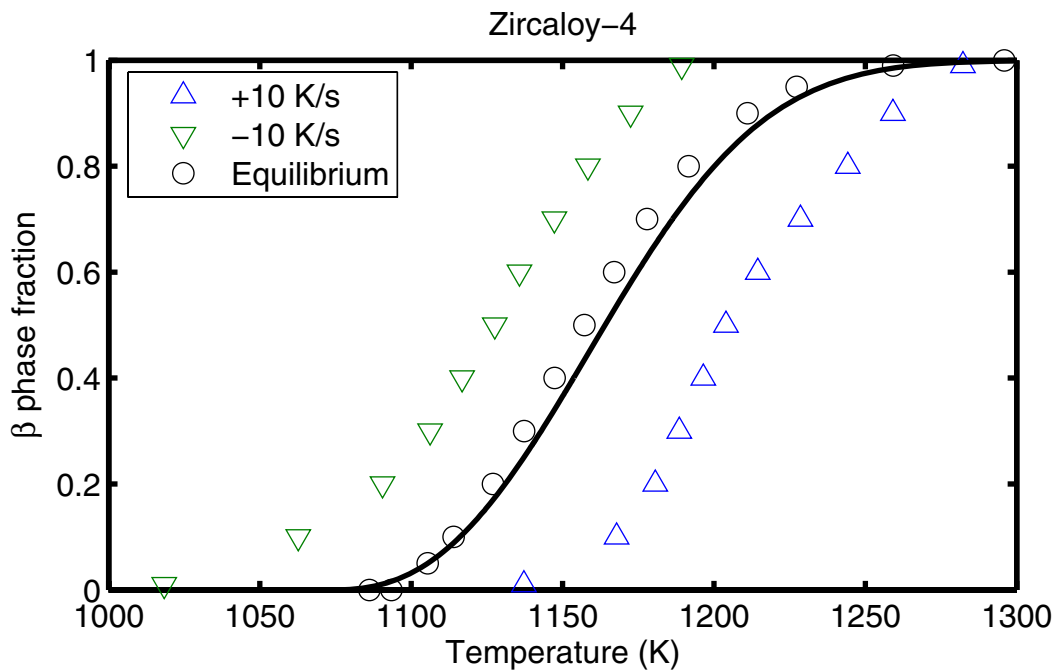


Figure 3.24: Fraction of β -Zr phase as a function of temperature in near-equilibrium condition and under heating and cooling at ± 10 K/s (Forgeron et al., 2000).

The hydride precipitation/dissolution temperatures, i.e., the inverse solubility limit for hydrogen in Zircaloy-4 and M5 alloy under the same kinetic condition have been determined by Brachet et al. (2002). Figure 3.26 shows the correlations obtained by curve fitting their results for the precipitation temperature as a function of hydrogen concentration for a cooling rate of 10 K/min.

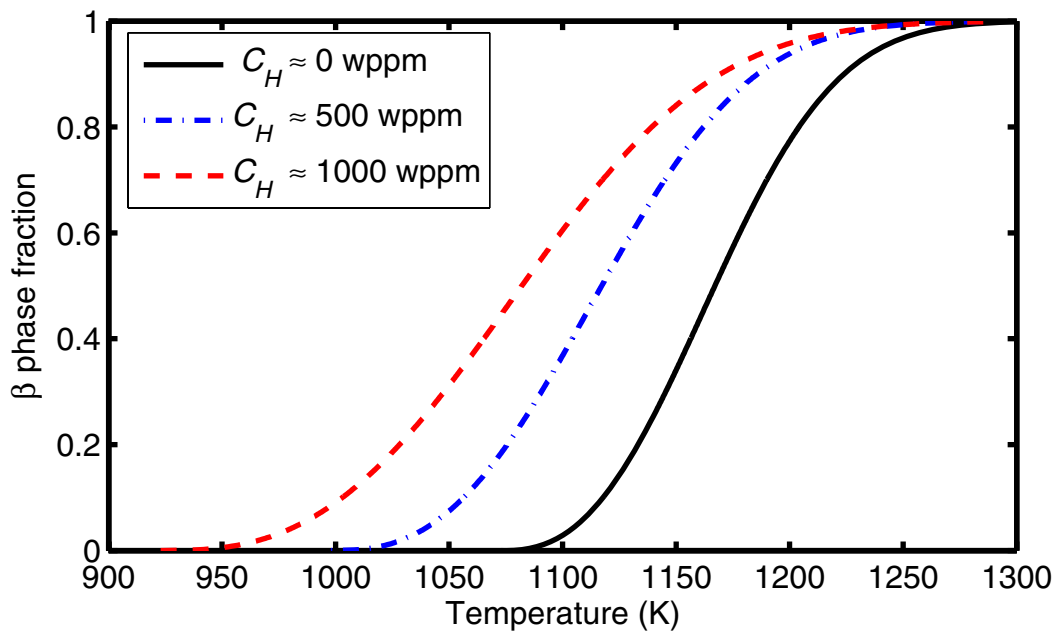


Figure 3.25: Fraction of β -Zr phase as a function of temperature in near-equilibrium condition in Zircaloy-4 at different hydrogen contents using empirical correlations fit to the data presented in (Brachet et al., 2002).

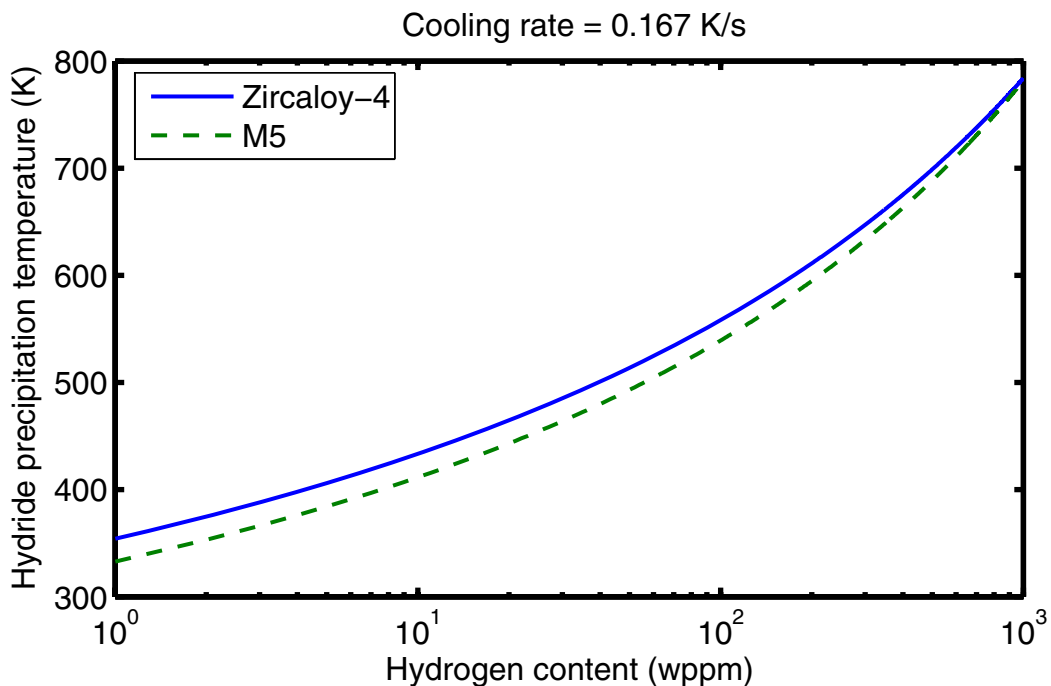


Figure 3.26: Best fit correlations to the hydride precipitation temperature versus hydrogen content data for Zircaloy-4 and M5 alloys (Brachet et al., 2002).

The effect of hydrogen on the $\alpha \leftrightarrow \beta$ phase transformation in Zircaloy-4 versus M5 was also alluded to by Brachet et al. (2002). They displayed plots of α/β phase transformation temperatures of Zircaloy-4 and M5 as a decreasing function of hydrogen for heating rate of 10 K/s, with M5 transition temperatures remaining below that of Zircaloy-4 at most by around 30 K.

3.4 Modelling

In this section, we delineate a method for modelling physical behaviour of cladding tube under LOCA conditions. A detailed description of the method and the numerics are subject of a subsequent stage in this project. The empirical correlations related to the phenomena treated in this section have already been discussed in the foregoing subsections and in the appendix regarding clad oxidation. The current available fuel rod modelling tool, the FRAPTRAN code, has been assessed in a separate report (Manngård, 2007).

Simulations of fuel clad behaviour during LOCA conditions require calculation of the tube equilibrium mechanical state, zirconium alloy oxidation, phase transformation, creep deformation laws, and burst criterion. The mechanical equilibrium provides the stresses in the tube as a function of position across tube wall, applied load (pressure), and the instantaneous tube radii.

The oxidation model, not only should be able to perform licensing calculations in the manner of Baker-Just or Cathcart-Pawel (appendix A), but also should be capable of predicting oxygen concentration across clad wall under transient conditions, e.g., the results presented in figure 3.1. For this kind of capability, a diffusion based mathematical model is necessary; e.g., similar to a method presented by Iglesias et al. (1985), in which one-dimensional diffusion equation is considered for oxygen concentration:

$$\frac{\partial C}{\partial t} = D \frac{\partial^2 C}{\partial r^2} , \quad (3.5)$$

where $C = C(r, t)$ is the oxygen concentration, being a function of position and time, and D is the oxygen diffusivity. Equation (3.5) is applied subject to specified oxygen concentration values at each layer boundary and conservation of oxygen atoms as the boundary moves (Tucker et al., 1978).

The phase transformation model should be based upon the classical theory of the kinetics of concurrent nucleation and growth reactions, the so-called KJMA^{vii} model (Christian, 2002). In the KJMA model, the fraction of the new phase ζ (e.g., β -Zr phase) is calculated according to a differential equation of the form:

$$\frac{d\zeta}{dt} = Kmt^{m-1}(1 - \zeta), \quad (3.6)$$

where m is an exponent whose value may vary from 1 to 4, depending on the morphology of the new phase but is independent of temperature. The parameter K , on the other hand, depends on the nucleation and growth rates and is therefore very sensitive to temperature.

Since in our applications, we need to treat thermal transients, where temperature is a function of time, $T = F(t)$, and inversely, $t = G(T)$, it is convenient to express equation (3.6) in terms of temperature variation, viz.

$$\frac{d\zeta}{dT} = \frac{KmG^{m-1}}{\dot{T}}(1 - \zeta), \quad (3.7)$$

where $\dot{T} = dT/dt$ is the heating/cooling rate.

Similar kind of analysis has been used in the past to model the kinetics of phase transition in zirconium alloys, for example an empirical model by Holt et al. (1980), and more recently a similar mode by Forgeron et al. (2000).

Having determined the volume fraction of the new phase, appropriate creep laws in each phase are invoked to calculate clad deformations. Finally, a burst criterion that combines the rupture stress in α -Zr and β -Zr phase is applied to assess the integrity of the clad. The method should also account for the effect of circumferential temperature variation on clad rupture (Ferner & Rosinger, 1985).

There are many ways to formulate a burst criterion for claddings in a LOCA. A simple empirical relation between burst stress in the hoop direction, σ_B and the burst temperature T_B was proposed by Erbacher et al. (1982) according to

$$\sigma_B = a \exp(-bT_B) \exp \left[- \left(\frac{w_{ox} - 0.12}{0.095} \right)^2 \right]. \quad (3.89)$$

Here a and b are constants determined experimentally over each of temperature ranges corresponding to the three phases of zirconium alloy, i.e., α , $(\alpha+\beta)$, β -phase and w_{ox} is the oxygen pickup (wt%) of the as-received clad.

The general equations for the computational method for clad behaviour under LOCA are outlined in Box 3.1.

1- Mechanical equilibrium

A tube with external and internal radii R_2 and R_1 with a pressure p inside and no pressure outside. The stress distribution as a function radius r is given by relations

$$\sigma_{rr} = \frac{pR_1^2}{R_2^2 - R_1^2} \left(1 - \frac{R_2^2}{r^2} \right), \quad \sigma_{\theta\theta} = \frac{pR_1^2}{R_2^2 - R_1^2} \left(1 + \frac{R_2^2}{r^2} \right)$$
$$\sigma_{zz} = \frac{2p\nu R_1^2}{R_2^2 - R_1^2}$$

where ν is Poisson's ratio.

2- Oxidation

The rate of oxidation is described by

$$\frac{dK_{ox}}{dt} = \frac{1}{K_{ox}} \frac{\delta^2}{2}$$

where K_{ox} is an oxygen kinetic parameter, e.g., total oxygen uptake by the clad and $\delta^2 / 2$ is the isothermal parabolic rate constant.

3- Phase transformation kinetics

The volume fraction of the new phase is described by

$$\frac{d\zeta}{dT} = \frac{KmG^{m-1}}{\dot{T}} (1 - \zeta)$$

where parameters entering this equation are defined in the text.

4- Creep deformation

The equivalent creep strain rate is proportional to the equivalent stress σ_{eq} by virtue of the following relation:

$$\frac{d\varepsilon_{eq}}{dt} = -A_i \exp(-Q_i / T) \sigma_{eq}^n$$

where the index i defines the phase domain.

5- Burst criterion

The calculated hoop stress becomes equal to the burst stress, namely

$$\sigma_{\theta\theta} = \sigma_B(\zeta, T)$$
$$\log \sigma_B(\zeta, T) = (1 - \zeta) \log \sigma_{B,\alpha} + \zeta \log \sigma_{B,\beta}$$

where $\sigma_{B,\alpha}$ and $\sigma_{B,\beta}$ are the burst stresses in the α and β phase, respectively.

Box 3.1: General equations describing cladding tube thermal-mechanical behaviour under loss-of-coolant conditions.

4 Integral LOCA tests

The experimental data discussed in the last two sections comprise basic material property data regarding creep strength, oxidation and embrittlement of cladding under LOCA conditions obtained by separate effect tests. A different class of tests, integral LOCA tests, has been performed to determine clad deformation and fracture subject to internal pressure on actual or dummy fuel rods under LOCA conditions. This class of tests may be divided into single rod tests and multi-rod tests, by type of heating, e.g. ohmic, internal, furnace, or nuclear heating, and according to the practicality of their external heat transfer conditions. Also the tests may be classified into in-reactor versus out-of-reactor tests. Many of these tests were carried out during the 1970s and 1980s. Parsons et al. (1986) offer a good review of these tests made prior to 1986 and recently Grandjean (2005) has made a state-of-the art review of these tests. Hence, we shall not delve deep into all these past important tests and maintain our focus on recent findings.

We should, however, briefly mention that the main series of multi-rod out-of-reactor tests were conducted at the US Oak Ridge National Laboratory (ORNL), Germany's Kernforschungszentrum Karlsruhe (KfK) and the Japan Atomic Energy Research Institute (JAERI). The ORNL tests on 4×4 and 8×8 bundles were conducted with low steam flows and consequently very low heat transfer coefficients, to provide data for evaluating specific requirements for the US Federal Regulations 10 CFR Part 50 Appendix K (cf. section 2.3). The ORNL test conditions were designed to result in large deformations and were selected to provide a realistic estimate of the upper limit of the amount of deformation that could be anticipated under LOCA. Moreover, the tests draw attention to the difference of the rods as single and in bundles and between small and large bundles. Nonetheless, the tests cannot be used directly to realize fuel bundle behaviour in accidents with reflood.

The KfK tests in the REBEKA program provided a more realistic situation in laboratory with simulated bottom reflood (Erbacher & Leistikow, 1987). These tests resulted in significant co-planar strains of claddings, but the restriction of sub-channels in bundles was acceptable. Also at KfK, in-reactor tests have been performed in the FR-2 reactor using PWR-type single rods (active length of 0.5 m) both fresh and irradiated (2.5 to 35 MWd/kgU) and simulating the second heat-up phase of a cold leg break. The in-reactor single rod tests, simulating large break LOCA, has been carried out in the Power Burst Facility at the Idaho National Engineering Laboratory in the USA. The test program (LOC) was designed to study the two major parameters determining clad strain during ballooning, i.e., clad temperature and differential pressure, using both fresh and irradiated rods. In this program, there were four separate 15×15 type PWR test rods, 0.91 m long, two of which were pressurized to values representative of PWR rods at beginning of life and two were pressurized to values representative of high burnup rods.

In this section, we focus our survey mainly on the tests performed recently, namely the single rod tests carried out at JAERI and the Argonne National Laboratory (ANL) tests in USA. Also some preliminary results of the recent Halden reactor LOCA testing; the IFA-650 series are briefly discussed. For the sake of completeness we also have included some highlights from the past multi-rod programs, PHEBUS-LOCA in France and the NRU tests in Chalk River Canada.

4.1 Thermal shock tests at JAERI

The current LOCA criteria on fuel safety used in Japan are not based on the concept of nil-ductility of clad, instead, the failure threshold value determined in the integral shock tests under restraint conditions is used (Nagase & Uetsuka, 2001). Consequently, the workers at the Japan Atomic Energy Research Institute (JAERI) have carried out a systematic research program with an outlook to obtain a wide range of database for evaluation of clad behaviour under LOCA conditions and in particular the influence of burnup.

The basic experimental setup used in the JAERI thermal shock tests is shown in figure 4.1. It is essentially the apparatus used originally by Uetsuka et al. (1983). The main components of the apparatus are an Instron-type tensile testing machine, a quartz reaction tube, an infra red image furnace equipped with tungsten halogen lamps, a steam generator, and a water supply system for flooding. The test rod is mounted vertically in the centre of the reaction tube and the bottom end is fixed to the testing machine. The test rod consists of alumina cylindrical pellets, Zircaloy cladding, and Zircaloy end plugs. The alumina pellets simulate UO_2 fuel pellets regarding the heat capacity (figure 4.2). LOCA conditions comprising clad oxidation at high temperature and quenching by flowing water are produced inside the quartz reaction tube (Nagase et al., 2000; Nagase & Fuketa, 2004b, 2005, 2006).

Figure 4.1 shows an example of a temperature history during the test. The temperature is measured with Pt-Pt/13%Rh thermocouples spot-welded on the outer surface of the clad at several axial positions. The test rod is heated at a rate of 10 K/s in a steam flow. Steam is introduced before the heat-up and the flow is maintained at a rate of around 36 mg/s during the oxidation stage. During the heat-up, usually clad inflates (balloons) and ruptures due to an increase in rod pressure and decrease in clad strength, upon which steam penetrates the fuel rod through rupture opening of clad. After the isothermal oxidation, for a predetermined period (minutes), the rod is slowly cooled to about 1000 K and then quenched by flooding water from the bottom (figure 4.1). The reflooding rate is typically in the range of 30 to 40 mm/s.

During a loss-of-coolant transient, a fuel rod would axially expand with the increase in temperature and then would contract with the decrease in temperature. Moreover, oxide layer formation on the clad would enhance fuel rod expansion. Since the contraction of fuel rods could be restricted within the fuel assembly, e.g., by friction between the clad and the spacer grid, tensile loads would be acting on the rod during this stage of LOCA. Hence in the JAERI experiments, the test rod can be axially restrained at the end of the isothermal oxidation to simulate the possible external axial loading. For instance, the tensile load is usually controlled and limited to three different levels of 390 ± 50 , 540 ± 50 and 735 ± 50 N (Nagase & Uetsuka, 2001) in order to achieve intermediate constraint conditions. Figure 4.1 shows typical load history curves measured during quenching. The applied tensile load on the test rod is measured with the load cell, and the obtained load data are used to adjust the restraint load by displacing the crosshead of the tensile machine.

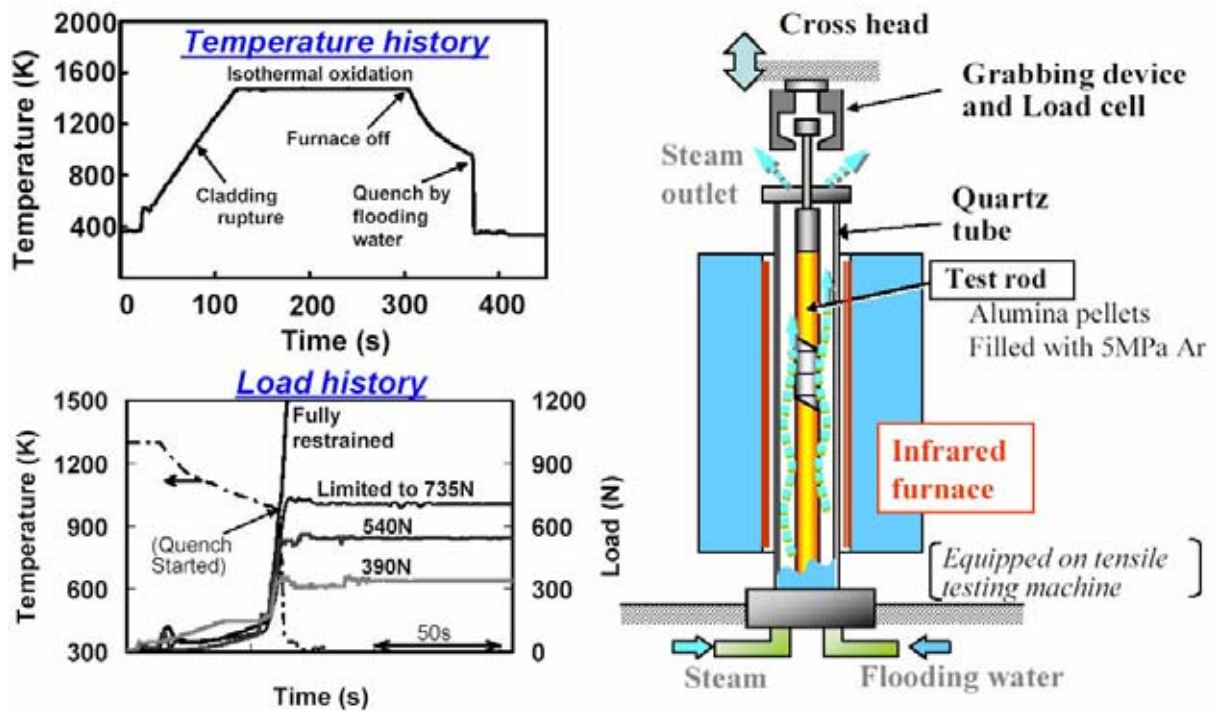


Figure 4.1: Cutaway view of apparatus used at JAERI for integral thermal shock tests (right), example of temperature history (upper left) and example of tensile load control under restraint conditions (lower left). After Nagase & Fuketa (2004a).

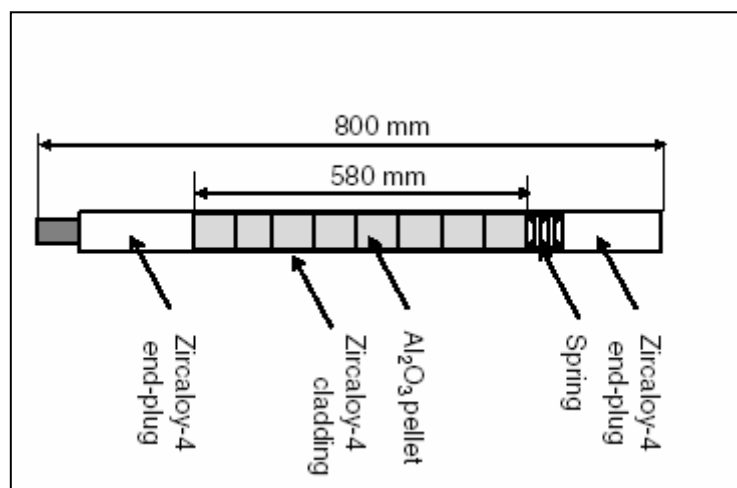


Figure 4.2: Cutaway view of a test rod used at JAERI for integral shock tests, Nagase & Fuketa (2004b). The test rod is pressurized with argon gas to a desired pressure.

In figure 4.3, we have plotted the early failure data of Uetsuka et al. (1983) in terms of the *equivalent oxidation time* (EOT) versus the inverse temperature (failure map) for test rods with length of 500 mm, standard PWR Zircaloy-4 clad, with inner and outer diameters of 9.48 and 10.72 mm, respectively, and 0.14 mm initial pellet-clad gap, with He gas to a pressure of 3 MPa at room temperature. About half of the rods failed on quenching in these tests both in the unconstrained and constrained conditions, which we have depicted in figure 4.3 in terms of their EOTs and oxidation temperatures. In the

constrained condition, the axial displacements of the rods, restrained during flooding, were estimated to be 2 mm in the thermal shock experiment. Uetsuka et al. (1983) point out that this value is close to the difference in the axial shrinkage between a clad and the guide tube in a PWR assembly in length of one spacer-grid span as calculated by the thermal expansion coefficient of Zircaloy. Figure 4.3, also depicts the oxidation conditions of $ECR = 0.15$, $= 0.2$ and $= 0.4$, calculated by the Baker-Just relation (appendix A).

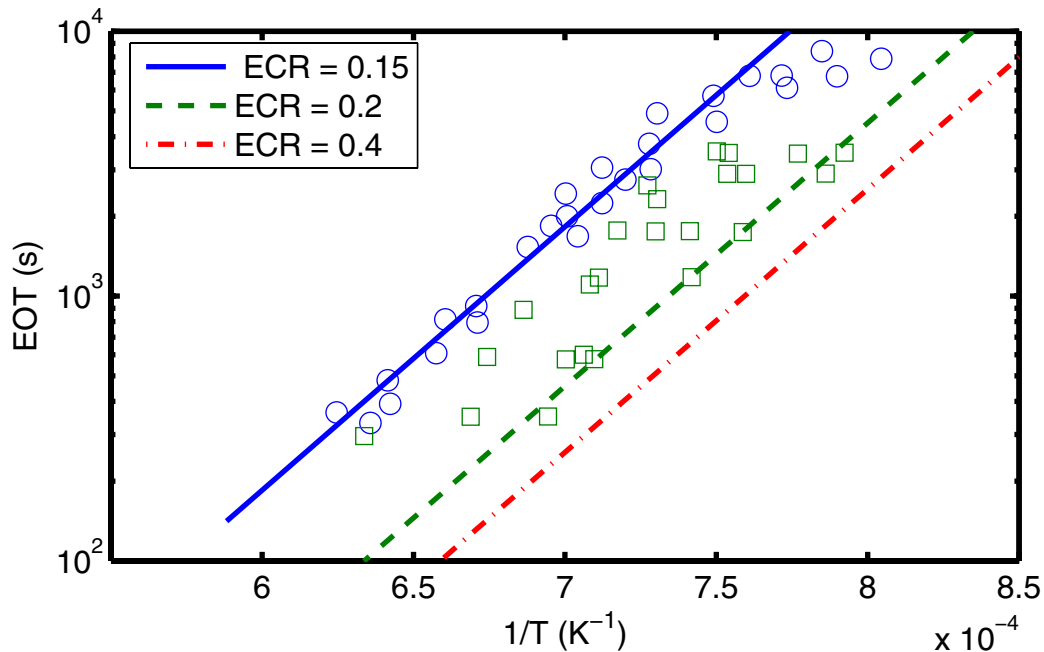


Figure 4.3: Equivalent oxidation time (EOT) versus inverse temperature for Zircaloy-4 clad during isothermal oxidation subjected to thermal shock experiment. The symbols represent failed test rods, unrestrained (circles) and restrained (squares) after rupture in steam. The lines are calculated according to the Baker-Just relation for several equivalent clad reacted (ECR) values. This figure is reproduced based on figures 5 and 6 of Uetsuka et al. (1983).

In these tests, the failure boundary oxidation condition of the clad on quenching with water under unrestrained condition laid in the region of $ECR \approx 0.35$ - 0.38 for the isothermal oxidation temperatures between 1323 and 1603 K. For temperatures in the range of 1243 to 1323 K, the boundary condition was somewhat lower than that obtained by Uetsuka and company at higher temperatures, most likely due to the breakaway oxidations at higher temperatures. For the constrained rods, the failure oxidation condition laid in the region of $ECR \approx 0.19$ - 0.24 for the oxidation temperatures of 1203 to 1583 K. This is sufficiently large compared with the ECCS acceptance criteria practiced in Japan (0.15) and elsewhere (0.17).

It is worth mentioning that the majority of the rods that failed on quenching under constraint were fractured at the positions between 20 and 30 mm away from the rupture opening, where high hydrogen content was absorbed by the clad. Thus hydrogen absorbed by the clad as well as the oxygen content played a pivotal role in the fracture behaviour of the rods during flooding under constraint condition (Uetsuka et al., 1983).

Nagase & Fuketa (2004b) conducted a similar experiment as the 1983 Uetsuka et al.'s, i.e. integral thermal shock tests, but on PWR 17×17-type low tin (1.3 wt% Sn) Zircaloy-4 clad with outer diameter of 9.50 mm and wall thickness of 0.57 mm. In addition, some of the clad samples, which had an initial hydrogen content ≈ 10 wppm, were hydrided to 400 and 600 wppm H, to simulate the range of hydrogen pickups expected during service in PWRs. The test rod pre-pressurization with argon gas was 5 MPa at room temperature. The test rods were quenched under unstrained and fully restrained conditions (see figure 4.1). Under the fully restrained condition, both ends of the test rod were restrained just before cooling was started. The tensile load was rapidly increased just after the start of quenching and reached loads in the range of 1400 to 2200 N in the situation where the clad survived the quench. Here, we present Nagase & Fuketa's results regarding the impact of full constraint and clad hydrogen content on rod failure as depicted in a failure map, i.e., EOT vs. inverse temperature diagram.

Figure 4.4a shows the failure map for the fractured rods under unrestrained condition for as-received and hydrided samples. The lines shown in the figure are calculated using the Baker-Just relation (appendix A) with $ECR=0.40$ and $ECR=0.46$ with clad wall thickness of 0.57 mm. Nagase & Fuketa's data indicate that the fracture/no-fracture threshold lies between the two contour lines. The threshold is comparable to that obtained by Uetsuka et al. (1983) for a thicker clad wall (0.62 mm) and unhydrided samples under no constraint (figure 4.3). The data also indicate that in the case of no constraint, hydriding in the range of 400 to 600 wppm does not noticeably affect the failure map. The fracture data for fully restrained (loaded) condition are depicted in figure 4.4b. In this case, it is seen that, hydriding has an impact, i.e., the hydrogenated samples have a lower threshold than the as-received ones. In fact, oxidation calculations à la Baker-Just show that the lower bound of the hydrided samples corresponds to $ECR=0.07$, which is significantly lower than the as-received samples with $ECR\approx 0.17$.

It should be noted that the load can vary over a wide range as influenced by the design of fuel assembly, irradiation time, and an accident scenario. Therefore, Nagase & Fuketa in their subsequent paper (Nagase & Fuketa, 2005) considered the effect of partial restraint and also higher hydrogen contents of the samples on the failure threshold.

In the 2005 JAERI study, the integral thermal shock tests were performed employing non-irradiated low-tin (1.3 wt% Sn) claddings, as the preceding work, with various hydrogen contents, 10 wppm for the as-received samples and 100 to 1450 wppm for hydrogenated samples. Moreover, the tensile load generated by restraining the test rods during the quench was controlled at intermediate restraint conditions. In particular, the maximum load was controlled by keeping the load levels of 390, 540 and 735 N using the automatic load adjusting operation of the tensile testing machine (figure 4.1). After the tests, the rods were sectioned into 15-mm segments for metallographic and hydrogen analysis.

A point worth noting is that under the isothermal high temperature oxidation of cladding tubes, significant hydrogen absorption occurs locally away from the rupture opening. The absorbed hydrogen emanates mainly as a result of clad oxidation at the inner surface by steam entering via the rupture opening. Nagase & Fuketa examined the effect of the initial hydrogen concentration on the peak hydrogen uptake (PHU) and found a trend between PHU and ECR, that is, the larger is the peak hydrogen content the higher becomes the value of ECR (figure 4.5). Although the dependency between hydrogen

uptake and ECR is not unambiguous, the trend indicates that cladding tubes having higher hydrogen contents, reach the ECR limit earlier under a LOCA, than the ones with lower H contents. Likewise, it is seen that pre-hydriding does not affect the secondary hydriding during oxidization.

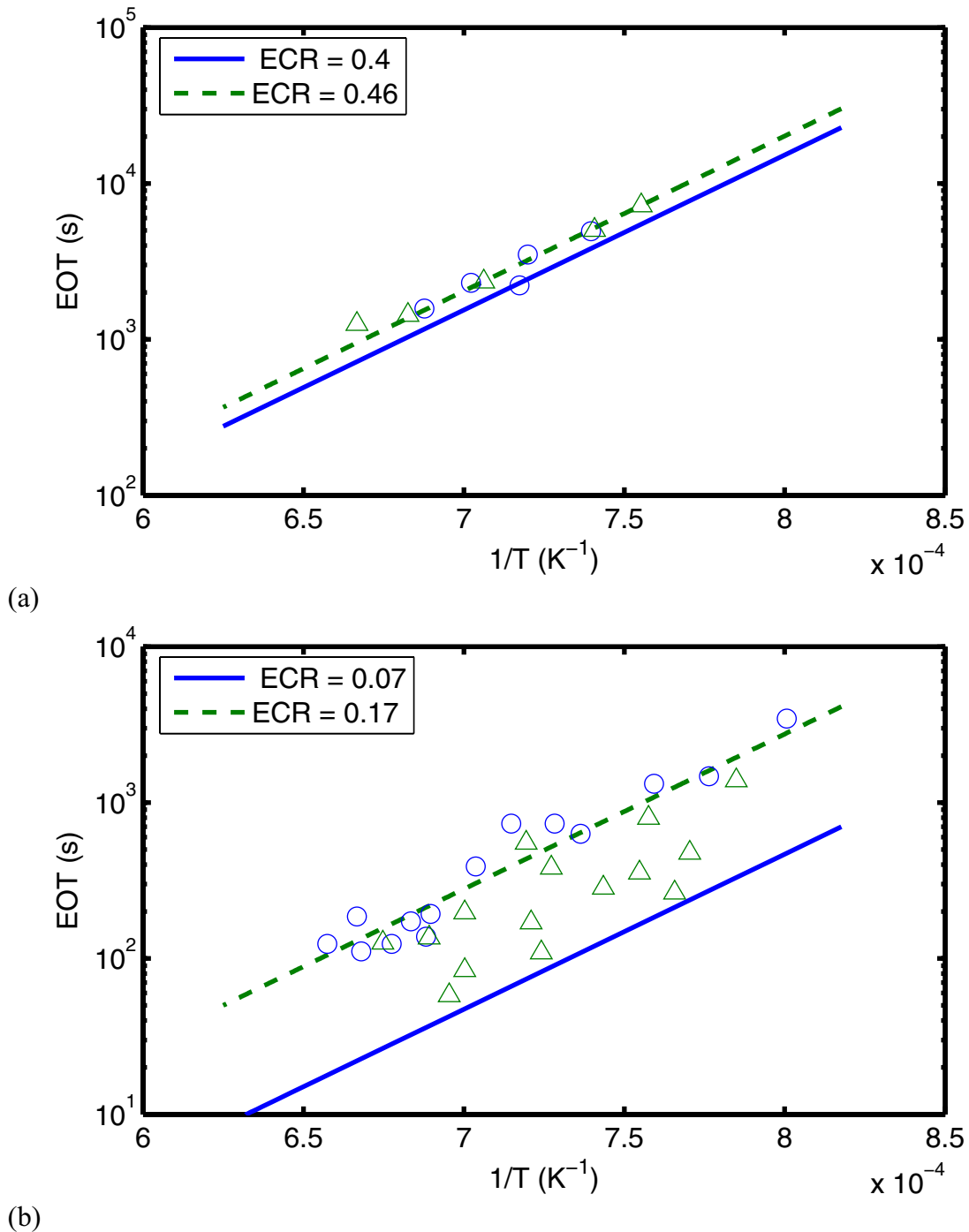


Figure 4.4 Equivalent oxidation time (EOT) versus inverse temperature for Zircaloy-4 clad during isothermal oxidation subjected to thermal shock experiment under: (a) unrestrained condition and (b) fully restrained condition. The symbols represent failed test rods, non-hydrided (circles) and hydrided (triangles) after rupture in steam (Nagase & Fuketa, 2004). The lines are calculated according to the Baker-Just relation for several ECR values with fixed clad wall thickness of 0.57 mm.

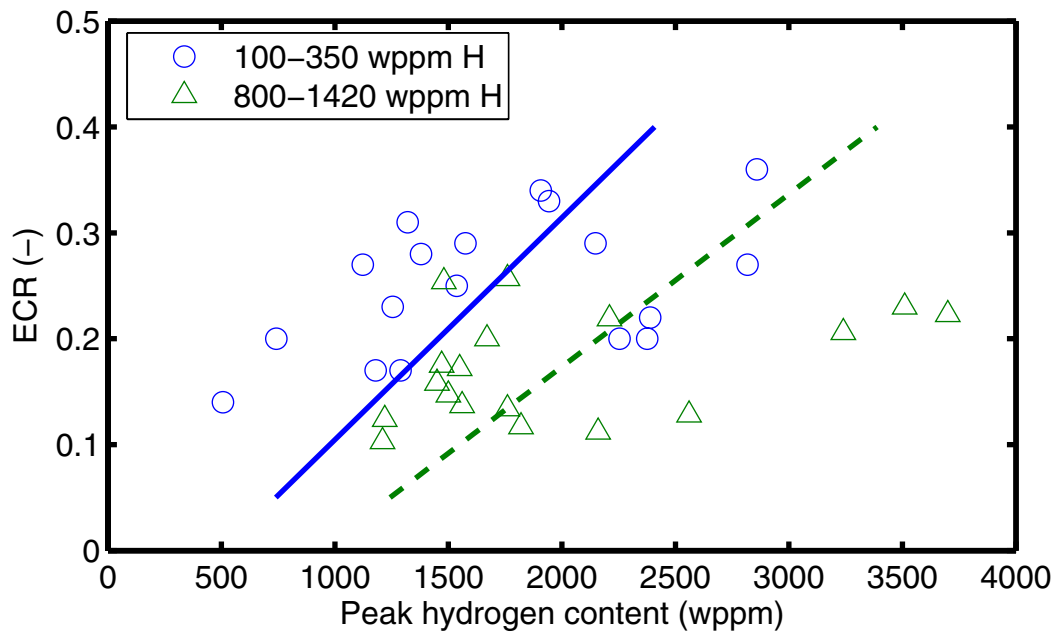


Figure 4.5: Trend between the peak hydrogen uptake and ECR during isothermal oxidation after thermal shock tests (Nagase & Fuketa, 2005). The data are split into two groups according to the initial hydrogen level of the samples: a low level (average 193 wppm) and a high level (average 974 wppm) content.

It is meaningful to show the fracture map relating EOT and temperature deduced by Nagase & Fuketa (2005) for the unrestrained, the intermediate, and the fully restrained conditions (figure 4.6). The initial wall thickness of the clad specimens tested under unrestrained condition was 0.57 mm and their initial hydrogen contents were between 400 and 600 wppm. Whilst, hydrogen contents of the clad specimens under restrained conditions were about 350 to 800 wppm. As can be seen (figure 4.6), the failure threshold reduces with an increase in restraint load. For instance, the difference between the fracture boundaries are equivalent to 95 and 185 K from 1473 K for $ECR \approx 0.17 \rightarrow 0.07$ and $ECR \approx 0.4 \rightarrow 0.17$, respectively, assuming a constant EOT. Nagase & Fuketa (2005) conclude that an increase in hydrogen concentration increases the precipitation of δ -hydrides and the oxygen content in the former β -Zr phase (cf. section 2.2). Hence, this can cause enhancement in embrittlement of oxidized Zircaloy specimens containing higher initial hydrogen contents.

In a recent paper, Nagase & Fuketa (2006) presented the results of experiments on Zircaloy-4 clad specimens, irradiated in the rod burnup range of 39 to 44 MWd/kgU in a PWR. The aim of the thermal shock tests was to investigate the high burnup fuel behaviour under LOCA conditions. The parent fuel rods were two PWR rods irradiated at the Takahama unit-3 reactor, Kansai Electric Power Company, in Japan. The clad material was low tin (1.3 wt% Sn) with as-fabricated outer diameter of 9.50 mm and wall thickness of 0.57 mm. The thickness of the oxide layer formed during irradiation ranged from 15 to 25 μm and the hydrogen content was calculated to range from 120 to 210 wppm assuming that 15% of the hydrogen generated is absorbed. The re-fabricated five test rods were pressurized to 5 MPa with Ar gas at room temperature. Similar test apparatus and procedure as illustrated in figure 4.1 were employed. The tensile load generated by restraining the test rod during the quench was kept at 540 N.

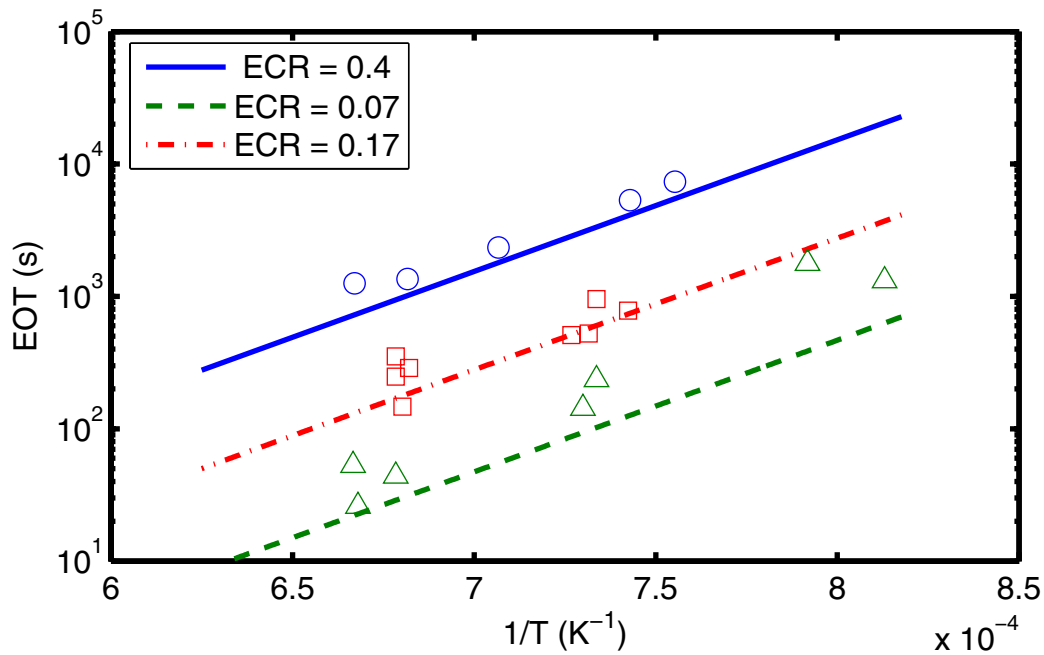


Figure 4.6: Effect of restraint load on fracture threshold in terms of the equivalent oxidation time (EOT) versus inverse temperature for Zircaloy-4 clad with H contents ranging from 350 to 800 wppm during isothermal oxidation subjected to thermal shock experiment. The symbols represent failed test rods unrestrained (circles), restrained with loads 390-735 N (squares) and fully restrained (triangles) after rupture in steam (Nagase & Fuketa, 2005). The lines are calculated according to the Baker-Just relation for several ECR values with fixed clad wall thickness of 0.57 mm.

According to Nagase & Fuketa (2006) two of the clad specimens oxidized to ECR \approx 0.26 to 0.29 were fractured during the quench, while four specimens, oxidized to ECR \approx 0.16 to 0.22 survived the quench. The results of Nagase & Fuketa (2006) vis-à-vis failure threshold for the 6 tested rods are shown in figure 4.7. The lines in this figure are calculated according to the Baker-Just relation for ECR values 0.3 (top line) and 0.17 (bottom line) with fixed clad wall thickness of 0.57 mm. We have calculated the ECR values for the individual rods, without reduction of clad wall due to ballooning; and the results are presented in table 4.1 together with the ECRs calculated by Nagase & Fuketa. As can be seen, our results (*here*) differ somewhat from those of Nagase & Fuketa (*NF*), though the general trend is the same.

Test No		1	2	3	4	5	6
Burnup	MWd/kgU	43.9	43.9	39.1	40.1	40.9	39.1
H content	wppm	170	210	140	140	120	120
Temperature	K	1449	1451	1427	1445	1303	1450
Time	S	486	120	200	363	2195	543
ECR (<i>NF</i>)	%	29	17	16	22	22	26
ECR (<i>here</i>)	%	25	13	14	21	22	27
Status	---	Failed	Intact	Intact	Intact	Intact	Failed

Table 4.1: Boundary conditions in the Nagase & Fuketa (2006) thermal shock tests.

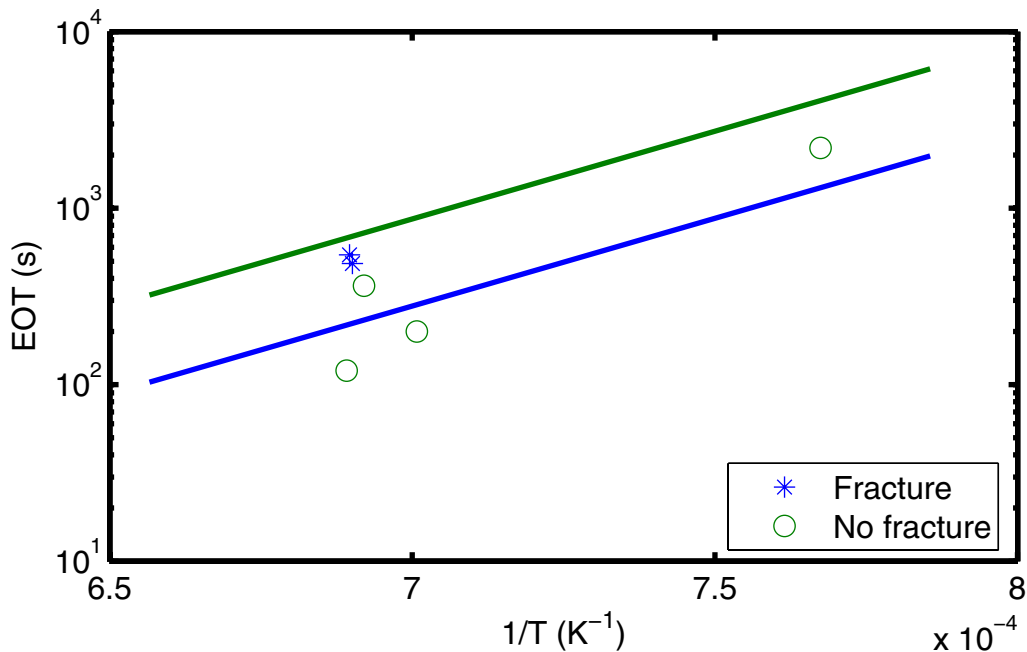


Figure 4.7: Equivalent oxidation time (EOT) versus inverse temperature for Zircaloy-4 clads irradiated in a PWR to rod burnups in the range of 39 to 44 MWd/kgU. The clad hydrogen contents were calculated to range from 120 to 210 wppm. The lines are calculated according to the Baker-Just relation for ECR values of 0.30 (top line) and 0.17 (bottom line) with fixed clad wall thickness of 0.57 mm.

The Nagase & Fuketa (2006) thermal shock tests showed that there are no significant differences between irradiated and unirradiated Zircaloy-4 clad specimens regarding the fracture threshold under quenching for the burnup levels (39-44 MWd/kgU) and hydrogen contents up to 210 wppm, however, the threshold is reduced as the pre-test hydrogen content of the specimen increases.

Nagase & Fuketa (2006) also measured axial profiles of the hydrogen concentration in irradiated samples, which experienced rupture, oxidation and quench and compared them with representative profiles of unirradiated specimens. It is known from earlier studies (Uetsuka et al., 1983; Nagase & Fuketa 2005) that clad absorbs significant amount of hydrogen during oxidation after rupture. Steam enters from the rupture opening, oxidizes the inner clad surface and produces hydrogen that is absorbed at the inner surface (secondary hydriding). The hydrogen distribution is nonuniform axially and is generally reported to peak at positions 30 to 50 mm away from the rupture location in unirradiated specimens. However, recent observations of Nagase & Fuketa (2006) show that the hydrogen content peak varies between irradiated specimens and they are different from those of the unirradiated specimens. Pellet-clad interaction during reactor operation can affect the surface chemistry of the inner clad, which can lead to multifaceted surface conditions depending on the degree of PCI, thereby causing variations of the hydrogen axial profile due to secondary hydriding in irradiated clad. Nagase & Fuketa believe that the size of ballooning, i.e., the gap between ballooned clad and pellet, and rupture opening could affect the axial hydrogen profile and suggest that hydriding in irradiated clad should be carefully investigated since the fracture boundary may be reduced if considerable hydrogen uptake occurs at the rupture position.

In another recent paper from the Japan Atomic Energy Agency, Udagawa et al. (2006) report the effects of cooling rate during the slow-cooling process and quench temperature on post-quench ductility of the oxidized cladding. Unirradiated 17×17 Zircaloy-4 clad specimens (1.3 wt% Sn) were oxidized in steam at 1373 or 1473 K, cooled at a rate from 2 to 7 K/s, and finally quenched from temperatures ranging from 1073 to 1373 K. The post-quench ductility of the specimens was examined by ring-compression test, and microscopic properties were analyzed by metallurgical examination, hardness test, and oxygen analysis. The morphology of the oxygen-rich α phase in the metallic former β phase layer changed depending on the cooling history. The area fraction of the α phase field increased and the post-quench ductility reduced with decrease in the quench temperature. Udagawa et al. note that because the α phase domain with low ductility provides favored paths for crack propagation, the increase in area fraction of the α phase domain can decrease the resistance to fracture, which leads to ductility reduction. Figure 4.8 shows the results of ring-compression tests for samples oxidized at 1473 K to various exposures, then quenched from 1173 K with cooling rates in the range of 2 to 7 K/s. The data are presented in terms of the normalized ductility index versus ECR. The normalized d -index is defined as a plastic deformation when the load is dropped to 80% of the maximum load during ring compression test, normalized by clad outer diameter (9.5 mm). The nominal clad wall thickness was 0.57 mm.

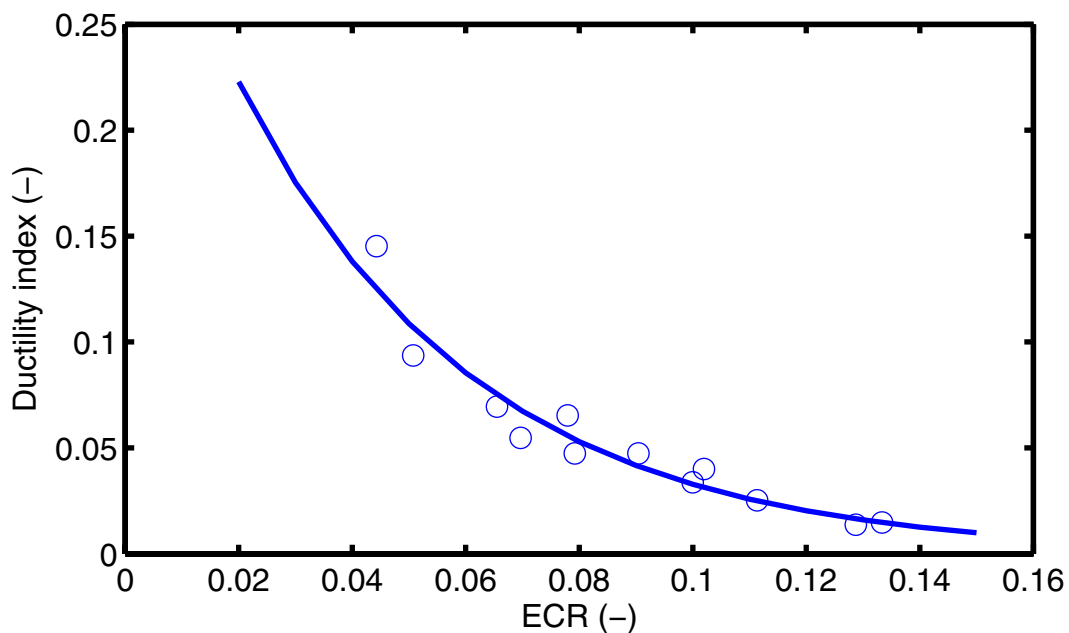


Figure 4.8: Normalized ductility index versus ECR for Zircaloy-4 clad specimens oxidized at 1473 K to various exposures, then quenched and subjected to ring compression tests; based on Udagawa et al. (2006).

Udagawa et al. also found that the area fraction is nearly constant irrespective of the rate of the slow cooling, and thus conclude that the effect of cooling rate on the post-quench ductility is negligible in the considered cooling rate range.

4.2 Thermal shock tests at KAERI

Similar thermal shock tests and methodology as the JAERI tests, discussed in the preceding section, have recently been employed by workers at the Korea Atomic Energy Research Institute (KAERI) to investigate the embrittlement behaviour of Zircaloy-4 clad during oxidation and water quench (Kim et al., 2005) and the effect of hydrogen content under LOCA conditions (Kim et al., 2006). In particular, Jun Hwan Kim and colleagues performed simulated LOCA tests on standard as-received Zircaloy-4 cladding (with outer diameter of 9.5 mm and wall thickness of 0.57 mm) to evaluate the consequence of thermal shock during the injection of emergency core coolant. Zircaloy-4 tubes of length 330 mm were used in a LOCA simulation test facility. To simulate the LOCA condition, the specimen was oxidized in a flowing steam at a prescribed temperature (1273-1523 K) and exposure time, and then the specimen was cooled at an intermediate temperature of 973 K for 100 s after oxidation, and then quenched in water at room temperature. After this test, compression test was performed on ring samples cut from the tube (15 mm) to examine the oxidized clad ductility (figure 4.9). In addition, the microstructure of the oxidized specimen was investigated by an optical microscope to measure the thickness of each layer. Absorbed hydrogen content was measured in the oxidized samples by gas analysis.

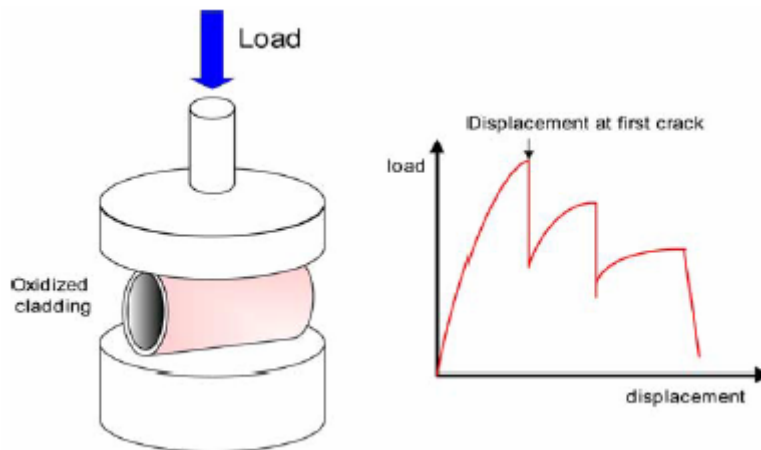


Figure 4.9: Schematic picture of the ring-compression test made by Kim et al. (2005).

The oxide layer growth followed a parabolic law according to Kawasaki's relation (appendix A). However, ECR was calculated for the specimens using the Baker-Just relation (appendix A). A correlation between the ring compression ductility and ECR was obtained for the oxidized Zircaloy-4. The correlation shows that the ductility decreases rapidly as ECR increases from about 7% to 25%. Above ECR \approx 25%, the cladding fragmented into pieces as observed by Kim et al. (figure 4.10). All the failed specimens during quenching showed a displacement prior to failure below 0.2 mm. Kim et al. (2005) also found a relationship between hydrogen uptake during the high temperature oxidation and ECR. The hydrogen uptake rate increases rapidly as oxidation proceeds and at ECR of about 25% failure occurs, while the absorbed hydrogen content varied between 300 to 800 wppm (figure 4.11).

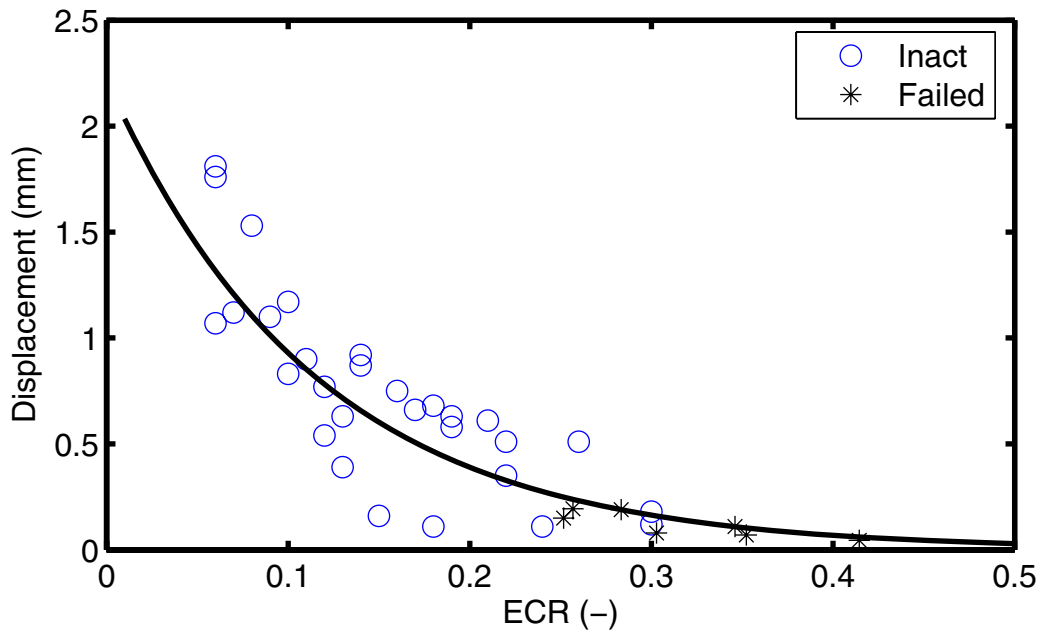


Figure 4.10: Relation between ECR and the displacement at the first crack (ductility) for oxidized Zircaloy-4 from ring-compression test (cf. figure 4.11) by Kim et al. (2005).

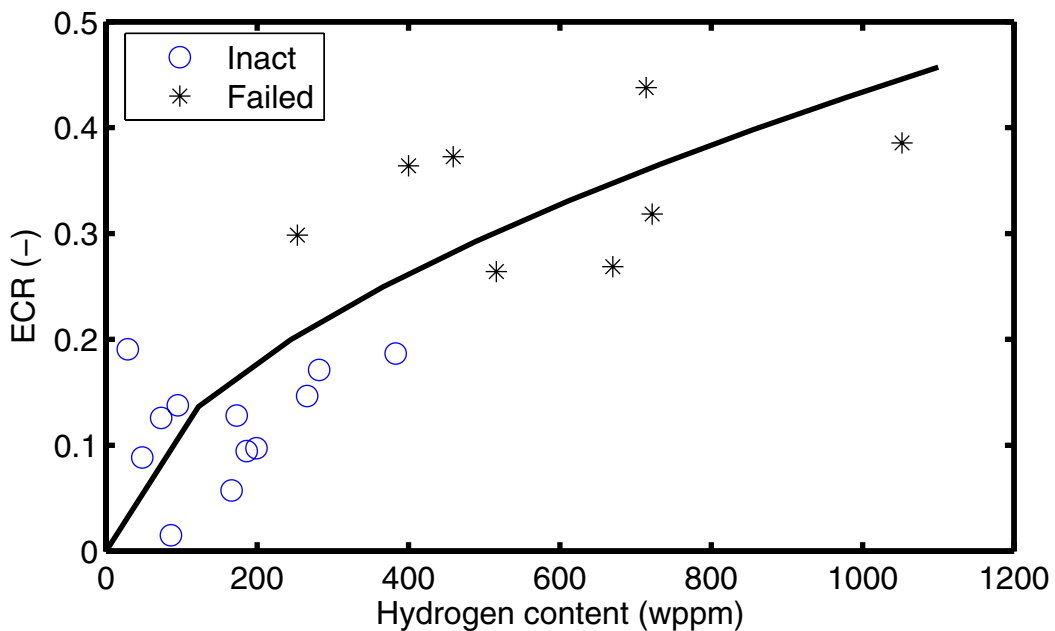


Figure 4.11: Relation between hydrogen pickup during oxidation and ECR for Zircaloy-4 by Kim et al. (2005), cf. figure 4.10.

The effect of pre-oxidation (up to 50 μm) and pre-hydring (up to 1000 wppm H) on the behaviour of Zircaloy-4 clad during LOCA was studied in a subsequent paper by the KAERI investigators (Kim et al., 2006), from which in section 3.2, we described some of their results concerning clad ballooning and burst temperature (table 3.2). This work indicated that the threshold ECR is reduced by pre-oxidation and pre-hydring; in particular, new data on ECR vs. displacement as in figure 4.10, showed that the ductility

of the as-received specimens became close to zero for $ECR \geq 20\%$, whereas the ductility of hydrogen charged specimens was sharply reduced regardless of the ECR value (figure 10 of Kim et al., 2006).

4.3 LOCA integral tests at ANL

The Argonne National Laboratory (ANL) workers have conducted integral LOCA tests on high burnup BWR Zircaloy-2 (Yan et al., 2004b) and PWR Zircaloy-4 cladding tubes. The Zircaloy-2 specimens were from Limerick BWR fuel rods irradiated to burnup of 56 MWd/kgU and the Zircaloy-4 specimens from H. B. Robinson PWR fuel rods. Since, only the BWR results were available to us, in a report form (Yan et al., 2003, 2004b), we focus our discourse on these rods. An overview of the PWR results is available from the USNRC archive as a slide presentation (Billone et al., 2005).

The aim of the integral LOCA tests on high burnup fuel rod segments from the BWR were to address the adequacy of the embrittlement criteria, the design oxidation correlations used and the effect of irradiation, in particular, the impact of water side corrosion and hydrogen uptake. The four LOCA tests consisted of: (1) The in-cell specimen (ICL#1) heated to rupture in argon gas and slowly cooled, (2) the specimen (ICL#2) was exposed to a LOCA sequence with exception of quench, (3) the specimen (ICL#3) subjected to a partial quench (1073 K to 713 K) before failure, (4) A full LOCA sequence on the test specimen (ICL#4). In the as-discharged condition, the Limerick clad (Zr-lined Zircaloy-2 GE-11 9×9 design) had a corrosion layer of about 10 μm , and a hydrogen content around 70 wppm. The specimens were internally pressurized to a gauge pressure of about 8.3 MPa at 573 K.

The ANL integral LOCA tests consist of rapidly heating (5 K/s) a 300 mm long fuel rod segment (with UO_2 pellets) under internal gas rod pressure in a steam environment, holding it at a temperature of about 1473 K for around 5 minutes or less, cooling it at the rate of 3 K/s to 1073 K, and then quenching the rod segment with room temperature water. An illustration of the LOCA test sequence vis-à-vis temperature and pressure history is shown in figure 4.12. The LOCA integral in-cell apparatus comprises radiant furnace, argon purge system, high pressure system to internally pressurize the 300 mm long test specimen, steam supply system and quench system. The study also included a reference rod, tested in the out-of-cell LOCA integral test facility for unirradiated specimens. The out-of-cell apparatus has the same features as the in-cell apparatus used for irradiated materials. The out-of-cell apparatus was used to obtain baseline data for unirradiated Limerick archival Zircaloy clad rod (Zr-lined Zircaloy-2 GE-11 9×9 design) with 11.18 mm outer tube diameter, wall thickness of 0.71 mm, and ZrO_2 dummy pellets (the out-of-cell specimen, OCL#11).

Some results of the tests from (Yan et al., 2004b) are summarized in table 4.2. The burst temperatures for the LOCA in-cell tests were in the range from 1003 to 1063 K, and their burst lengths were in the range of 11-15 mm. The concentrations of oxygen and hydrogen were determined by the method described in (Yan et al., 2003).

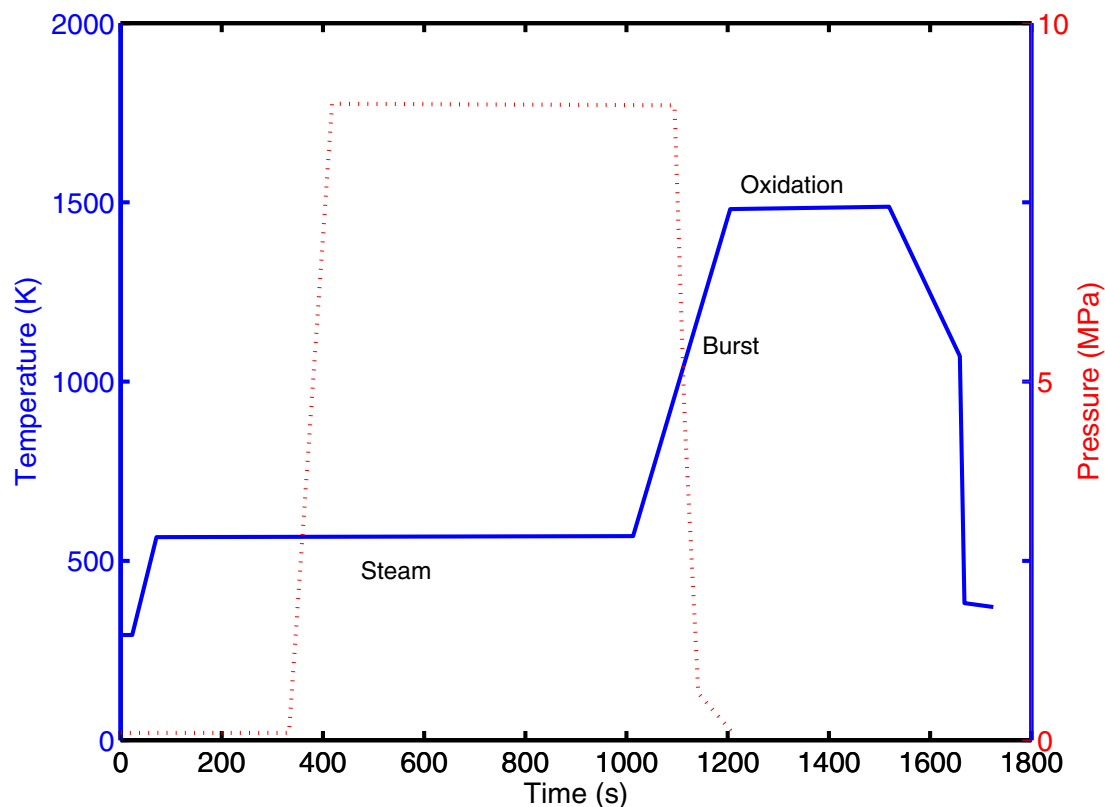


Figure 4.12: Temperature and pressure (red dotted line) histories for the full LOCA integral test sequence employed by Yan et al. (2004b).

Parameter	ICL#1	ICL#2	ICL#3	ICL#4	OCL#11
Hold time, s	0	300	300	300	300
Max. pressure, MPa	8.96	8.87	9.0	8.86	8.61
Burst pressure, MPa	≤ 8.61	≤ 8.01	8.6	8.0	≤ 7.93
Burst temperature, K	1028	1023	1003	1063	1023
Max $\Delta D / D_0$, %	38 ± 9	39 ± 10	43 ± 9	36 ± 9	43 ± 10
Max calculated ECR, %	0	20	21	20	21
Max hydrogen pickup, wppm	...	> 220	≥ 2900	...	3900

Table 4.2: Some data on ANL in-cell LOCA integral tests (ICL) with high-burnup clad specimens from the Limerick BWR. Included are also results of an out-of-cell test OCL#11 with unirradiated Zircaloy-2 clad (Yan et al., 2004b).

The ECR values listed in table 4.2 were calculated for two-sided oxidation using the Cathcart-Pawel relation (appendix A). As can be seen from table 4.2, the results of the high burnup rod segments are very similar to the unirradiated rod, i.e., the irradiation to high burnup did not affect the LOCA behaviour in the integral tests. Nevertheless, we should note that the selected high burnup rod had a low oxide layer thickness (10 μm) and low hydrogen content (70 wppm) and due to this, the results are not unexpected. It would be more challenging to test high burnup BWR rod segments with oxide thicknesses $\approx 70 \mu\text{m}$ and hydrogen contents ≥ 500 wppm. Also, the integral tests should be performed under mechanical constraint, as in the JAERI program, to emulate a more realistic boundary condition.

The axial distributions of measured ECR and hydrogen pickup are presented in figures 4.13 (unirradiated rod) and 4.14 (irradiated rods). For the unirradiated rod the axial distribution of ECR peaks at the centre of the burst region where the clad is thinnest and the oxidation is completely two-sided. The ECR drops down away from the burst centre where the clad wall thickness increases and the extent of the inner surface oxidation reduces. On the other hand, the hydrogen pickup during oxidation peaks near the balloon neck sections and is minimal at the burst centre. Since the hydrogen ridges cause embrittlement of clad, Yan and company decided to determine the magnitude of such phenomenon in high burnup BWR clad specimens (figure 4.14). It is seen that for the irradiated specimens the hydrogen crests are shifted toward the burst centre, compared with the unirradiated samples. The peak hydrogen pickup numbers, however, are comparable between these specimens.

As alluded earlier, the ANL group has also examined high burnup Zircaloy-4 specimens from H. B. Robinson (HBR) PWR fuel rods. The HBR specimens' burnup were around 64 MWd/kgU with a waterside corrosion resulting in an oxide layer thickness of around 70 μm and hydrogen content up to 760 ± 60 wppm (Billone et al., 2005). The clad, which had a residual metal thickness of 0.72 mm, was de-fuelled and subjected to two-sided oxidation according to a prescribed temperature history. Afterward, ring compression tests were made at 408 K. According to a recent article (Vitanza, 2006), the ductile-to-brittle transition for this sample occurred at $\text{ECR} \approx 0.11$ (calculated with the Baker-Just relation, appendix A), which is a moderate reduction from the acceptance limit of $\text{ECR} = 0.17$. In terms of temperature reduction, this gives roughly 80 K reduction in clad temperature limit, i.e., the temperature limit is reduced from 1473 K to 1393 K.

Recently, R. O. Meyer (2006) also presented some data (without reference to their source), which showed that an ample reduction in ductility by comparing a high burnup Zircaloy-4 specimen (80 μm oxide layer) and a fresh Zircaloy-4 sample. More specifically, the measured ductility as a function of calculated ECR (using the Cathcart-Pawel relation, appendix A) at 1473 K showed nearly nil-ductility behaviour at $\text{ECR} \approx 0.17$ for the unirradiated sample and $\text{ECR} \approx 0.10$ for the irradiated sample, both tested at 408 K.

ANL's ring compression tests at 408 K on hydrogenated, unirradiated 15 \times 15 PWR Zircaloy-4 clad samples (with outer diameter 10.75 mm, wall thickness 0.76 mm) oxidized at 1477 K, indicated a ductile-brittle transition at the calculated (Baker-Just) $\text{ECR} = 0.063$ for hydrogen content ≥ 600 wppm and at $\text{ECR} \approx 0.095$ for H content ≈ 400 wppm (Vitanza, 2006). For 17 \times 17 Zircaloy-4 clad (outer diameter 9.5 mm, wall thickness 0.57 mm), the ductile-brittle transition occurred at $\text{ECR} \approx 0.13$ for H content ≥ 300 wppm (Vitanza, 2006). Results from similar tests on ZIRLO and M5 alloys will be reported (Yan et al., 2004a). The results of oxidation of the latter two alloys and Zircaloy-4 were compared in section 3.1.4.

To our knowledge, the aforementioned results of the ANL group have not yet been published as journal articles subjected to peer-review and independent scrutiny, where necessary details are to be provided. Nevertheless, if the ANL results are accurate and reproducible, new modifications of the LOCA criteria for high burnup fuel rods may become necessary.

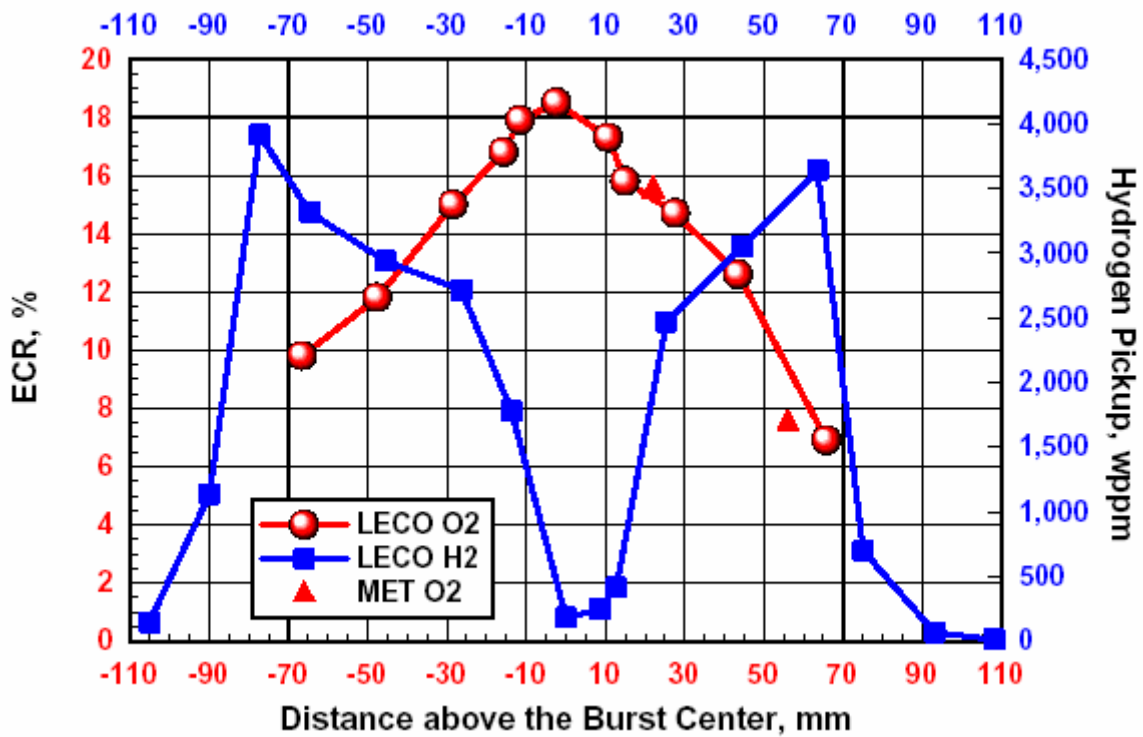


Figure 4.13: Axial distributions of hydrogen pick up and ECR for ANL out-of-cell LOCA test OCL#11 with unirradiated Zircaloy-2 clad (Yan et al., 2004b).

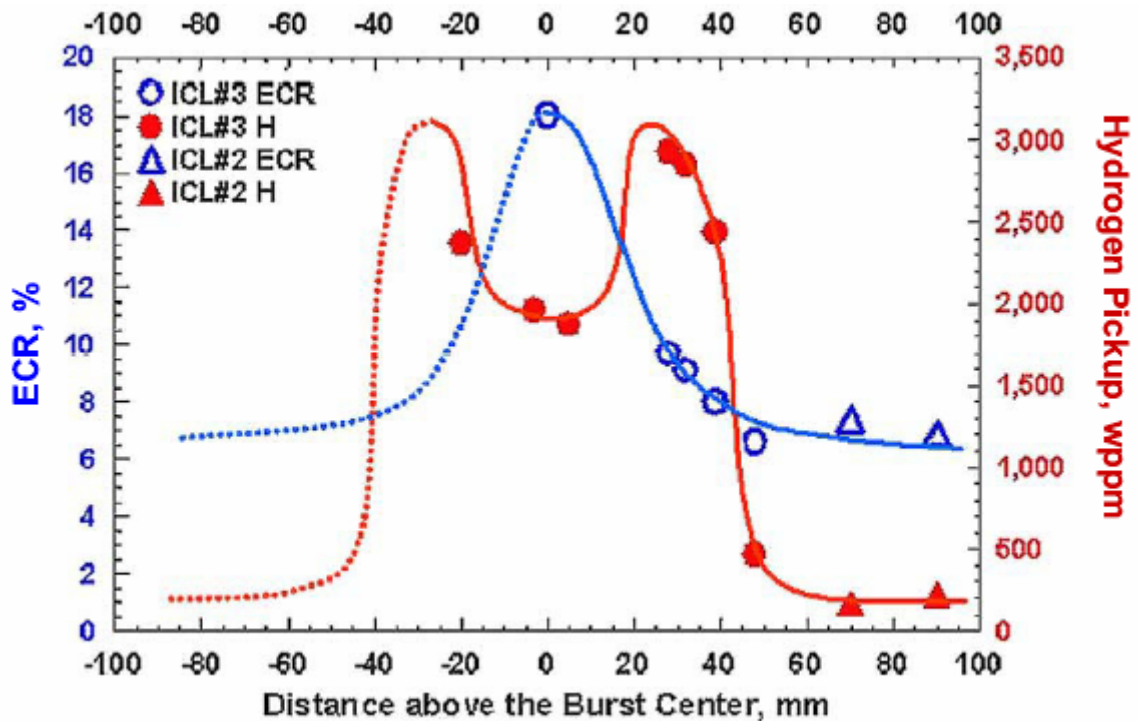


Figure 4.14: Axial distributions of hydrogen pickup and ECR for ANL in-cell LOCA tests (ICL#2, ICL#3) with high burnup BWR Zircaloy-2 clad (Yan et al., 2004b).

4.4 Multi-rod tests at NRU

Multi-rod tests simulating LOCA conditions in a test loop of the NRU reactor at Chalk River, Canada, were conducted with the objective of understanding the deformation and flow blockage behaviour within a fuel bundle of 32 PWR full-length rods. Parsons et al. (1986) and recently Grandjean (2005) have reviewed these experiments and the interested reader can refer to these reviews and the references therein for more details. The test assembly consisted of a 6×6 bundle with the 4 corner rods removed, the 20 non-pressurized rods making a protection rig for the 12 inner pressurized rods. The rods were full-length 17×17 type PWR rods with an active length of 3.66 m. The tests were conducted with fresh UO₂ fuel “conditioned” by rapidly raising to full power three times just prior to the experiment.

Seven LOCA experiments were conducted from October 1980 to May 1982. They comprised three thermal-hydraulic tests (HTs) and four so-called material tests (MTs). The HTs were used for calibration of the boundary conditions of the MTs. The main results of the material tests are summarized in table 4.3 below. In addition, the maximum of mean assembly deformation, defined as the maximum value of the average deformation at a given axial level, for tests MT-1 and MT-2 were reported to be 37.2% and 36.5%, respectively, corresponding to flow blockage ratios of 70% and 67%, respectively (Grandjean, 2005). In MT-3 and MT-4 the flow blockage values were 68% and 100%, respectively.

The rod deformations were reported to be co-planar especially in MT-3 due to the impact of spacer grids that restrained the deformation locally. The influence of flow reduction on the heat transfer in the deformed region seems to be balanced by the increase in turbulence. It was concluded that the coolability of deformed bundle is relatively insensitive to the extent of average deformation, over the range of blockages exhibited in these tests.

Test #	PCT K	Failed/Total #	Reflood start time s	Rupture time s	Max. strain %
MT-1	1144	6/11	32	70	60
MT-2	1161	8/11	...	65	70
MT-3	1067	12/12	9	133	94
MT-4	1094	12/12	57	55	96

Table 4.3: Some data on multi-rod LOCA material tests performed at NRU. PCT is the peak clad temperature, Failed/Total designates the number of failed pressurized rods relative to the total number of pressurised rods. Maximum strain is the clad peak axial, radial average strain.

4.5 The PHEBUS-LOCA program

The PHEBUS-LOCA program conducted by CEA Cadarache simulated in-pile LOCA experiments on fuel rods in a bundle configuration. As an integral test, the main

objective of PHEBUS-LOCA was to generate pertinent data for validation of predictive computer codes for large break LOCA analysis of PWRs in France (Réocreux & Scott de Martinville, 1990). Recently, Grandjean (2005) has reviewed this program and we refer the interested reader to this report and the references therein; here we only delineate a few highlights of the program.

Other missions of the program were (Réocreux & Scott de Martinville, 1990):

- a. Verification of clad deformation and rupture data obtained by separate effect tests (EDGAR tests, see section 3).
- b. Quantification of maximum flow blockage ratios that could occur during a LOCA and their impact on possible clad failure propagation modes, also generation of data for evaluation of the coolability of damaged assemblies.
- c. Provision of data on clad oxidation under LOCA, the axial extent of internal oxidation in failed rods, structure of oxidized clad, i.e., the extent of ZrO_2 and α -Zr (O) brittle layers.
- d. An appraisal of the actual performance of deformed clad oxidized up to 17% wall thickness to withstand thermal shock during a PWR prototype reflooding (LOCA criterion).

The experimental PHEBUS-LOCA program was conducted from 1980 to 1984. It included 3 single rod tests and 22 tests with 5×5 fuel rod bundles. Among the bundle tests, only 7 contained pressurized rods, the remaining non-pressurized rods were used mostly to examine the thermal-hydraulic behaviour from the blowdown to reflood stage of LOCA and to adjust the experimental procedure for the pressurized rods. The rods had an active length of 800 mm and were of 17×17 PWR type with standard Zircaloy-4 clad.

The first test series consisted of eight thermal-hydraulic experiments using un-pressurized rods and one burst test. These experiments were conducted with the fuel rod bundle contained within an unheated shroud. In the burst test, 21 of the rods were initially pressurized to 4 MPa in order to make them burst in the high α -Zr phase region, the remaining rods did not deform owing to their low internal pressure.

The pressurized rods ruptured within 14 s of one another at the top of ramp level of the transient at about 1110 K in steam, just prior to reflooding. The scatter in rupture times was considered to have resulted from non-uniform rewetting which affected clad deformation by accentuating circumferential temperature gradients. Examination of the bundle revealed clad deformations with hoop strains greater 33% over an axial distance of about 80 mm in the rods in the central 3×2 array, which had not been affected by the non-uniform rewetting.

The strains in the peripheral rods were considerably lower, 15-35% compared with those positioned in the central 3×2 array, 43-53%. This was due to the steep circumferential temperature gradients caused by unheated shroud. The four tie rods in the bundle provided sufficient mechanical restraint to induce ballooning in the 3×2 array. The average flow restriction for the central 3×3 (including 3 rods with low strains) was 65%. However, the largest single flow channel reduction was about 80%.

4.6 LOCA testing at Halden

The Halden LOCA testing is an ongoing program designed to conduct single rod integral in-pile tests under LOCA conditions in the Halden reactor, Halden, Norway. The tests will examine LWR fuel rods irradiated to various burnups (40-60 MWd/kgU) and will focus on the effects that are different from those studied in out-of-pile tests (Lestinen et al., 2003; Kolstad et al., 2004a). Particularly, the test conditions are selected: (i) to maximize clad ballooning under LOCA conditions for enhancing fuel relocation and to examine its possible impact on clad temperature and oxidation, (ii) to investigate the extent of secondary hydriding on the inner side of the clad close to the burst region. Target peak clad temperatures are set at 1073 K and 1373 K.

Tests have been performed on fresh fuel rods for calibration and baseline data on Zircaloy-4 clad (Kolstad et al., 2004a). For example, a test on a fresh PWR fuel rod was performed in IFA-650.2 that consisted of a blowdown phase, heat-up, hold at peak clad temperature of 1323 K and termination by reactor scram, figure 4.15 (Kolstad et al., 2004b). The rod rupture occurred at 1073 K as revealed by the rod pressure and elongation measurements as well as by gamma ray monitoring. The hold time above 1173 K was 390 s and the average temperature increase rate, between 873 and 1073 K, was about 7 K/s. The circumferential temperature variation was within $\Delta T = \pm 2 - 3$ K and the tensile hoop stress ≈ 55 MPa. According to Kolstad et al. (2004b), computations made with the programs GENFLO/FRAPTRAN on peak clad temperature, the time to rupture and the rupture temperature agreed well with the results of measurements.

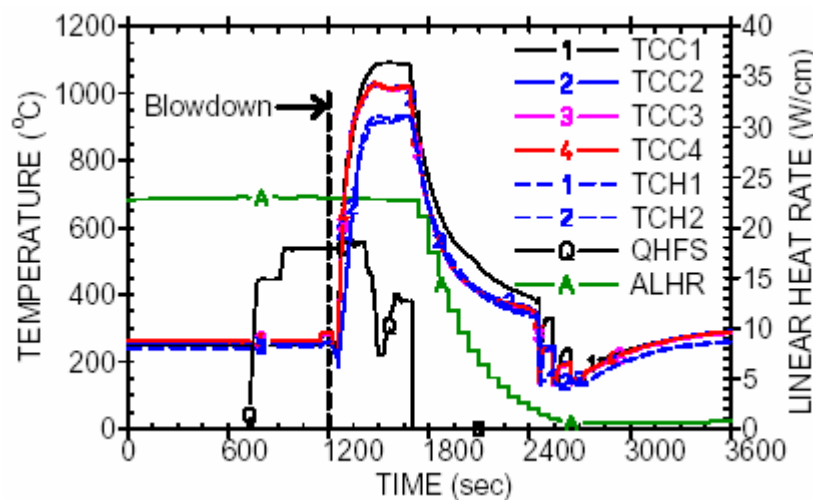


Figure 4.15: Clad, heater, loop inlet and outlet temperatures during the trial Halden LOCA test. Also fuel and heater powers are shown. A = fuel power, Q = heater power, I = inlet loop temperature, dashed 1-2 = heater temperature (Kolstad et al., 2004a).

5 Conclusions

In this report we delineated some past important and recent experimental results for modelling LWR fuel clad behaviour during LOCA conditions. We discussed the background to the acceptance criteria for LOCA, that is to say, clad embrittlement phenomenology, clad embrittlement criteria (maximum clad oxidation and peak clad temperature) and the experimental bases for the criteria.

Two broad kinds of tests have been carried out to understand and quantify fuel rod behaviour under LOCA conditions: (i) Separate effect tests to study clad oxidation, clad deformation and rupture, and zirconium alloy allotropic phase transition during LOCA. (ii) Integral LOCA tests, in which the entire LOCA sequence is simulated on a single rod or a multi-rod array in a fuel bundle, in laboratory or in a test reactor, to study the overall behaviour of fuel rod under LOCA. These tests provide the foundation for LOCA acceptance criteria and design of LWR systems.

The results of recent experimental studies conferred in this report indicate that clad alloy composition and high burnup effects influence LOCA acceptance criteria margins. Replacement of Zircaloy-4 clad in many PWRs (which form the bulk of experimental data generated on LOCA conditions) with Zr-Nb base alloys affects both thermodynamics and mechanical properties of clad under LOCA. Niobium stabilizes the β -Zr phase, while tin (in Zircaloy) is an α -Zr stabilizer. Oxygen is also an α -Zr stabilizer. So the thermodynamics of the ternary system Zr-Sn-O is different from Zr-Nb-O. High burnup effects on clad, namely corrosion and in particular hydriding affect thermodynamics and mechanical properties. Recent research on the Zr-O-H system has established that $\alpha/(\alpha+\beta)$ and $(\alpha+\beta)/\beta$ phase boundaries in the Zr-O binary shifts to lower temperatures with the presence of hydrogen and the dissolved hydrogen causes the oxygen content of β phase to increase, hence enhancing embrittlement in the prior β phase during the quenching stage of LOCA. The thermodynamics assessment of the ternary Zr-Nb-H and quaternary Zr-Nb-O-H systems will help to resolve existing ambiguities.

Review of oxidation experiments and models indicates that the Baker-Just relation in general bounds the oxidation data, while the Cathcart-Pawel relation provides a best-estimate description. Furthermore, the method of oxidation calculation is appropriate. However, recent experiments on Zircaloy-4 show that the Baker-Just relation underestimates the oxidation rate at temperatures below 1000 K. Furthermore, these relations are appropriate at atmospheric pressure. At pressures from 5 MPa and higher the relations underestimate the oxidation rate increasingly. Some oxidation tests on high burnup PWR fuel (49 MWd/kgU) clad have shown that the oxide mass gain for irradiated clad is similar to unirradiated clad under LOCA conditions. Pre-oxidized clad exhibited less oxide mass gain and no effect of hydrogen absorption (740 wppm) on oxidation behaviour was detected. In contrast, some investigators' results show that at 1323 K and 1523 K, the oxidation rate of Zircaloy-4 samples (hydrogenated to 500 wppm) increases relative to the as-received specimens, by about 9% and 23%, respectively. Nevertheless, this enhancement in mass gain disappeared for hydrogen contents larger than 1000 wppm. More investigation on this effect deems to be necessary to resolve the issue.

The clad creep strength tests indicate that a Zr-1Nb alloy has slightly lower creep strength than Zircaloy, that is to say, the clad burst time is slightly shorter in Zr-1Nb alloy than in Zircaloy-4. This is attributed to a lower allotropic phase transition temperature of Zr-1Nb alloy compared to Zircaloy. Moreover, in the ($\alpha+\beta$)-phase temperature domain, the burst stress of the Zr-1Nb is lower than in Zircaloy-4. As regards the effect of hydrogen, Zircaloy-4 samples, pre-hydrided to 600 wppm H, had a lower burst stress than the as-received ones (which usually contain about 8 wppm H).

In regard to recent separate effect data, we suggest that the following phenomena should be modelled in the available thermal-mechanical fuel rod code for LOCA.

- The phase transformation kinetics of Zr-Nb base alloy should rigorously be modelled, including the impact of high hydrogen content.
- The clad burst criterion for Zr-Nb base alloy should be evaluated and the effect of hydrogen should be modelled.
- The effect of pressure on clad oxidation should be accounted for in the oxidation model.
- The ductility of Zr-Nb base alloy and the effect of high hydrogen content need further experiments and evaluation.

The general equations and calculation methodology have already been outlined in section 3.4.

The LOCA integral tests discussed in section 4 offer the wealth of data for modelling fuel rod behaviour under the different stages of LOCAs. Valuable data have been and are being produced by the JAERI integral thermal shock tests and the ANL LOCA integral tests. The ongoing LOCA testing in the Halden reactor (IFA-650 series) will also produce useful data for modelling and code verification. The evaluation of the integral tests requires an appropriate thermal-hydraulic code to describe the test boundary conditions coupled to a fuel rod behaviour code to describe clad performance under LOCA.

Acknowledgement

The author is indebted to Tero Manngård for a careful reading of the manuscript and valuable suggestions thereof. And thanks are also due to Jan In de Betou for critical comments.

6 References

- Abriata, J. P., Garces, J., Versaci, R., 1986.
The O-Zr (oxygen-zirconium) system,
Bulletin of Alloy Phase Diagram 7, 116-124.
- AEC, 1973.
Opinion of the commission,
Docket No. RM-50-1.
- Arias, D., Guerra, C., 1987.
Phase transition temperature in Zircaloy-2,
J. Nucl. Mater. 144, 196-199.
- Bai, J. B., Prioul, C., Francois, D., 1994.
Hydride embrittlement in Zircaloy-4 plate: Part I. Influence of microstructure on hydride embrittlement in Zircaloy-4 at 20°C and 350 °C,
Metallurgical and Materials Transactions A, 25A, 1185-1197.
- Baker, L., Just, L. C., 1962.
Studies of water-metal reactions at high temperatures III. Experimental and theoretical studies of zirconium water reactions,
Technical Report ANL-6548, Argonne National Laboratory, Argonne, IL, USA.
- Ballinger, R. G., Dobson, W. G., Biederman, R. R., 1976.
Oxidation reaction kinetics of Zircaloy-4 in an unlimited steam environment,
J. Nucl. Mater. 62, 213-220.
- Baum, W. L., 1963.
Phase transformations at high temperatures in hafnia and zirconia,
Science 140, 1330-1331.
- Billone, M. C., Yan, Y., Burtseva, T. A., 2004a.
Post-quench ductility of advanced alloy cladding,
Transactions of the 2004 Nuclear Safety Research Conference, Washington DC,
October 25-27, 2004, NUREG/CP-0180, 43-45.
- Billone, M. C., Yan, Y., Burtseva, T., 2004b.
Post-quench ductility of Zircaloy, ZIRLO, M5 and E110,
SEGFSM Topical Meeting on LOCA Issues, Argonne National Laboratory, May 25-26,
2004.
- Billone, M.C., Yan, Y., Burtseva, T., Chung, H., 2005.
H. B. Robinson high burnup PWR oxidation and post-quench ductility,
Presentation slides, Argonne National Laboratory, February 10, 2005.
- Bodansky, D., 2004.
Nuclear Energy, 2nd Edition,
Springer AIP Press, New York, 2004.

- Brachet, J. C., Portier, L., Forgeron, T., et al., 2002.
Influence of hydrogen content on the α/β phase transformation temperatures and on the thermal-mechanical behaviour of Zy-4, M4 (ZrSnFeV) and M5TM (ZrNbO) alloys during the first phase of LOCA transient,
Zirconium in the Nuclear Industry, 13th International Symposium., Moan, G. D., Rudling, P. (Eds), ASTM STP 1423, American Society for Testing and Materials, West Conshohocken, PA, USA, 673-701.
- Bradhurst, D. H., Heuer, P. M., 1975.
The effects of deformation on the high-temperature steam oxidation of Zircaloy-2,
J. Nucl. Mater. 55, 311-326.
- Bramwell, I. L., Haste, T. J., Worswick, D., Parsons, P. D., 1994.
An experimental investigation into the oxidation of Zircaloy-4 at elevated pressures in the 750 to 1000°C temperature range,
Zirconium in the Nuclear Industry, 10th International Symposium, Garde, A. M., Bradley, E. R. (Eds), ASTM STP 1245, American Society for Testing and Materials, Philadelphia, PA, USA, 450-465.
- Brown, A. F., Healey, T., 1980.
The kinetics of total oxygen uptake in steam-oxidized Zircaloy-2 in 1273-1673 K,
J. Nucl. Mater. 88, 1-6.
- Bunnell, L. R., Bates, J. L., Mellinger, G. B., 1983.
Some high-temperature properties of Zircaloy oxygen alloys,
J. Nucl. Mater. 116, 219-232.
- Burton, B., 1983.
Creep fracture processes in Zircaloy,
J. Nucl. Mater. 113, 172-178.
- Böhmert, J., 1992.
Embrittlement of ZrNb1 at room temperature after high-temperature oxidation in steam atmosphere,
Kerntechnik 57, 55-58.
- Böhmert, J., Dietrich, M., Linek, J., 1993.
Comparative studies on high-temperature corrosion of ZrNb1 and Zircaloy-4,
Nucl. Engin. & Design 147, 53-62.
- Canay, M., Danon, C. A., Arias, D., 2000.
Phase transition temperatures in the Zr-rich corner of Zr-Nb-Sn-Fe alloys,
J. Nucl. Mater. 280, 365-371.
- Cathcart, J. V., Pawel, R. E., McKee, R. A., et al., 1977.
Zirconium metal-water oxidation kinetics: IV. Reaction rate studies,
Technical report ORNL/NUREG-17, Oak Ridge National Laboratory, TN, USA.

- Christian, J. W., 2002.
The theory of phase transformations in metals and alloys,
Pergamon, Amsterdam, 2002.
- Chung, H. M., 2005.
Fuel behavior under loss-of-coolant accident situations,
Nucl. Engin. & Technol. 37, 327-362.
- Chung, H. M., Garde, A. M., Kassner, T. F., 1976.
Mechanical properties of Zircaloy containing oxygen,
in, Light Water Reactor Safety Research Program Quarterly Report, ANL-77-10,
Argonne National Laboratory, Argonne, IL, USA.
- Chung, H. M., Garde, A. M., Kassner, T. F., 1977.
*Deformation and rupture behavior of Zircaloy cladding under simulated loss-of-coolant
accident conditions*,
Zirconium in the Nuclear Industry, ASTM STP 633, Lowe Jr., A. L., Parry, G. W.
(Eds.), American Society for Testing and Materials, 82-97.
- Chung, H. M., Kassner, T. F., 1979.
Pseudobinary Zircaloy-oxygen phase diagram,
J. Nucl. Mater. 84, 327-339.
- Chung, H. M., Kassner, T. F., 1980.
*Embrittlement criteria for Zircaloy fuel cladding applicable to accident situations in
light-water reactors: summary report*,
NUREG/CR-1344, ANL-79-48, Argonne National Laboratory, Argonne, IL, USA.
- Comstock, R. J., Schoenberger, G., Sabol, G. P., 1996.
*Influence of processing variables and alloy chemistry on the corrosion behaviour of
ZIRLO nuclear fuel cladding*,
Zirconium in the Nuclear Industry, 11th International Symposium, Bradley, E. R., Sabol,
G. P. (Eds), ASTM STP 1295, American Society for Testing and Materials, West
Conshohocken, PA, USA, 710-725.
- Donaldson, A. T., Evans, H. E., 1981.
Oxidation-induced creep in Zircaloy-2,
J. Nucl. Mater. 99, 38-46.
- Douglass, D. L., 1971.
The metallurgy of zirconium,
Supplement 1971, International Atomic Energy Agency, Vienna, Austria.
- Erbacher, F. J., 1981.
*LWR cladding deformation in a LOCA and its interaction with the emergency core
cooling*,
ANS/ENS Meeting on Reactor Safety Aspects of Fuel Behaviour, Sun valley, Idaho,
USA, 2-6 August, 1981.

Erbacher, F. J., Neitzel, H. J., Wiehr, K., 1978.
Interaction between thermohydraulics in a LOCA – results of the REBEKA multi-rod burst tests with flooding,
The 6th Water Reactor Safety Information Meeting, Gaithersburg, MD, USA, November 1978.

Erbacher, F. J., Neitzel, H. J., Rosinger, H., Schmidt, H., Wiehr, K., 1982.
Burst criterion of Zircaloy fuel claddings in a loss-of-coolant accident,
Zirconium in the Nuclear Industry, ASTM STP 754, Franklin, D. G. (Ed), American Society for Testing and Materials, 271-283.

Erbacher, F. J., Leistikow, S., 1987.
Zircaloy fuel cladding behavior in a loss-of-coolant accident,
Zirconium in the Nuclear Industry, 7th International Symposium, Adamson, R. B., Van Swam, L. F. P. (Eds), ASTM STP 939, American Society for Testing and Materials, Philadelphia, PA, USA, 451-488.

Ferner, J., Rosinger, H. E., 1983.
The effect of oxygen on the failure of reactor fuel sheaths during a postulated loss-of-coolant accident,
Atomic Energy of Canada Limited, report AECL-7791.

Ferner, J., Rondeau, R. K., Rosinger, H. E., 1985.
A study of the effect of circumferential temperature variation on fuel-sheath strain in an inert atmosphere,
Atomic Energy of Canada Limited, report AECL-7789.

Ferner, J., Rosinger, H. E., 1985.
The effect of circumferential temperature variation on fuel-cladding failure,
J. Nucl. Mater. 132, 167-172.

Forgeron, T., Brachet, J. C., Barcelo, F., et al., 2000.
Experiment and modeling of advanced fuel rod cladding behavior under LOCA conditions: alpha-beta phase transformation kinetics and EDGAR methodology,
Zirconium in the Nuclear Industry, 12th International Symposium, Sabol, G. P., Moan, G. D. (Eds), ASTM STP 1354, American Society for Testing and Materials, West Conshohocken, PA, USA, 256-278.

Furuta, T., Uetsuka, H., Kawasaki, S., 1981.
Ductility loss of Zircaloy by inner surface oxidation during high temperature transient,
J. Nucl. Sci. Technol. 18, 802-810.

Grandjean, C., Cauvin, R., Waeckel, N., 1996.
French investigations of high burnup effect on LOCA thermomechanical behaviour, Part Two: Oxidation and quenching experiments under simulated LOCA conditions with high burnup clad material,
Twenty-fourth Water Reactor Safety Information Meeting, Vol. 1, Bethesda, Maryland, October 21-23, 1996. NUREG/CP-0157, 161-172.

- Grandjean, C., Cauvin, R., Jacques, P., 1998.
Oxidation and quenching experiments under simulated LOCA conditions with high burnup cladding under LOCA conditions. Revisions of previous data and main trends of recent tests,
Twenty-sixth Water Reactor Safety Information Meeting, Vol. 3, Bethesda, Maryland, October 26-28, 1998. NUREG/CP-0166, 191-199.
- Grandjean, C, 2005.
A state-of-the-art review of past programs devoted to fuel behaviour under LOCA conditions 1st Part. Clad swelling and rupture, assembly flow blockage,
IRSN Technical Report DPAM/SEMCA 2005/XX, Draft.
- Guillermet, A. F., 1991.
Thermodynamic analysis of the stable phases in the Zr-Nb system and calculation of the phase diagram,
Z. Metallkunde 82, 478-487.
- Hache, G., Chung, H. M., 2001.
The history of LOCA embrittlement criteria,
Proc. OEDC meeting on LOCA Fuel Safety Criteria, Aix-en-Provence, France March 22-23, 2001, NEA/CSNI/R (2001)18.
- Hehemann, R. F., 1972.
Transformations in zirconium-niobium alloys,
Canadian Metall. Quart. 11, 201-211.
- Higgins, G. T., Banks, E. E., 1966.
The basic features of the isothermal promonotectoid transformation in zirconium-2½ weight percent niobium alloy,
Electrochemistry Technology 4, 341-346.
- Hobson, D. O., 1973.
Ductile-brittle behavior of Zircaloy fuel cladding,
ANS Topical Meeting on Reactor Safety, Salt Lake City, UT, March 26 1973.
- Hobson, D. O., Rittenhouse, P. L., 1972.
Embrittlement of Zircaloy clad fuel rods by steam during LOCA transients,
Technical report ORNL-4758, Oak Ridge National Laboratory, TN, USA.
- Hofmann, P., Politis, C., 1979.
The kinetics of the uranium dioxide-Zircaloy reactions at high temperatures,
J. Nucl. Mater. 87, 375-397.
- Hofmann, P., Kerwin-Peck, D., 1984.
UO₂/Zircaloy chemical interactions from 1000 to 1700°C under isothermal and transient temperature conditions,
J. Nucl. Mater. 124, 80-105.

Holt, R. A., Sills, H. E., Sagat, S., 1980.
Models for kinetics of the phase transformations in Zircaloy-4,
Presented at the IAEA Specialist Meeting on Water Reactor Fuel Element Performance
Modelling, Blackpool, UK, 1980.

Hunt, C. E. L., Foot, D. E., 1977.
High temperature strain behavior of Zircaloy-4 and Zr-2.5% Nb fuel sheaths,
Zirconium in the Nuclear Industry, ASTM STP 633, Lowe Jr., A. L., Parry, G. W.
(Eds), American Society for Testing and Materials, 50-65.

IAEA, 2001.
Thermohydraulic relationships for advanced water cooled reactors,
Report IAEA-TECDOC-1203, International Atomic Energy Agency, Vienna, Austria.

Iglesias, F. C., Ducan, D. B., Sagat, S., Sills, H. E., 1985
*Verification of the FROM model for Zircaloy oxidation during high temperature
transients*,
J. Nucl. Mater. 130, 36-44.

Jones, P. M., Casadei, F., Laval, H., 1984.
*Modelling of azimuthal effects arising from interaction between clad deformation and
heat transfer under LB LOCA conditions*,
Nucl. Engin. & Design 79, 267-276.

Kawasaki, S., Furuta, T., Suzuki, M., 1978.
*Oxidation of Zircaloy-4 under high temperature steam atmosphere and its effect on
ductility of cladding*,
J. Nucl. Sci. Technol. 15, 589-596.

Kim, J. H., Lee, M. H., Choi, B. K., Jeong, Y. H., 2004.
Deformation of Zircaloy-4 cladding during LOCA transient up to 1200°C.
Nucl. Engin. & Design 234, 157-164.

Kim, J. H., Lee, M. H., Choi, B. K., Jeong, Y. H., 2005.
Embrittlement behavior of Zircaloy-4 cladding during oxidation and water quench,
Nucl. Engin. & Design 235, 67-75.

Kim, J. H., Choi, B. K., Baek, J. H., Jeong, Y. H., 2006.
*Effects of oxide and hydrogen on the behavior of Zircaloy-4 cladding during the loss-of-
coolant accident (LOCA)*,
Nucl. Engin. & Design 236, 2386-2393.

Kolstad, E., Wiesenack, W., Grismanovs, V., 2004a.
LOCA testing at Halden,
Proceedings of the Nuclear Fuel Sessions of the 2004 Nuclear Safety Research
Conference, Washington DC, October 25-27, 2004, NUREG/CP-0192, 159-161.

Kolstad, E., Grismanovs, V., Wiesenack, W., 2004b.
LOCA testing at Halden, second in-pile test in IFA-650.2,
Proceedings of the Nuclear Fuel Sessions of the 2004 Nuclear Safety Research
Conference, Washington DC, October 25-27, 2004, NUREG/CP-0192, 189-195.

- Leistikow, S., Schanz, G., v. Berg, A. E., 1979.
Investigations into the temperature transient steam oxidation in Zircaloy-4 cladding material under hypothetical PWR loss-of-coolant accident conditions,
 Karlsruhe Research Center Report, KfK 2810, Karlsruhe, Germany.
- Leistikow, S., Schanz, G., 1987.
Oxidation kinetics and related phenomena of Zircaloy-4 fuel cladding exposed to high temperature steam and hydrogen-steam mixtures under PWR accident conditions,
 Nucl. Engin. & Design 103, 65-84.
- Lehr, P., Debuigne, J., 1963.
Fragilisation du zirconium par l'oxygène en insertion,
 Proc. VIe Colloque de Métallurgie, North Holland Publishing Co., Amsterdam, 139.
- Lestinen, V., Kolstad, E., Wiesenack, W., 2003.
LOCA testing at Halden, trial runs in IFA-650,
 Proceedings of the 2003 Nuclear Safety Research Conference, Washington DC, October 20-22, 2003, NUREG/CP-0185, 299-309.
- Lemaignan, C., Motta, A. T., 1994.
Zirconium alloys in nuclear applications,
 Material Science and Technology, Nuclear Materials, Vol. 10B, Cahn, R.W., Haasen, P., Kramer, E.J. (Eds), VCH, Weinheim, Germany, chap. 7.
- Liang, P., Dupin, N., Fries, S. G., et al., 2001.
Thermodynamic assessment of the Zr-O binary system,
 Z. Metallkunde 92, 747-756.
- Lide, D. P., 2003.
CRC Handbook of Chemistry and Physics, 84th Edition,
 CRC Press, Boca Raton, FL, USA.
- Mallett, M. W., Albrecht, W. M., Wilson, P. R., 1959.
The diffusion of oxygen in alpha and beta Zircaloy-2 and Zircaloy-3 at high temperatures,
 J. The Electrochemical Soc. 106, 181-184.
- Manngård, T., 2007.
Evaluation of the FRAPTRAN-1.3 computer code,
 Quantum Technologies Technical Report, TR 06-007.
- Mardon, J. P., Charquet, D., Senevat, J., 2000.
Influence of composition and fabrication process on out-of-pile and in-pile properties of M5 alloy,
 Zirconium in the Nuclear Industry, 12th International Symposium, Sabol, G. P., Moan, G. D. (Eds), ASTM STP 1354, American Society for Testing and Materials, West Conshohocken, PA, USA, 505-522.

Mardon, J. P., Lesbros, A., Bernaudat, C., Waeckel, N., 2004.
Recent data on M5TM alloy under RIA and LOCA conditions,
In: Proceedings of the 2004 International Meeting on LWR Fuel Performance, Orlando,
Florida, September 19-22, 507-515.

Massih, A. R., Andersson, T., Witt, P., et al., 2004.
The effect of quenching rate on the alpha-to-beta phase transformation structure in zirconium alloys,
J. Nucl. Mater. 322, 138-151.

Massih, A. R., Dahlbäck, M., Limbäck, M., et al., 2006.
Effect of beta-to-alpha phase transition rate on corrosion behaviour of Zircaloy,
Corrosion Science 48, 1154-1181.

Meyer, R. O., 2006.
The U.S. Nuclear Regulatory Commission's research on fuel behaviour under accident conditions,
2006 International Meeting on LWR Fuel Performance, 22-26 October 2006,
Salamanca, Spain.

Miquet, A., Charquet, D., Allibert, C. H., 1982.
Solid state phase equilibria of Zircaloy-4 in the temperature range 750-1050°C,
J. Nucl. Mater. 105, 132-141.

Moalem, M., Olander, D. R., 1991.
Oxidation of Zircaloy by steam,
J. Nucl. Mater. 182, 170-194.

Nagase, F., Otomo, T., Tanimoto, M., Uetsuka, H., 2000.
Experiments on high burnup fuel behavior under LOCA conditions at JAERI,
Proceedings of ANS Topical Meeting on LWR Fuel Performance, Park City, Utah, 10-
13 April, 2000.

Nagase, F., Uetsuka, H., 2001.
Study of high burnup fuel behaviour under LOCA conditions at JAERI: hydrogen effects on the failure-bearing capability of cladding tubes,
Twenty-Ninth Water Reactor Safety Information Meeting, Washington DC, October 22-
24, 2001. NUREG/CP-0176, 335-342.

Nagase, F., Otomo, T., Uetsuka, H., 2003.
Oxidation kinetics of low-Sn Zircaloy-4 at the temperature range from 773 to 1573 K,
J. Nucl. Sci. Technol. 40, 213-219.

Nagase, F., Fuketa, T., 2004a.
Thermal shock resistance of irradiated PWR claddings,
Presentation in SEGFSM Topical Meeting on LOCA Issues, Argonne National
Laboratory, Argonne Illinois, USA, 25-26 May, 2004.

Nagase, F., Fuketa, T., 2004b.
Effect of pre-hydriding on thermal shock resistance of Zircaloy-4 cladding under simulated loss-of-coolant accident conditions,

J. Nucl. Sci. Technol. 41, 723-730.

Nagase, F., Fuketa, T., 2005.

Behavior of pre-hydrided Zircaloy-4 cladding under simulated LOCA conditions,
J. Nucl. Sci. Technol. 42, 209-218.

Nagase, F., Fuketa, T., 2006.

Fracture behaviour of irradiated Zircaloy-4 cladding under simulated LOCA conditions,
J. Nucl. Sci. Technol. 43, 1114-1119.

Neitzel, H. J., Rosinger, H., 1980.

The development of burst criterion for Zircaloy fuel cladding under LOCA conditions,
Atomic Energy of Canada Limited, report AECL-6420.

Nikulina, A. V., 2004.

Structural materials for elements of nuclear-reactor active zones, zirconium alloys in nuclear power engineering,
Metal Science and Heat Treatment, 46, 458-462.

Ocken, H., 1980.

An improved evaluation model for Zircaloy oxidation,
Nuclear Technology 47, 343-357.

Ozawa, M., Takahashi, T., Homma, T., Goto, K., 2000.

Behavior of irradiated Zircaloy-4 fuel cladding under simulated LOCA conditions,
Zirconium in the Nuclear Industry, 12th International Symposium, Sabol, G. P., Moan, G. D. (Eds), ASTM STP 1354, American Society for Testing and Materials, West Conshohocken, PA, USA, 279-299.

Park, K., Kim, K., Whang, J., 2000.

Pressure effects on high temperature Zircaloy-4 oxidation in steam,
ANS Topical Meeting on Light Water Reactor Fuel Performance, Park City, Utah, April 10-13, 2000.

Parsons, P. D., Hindle, E. D., Mann, C. A., 1986.

The deformation, oxidation and embrittlement of PWR fuel cladding in a loss-of-coolant accident: A state of the art report,
OECD NEA CSNI Report 129, December 1986.

Pawel, R. E., 1974.

Oxygen diffusion in beta Zircaloy during steam oxidation,
J. Nucl. Mater. 50, 247-258.

Pawel, R. E., Perkins, R. A., McKee, R. A., et al., 1977.

Diffusion of oxygen in beta-Zircaloy and high temperature Zircaloy-steam reaction,
Zirconium in the Nuclear Industry, ASTM STP 633, Lowe Jr., A. L., Parry, G. W. (Eds.), American Society for Testing and Materials, 119-133.

Pawel, R. E., Cathcart, J. V., McKee, R. A., 1979.

The kinetics of oxidation of Zircaloy-4 in steam at high temperatures,

J. The Electrochemical Soc. 126, 1105-1111.

Pawel, R. E., Cathcart, J. V., McKee, R. A., 1980.
Anomalous oxide growth during transient-temperature oxidation of Zircaloy-4,
Oxidation of Metals 14, 1-13.

Pemsler, J. P., 1962.
Studies on the oxygen gradients in corroding zirconium alloys,
J. Nucl. Mater. 7, 16-25.

Pemsler, J. P., 1965.
*Studies on the oxygen gradients in corroding zirconium alloys: III kinetics of the
oxidation of zirconium at high temperatures,*
J. The Electrochemical Soc. 112, 477-484.

Perez, R. J., Massih, A. R., 2007.
Thermodynamic evaluation of the Nb-O-Zr system,
J. Nucl. Mater. 360, 242-254.

Portier, L., Bredel, T., Brachet, J-C., et al., 2005.
*Influence of long service exposures on the thermal-mechanical behavior of Zy-4 and
M5™ alloys in LOCA conditions,*
J. ASTM International, February 2005, vol. 2, Paper ID JAI12468.

Réocreux, M., Scott de Martinville, E. F., 1990.
*A study of fuel behaviour in PWR design basis accident: an analysis of results from
PHEBUS and EDGAR experiments,*
Nucl. Engin. & Design 124, 363-378.

Rohatgi, U. S., Saha, P., Chexal, V. K., 1987.
*Considerations for realistic emergency core cooling system evaluation methodology for
light water reactors,*
Nuclear Technology 76, 11-26.

Rosinger, H. E., 1984.
*A model to predict the failure of Zircaloy-4 fuel sheathing during postulated LOCA
conditions,*
J. Nucl. Mater. 120, 41-54.

Rosinger, H. E., Bera, P. C., Clendening, W. R., 1978.
Steady-state creep of Zircaloy-4 fuel cladding from 940 to 1873 K,
Atomic Energy of Canada Limited, report AECL-6193.

Rosinger, H. E., Bera, P. C., Clendening, W. R., 1979.
Steady-state creep of Zircaloy-4 fuel cladding from 940 to 1873 K,
J. Nucl. Mater. 82, 286-297.

Rubenstein, L. S., Goodwin, J. G., Shubert, F. L., 1961.
Effect of oxygen on the properties of Zircaloy-2,
Trans. Am. Soc. Metals 54, 20-30.

- Sawatzky, A., Ledoux, G. A., Jones, S., 1977.
Oxidation of zirconium during a high-temperature transient,
 Zirconium in the Nuclear Industry, ASTM STP 633, Lowe Jr., A. L., Parry, G. W.
 (Eds.), American Society for Testing and Materials, 134-149.
- Setoyama, D., Yamanaka, S., 2003.
Calculated phase diagram for zirconium-oxygen-hydrogen ternary system,
 Transactions of Atomic Energy Society of Japan, 2, 74-81 (in Japanese).
- Schanz, G., 2003.
*Recommendation and supporting information on the choice of zirconium oxidation
 models in severe accident codes*,
 Forschungszentrum Karlsruhe Report, FZKA 6827, Karlsruhe, Germany.
- Shewfelt, R. S. W., 1988.
The ballooning of fuel cladding tubes: theory and experiment,
 Res Mechanica 25, 261-294.
- Shewfelt, R. S. W., Godin, D. P., 1986.
Ballooning of thin wall tubes with circumferential temperature variations,
 Res Mechanica 18, 21-33.
- Singh, K. P., Parr, J. G., 1963
Hydrogen solubility of Zr-O alloys,
 Transactions of Faraday Society, 59, 2248-2255.
- Toffolon, C., Brachet, J-C., Servant, C. et al. (2002)
*Experimental study and preliminary thermodynamic calculations of the pseudo-ternary
 Zr-Nb-Fe-(O,Sn) system*,
 Zirconium in the Nuclear Industry, 13th International Symposium., Moan, G. D.,
 Rudling, P. (Eds), ASTM STP 1423, American Society for Testing and Materials, West
 Conshohocken, PA, USA, 361-383.
- Tucker, M. O., Brown, A. F., Healey, T., 1978.
Partitioning behaviour of oxygen in steam-oxidized Zircaloy,
 J. Nucl. Mater. 74, 41-47.
- Udagawa, Y., Nagase, F., Fuketa, T., 2006.
Effect of cooling on cladding ductility under LOCA conditions,
 J. Nucl. Sci. Technol. 43, 844-850.
- Uetsuka, H., Furuta, T., Kawasaki, S., 1981.
*Zircaloy-4 cladding embrittlement due to inner surface oxidation under simulated loss-
 of-coolant condition*,
 J. Nucl. Sci. Technol. 18, 705-717.
- Uetsuka, H., Furuta, T., Kawasaki, S., 1983.
*Failure-bearing capability of oxidized Zircaloy-4 cladding under simulated loss-of-
 coolant condition*,
 J. Nucl. Sci. Technol. 20, 941-950.

- Urbanic, V. F., Heidrick, T. R., 1978.
High-temperature oxidation of Zircaloy-2 and Zircaloy-4 in steam,
 J. Nucl. Mater. 75, 251-261.
- US Code of Federal Regulations, 1981.
 Title 10, Part 50.46 and Appendix K (Rev. Jan., 1981).
- US NRC, 1988.
Compendium for ECCS research for realistic LOCA analysis: final report,
 US Nuclear Regulatory Commission Report NUREG 1230.
- Varty, R. L., Rosinger, H. E., 1982.
Comparison of fuel sheath model with published experimental data,
 Atomic Energy of Canada Limited, report AECL-6806.
- Vitanza, C., 2006.
RIA failure threshold and LOCA limit at high burnup,
 J. Nucl. Sci. Technol. 43, 1074-1079.
- Williford, R. E., 1986.
*Safety margins in Zircaloy oxidation and embrittlement criteria for emergency core
 cooling system acceptance*,
 Nuclear Technology 74, 333-345.
- Yan, Y., Burtseva, T., Billone, M. C., 2003.
LOCA results for advanced –alloy and high burnup Zircaloy cladding,
 Proceedings of the 2003 Nuclear Safety Research Conference, Washington DC, October
 20-22, 2003, NUREG/CP-0185, 97-121.
- Yan, Y., Burtseva, T., Billone, M. C., 2004a.
I-Post-quench ductility results for Zry-4 and ZIRLO oxidized at 1000°C and 1100°C,
 31 January, 2004,
II-Post-quench ductility results for Zry-4 and M5 oxidized at 1000°C and 1100°C,
 31 January, 2004,
*III- Post-quench ductility results for Zry-4 and ZIRLO oxidized at 1200°C, slow cooled
 to 800°C and quenched*, 22 March, 2004,
*IV- Post-quench ductility results for Zry-4 and M5 oxidized at 1200°C, slow cooled to
 800°C and quenched*, 23 March, 2004,
 E-prints, NRC ADAMS document centre at <www.nrc.gov>.
- Yan, Y., Billone, M. C., Burtseva, T., Chung, H. M., 2004b.
LOCA Integral test results for high burnup fuel,
 Proceedings of the Nuclear Fuel Sessions of the 2004 Nuclear Safety Research
 Conference, Washington DC, October 25-27, 2004, NUREG/CP-0192, 138-158.
- Yoo, J. S., Kim, I. S., 1991.
Effect of ($\alpha+\beta$) heat treatment on the mechanical properties of Zircaloy-4,
 J. Nucl. Mater. 185, 87-95.
- Zuzek, E., Abriata, J. P., San-Martin, A., Manchester, F. D., 2000.
H-Zr (hydrogen-zirconium), Phase Diagrams of Binary Hydrogen Alloys, 309-322,
 ASM International, Materials Park, OH 44073-0002, USA.

Appendix A: Clad oxidation rate correlations

The basic licensing model used for LOCA analysis is the Baker & Just (BJ) correlation (Baker & Just, 1962) for fuel cladding oxidation. The BJ correlation describes the rate at which oxygen is consumed in Zircaloy as a function of temperature. Baker & Just (1962) conducted experiments at the melting point of zirconium (2123 K) then combined their results with those of earlier workers at lower temperatures to obtain an empirical correlation spanning over temperatures from about 773 to 2123 K. The BJ correlation has a number of restrictions, which include the following details. Oxidation rates were determined from hydrogen evolved during the reaction of electrically heated wire specimens immersed in water. Specimen temperatures were inferred from experimental conditions rather than measured. The appearance of droplets of zirconium-zirconia in experimental apparatus was supposed to represent oxidation at melting temperature; however, self-heating of specimen by the exothermic reaction was disregarded. In addition, the BJ correlation was obtained by interpolating between low and high temperatures with no verifying data in between. The BJ correlation and other known correlations are listed in table A.1.

To be more precise, the rate constants applicable to several kinetic parameters of interest, namely, the oxygen absorption density and thicknesses of different phases containing oxygen, may be determined for each reaction temperature as follows. If the rate of reaction under the conditions of interest obeys a parabolic law, using the notation of Pawel et al. (1977, 1979), we write

$$\frac{dK}{dt} = \frac{1}{K} \frac{\delta_K^2}{2}, \quad (\text{A.1})$$

where K is a kinetic (rate) parameter, e.g., the oxide layer thickness ϕ , the total oxygen consumed τ or the oxide plus α -Zr(O) thickness, ξ . Integration of (A1) yields:

$$K = \delta_K \sqrt{t}. \quad (\text{A.2})$$

The rate parameters δ_τ obtained by various workers including the BJ correlation as well as their temperature ranges of applicability are listed in table A.1.

One noteworthy study was the experimental works of Cathcart et al. (1977) and Pawel et al. (1977, 1979) who examined the kinetics of oxidation of Zircaloy-4 in steam under isothermal conditions in the temperature range of 1173-1773 K. Oxidation rate data describing the growth of the reaction product layers, oxide (ZrO_2) and oxygen stabilized α -Zr, were obtained under well-defined experimental conditions. The early stages of oxidation for temperatures above 1273 K were virtually parabolic; below 1273 K, however, deviations from parabolic behaviour were noted. Statistical analyses of data in terms of rate constants and the Arrhenius parameters established accurate correlations for oxidation rates. The parabolic rate parameters for the mass of oxygen consumed per unit area in for this correlation (CP = Cathcart-Pawel) are given table A.1.

Correlation	Range K	A (g/cm ²) ² /s	Q/R -	Source
BJ	773-2125	2.0400	22899	Baker-Just, 1962
Klepfer	1255-1785	0.0219	16860	Ballinger et al., 1976
BDB	1144-1755	0.0190	16794	Ballinger et al., 1976
CP	1273-1773	0.1811	20101	Cathcart-Pawel, 1977
KFS	1273-1603	0.2340	20488	Kawasaki et al., 1978
Komatsu	1223-1573	0.1094	19124	Kawasaki et al., 1978
UH	1323-1853	0.0181	16820	Urbanic-Heidrick, 1978
LSB	1173-1773	0.2621	20962	Schanz, 2003
PC	1783-2673	16.7380	26440	Schanz, 2003
BH	1273-1473	0.1023	19620	Brown-Healey, 1980
	1473-1673	0.2228	20950	
NOU	773-1123	860	15191	Nagase et al., 2003
	1173-1273	4.56×10 ⁷	27652	
	1323-1573	1.84×10 ⁵	20447	

Table A.1: Parabolic rate constants for the total oxygen consumed by Zircaloy according to $\delta^2/2 = A \exp(-Q/RT)$, where T is temperature in K and A is in (g O₂/cm²)²/s. Correlations NOU are based on low-Sn Zircaloy-4 data.

Figure A.1 compares the correlations for oxidation rate listed in table 1 for the temperature range of 1273 to 1773 K. All these correlations are considered as best-estimate, meaning that the scatter for each individual correlation is ignored. It is seen that the BJ correlation bound all the other correlations with large margin at higher temperatures. However, at temperatures roughly below 1370 K the margin associated with the BJ correlation vanishes. The CP correlation lies mostly in the middle of the considered correlations. It is considered to offer a best-estimate relation for calculation of oxidation rate of Zircaloy during LOCA, thus replacing the BJ correlation for a more realistic assessment of the ECCS acceptance criteria.

The three NOU correlations listed in table A.1 are best fit to measurements made on low-Sn (1.3 wt% Sn) Zircaloy-4 (Nagase et al., 2003 and section 3.1). Figure A.2 compares these correlations with the BJ and CP correlations. It is seen that both the BJ and CP correlations underestimate the oxidation rate below 1000 K relative to the data (correlation) of Nagase et al. (2003).

The best-fit to the Pawel et al. (1977, 1979) data to Arrhenius relations for the rate of oxide layer growth (δ_ϕ) and the oxygen stabilized α -Zr layer thickness (δ_α) (in the common units used) are:

$$\frac{\delta_\phi^2}{2} = 0.01126 \exp(-35890/RT) \quad \text{cm}^2/\text{s} \quad (\text{A.3})$$

$$\frac{\delta_\alpha^2}{2} = 0.7615 \exp(-48140/RT) \quad \text{cm}^2/\text{s} \quad (\text{A.4})$$

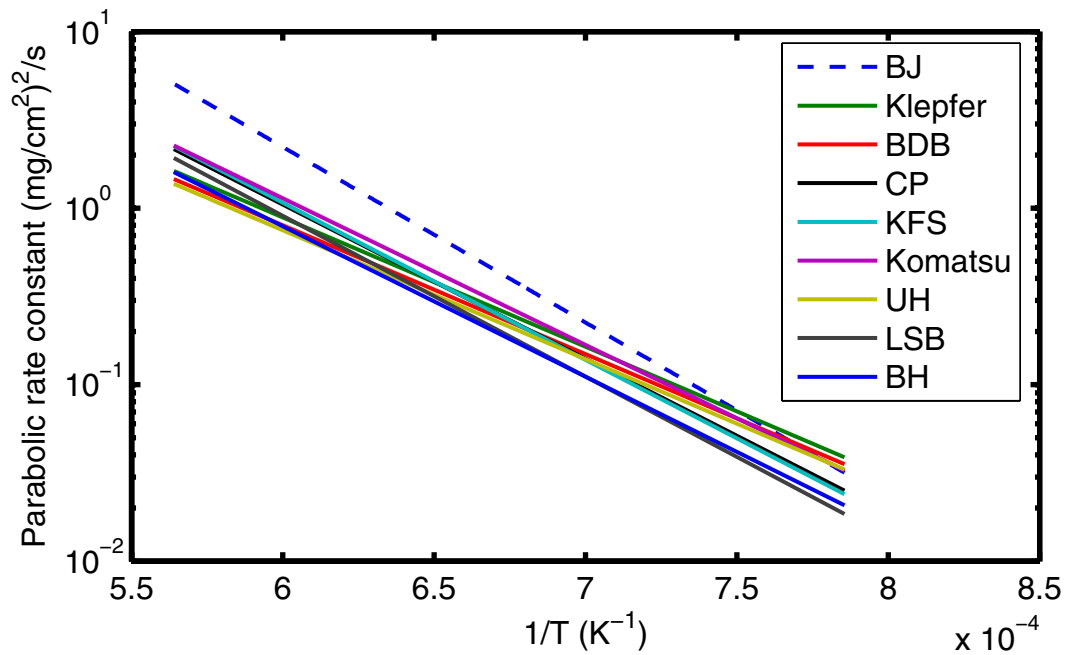


Figure A.1: Temperature dependence of parabolic rate constant of Zircaloy oxidation in steam in the temperature range of 1273 to 1773 K (table A.1).

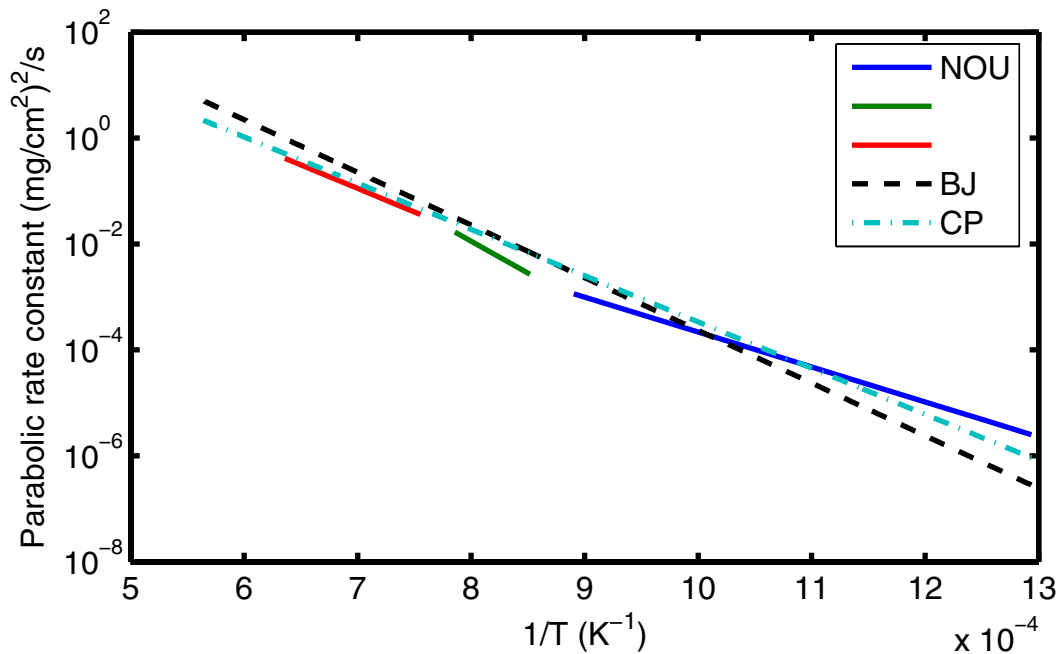


Figure A.2: Temperature dependence of parabolic rate constant of low-Sn Zircaloy-4 oxidation in steam compared to that of the BJ and CP correlations in the temperature range of 773 to 1773 K (table A.1).

In figure A.3, we depict growth of oxide layer and oxygen stabilized α -Zr thickness vs. time, using equations (A2)-(A4), i.e., the recasting of the CP correlations, for isothermal temperatures of 1426 and 1777 K, respectively. It is noted that at the lower temperature, the oxide layer is somewhat larger than the α -Zr layer and vice versa by a wider difference. Isothermal steam oxidation tests made at these temperatures on Zircaloy-4 agree with the results of the correlations displayed in figure A.3 (Pawel et al., 1979).

As conferred in section 2.3, the key parameter of concern is the equivalent clad reacted (ECR) during the oxidation process. In figure A.4, we have presented the results of calculations of ECR using the BJ correlation and the CP correlation as a function of time at isothermal temperatures ranging from 1300 to 1700 K. For these calculations, we have assumed that the density of ZrO_2 is 5.68 g/cm^3 (Lide, 2003), the oxide/metal volume ratio of 1.56 (Lemaignan & Motta, 1994) and a clad wall thickness of 0.57 mm. From figure A.4, it is seen that after about 88 s at 1700 K, the BJ correlation calculates an ECR of 17% (acceptance limit), whereas the CP correlation predicts ECR=11.6%.

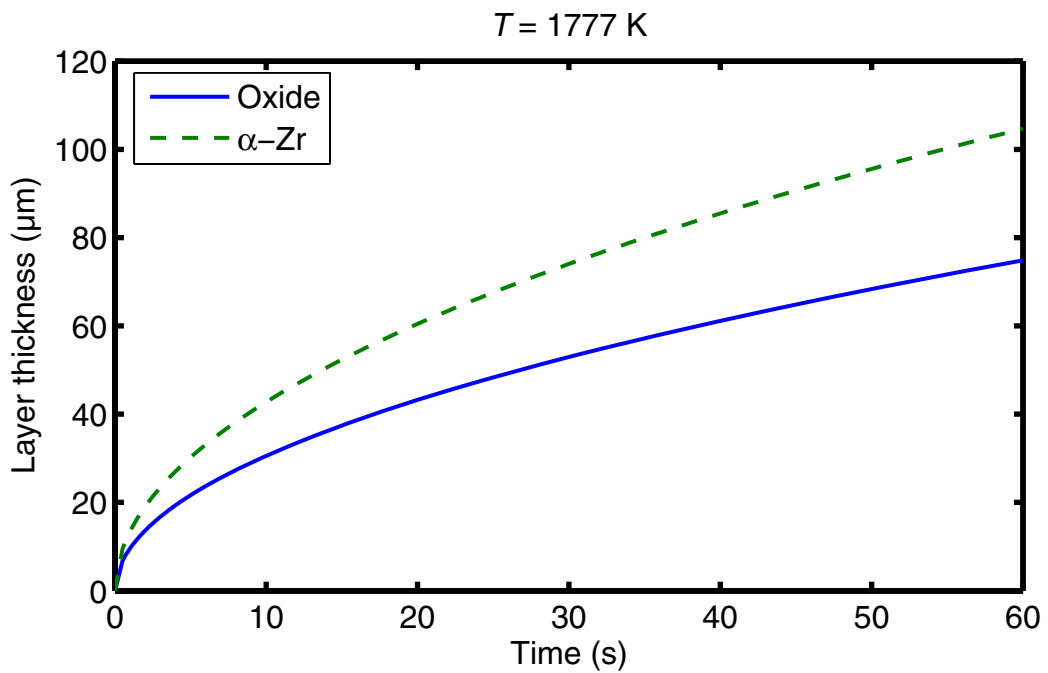
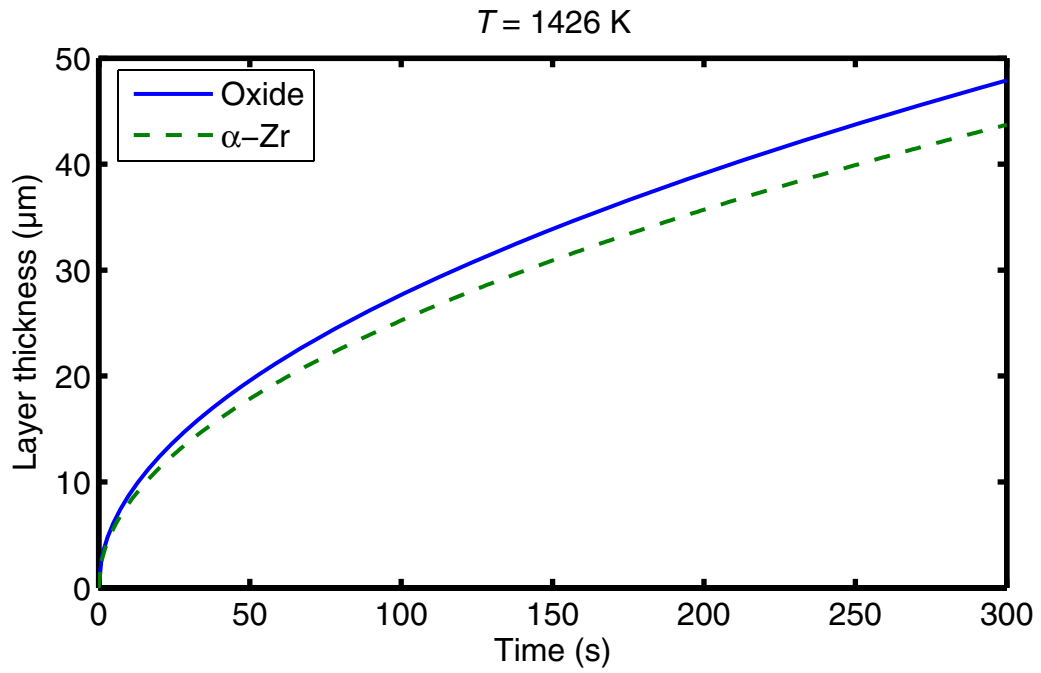


Figure A.3: Growth of oxide and α -Zr layers on Zircaloy-4 in steam at 1426 K (upper) and 1777 K (lower) using the Cathcart-Pawel correlations (A.3) and (A.4), respectively.

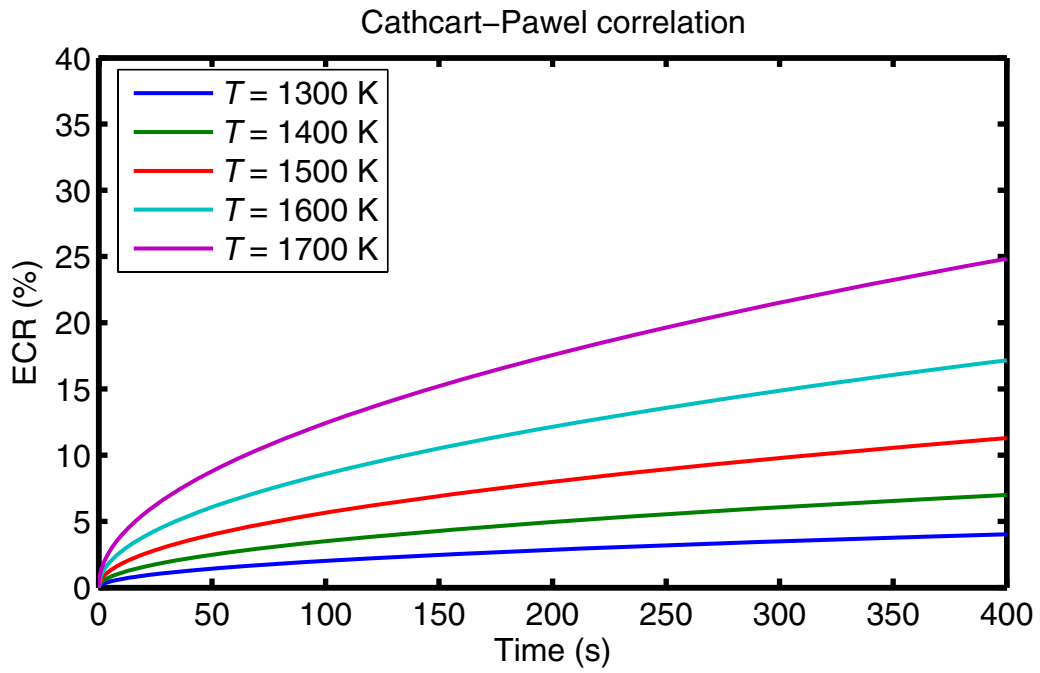
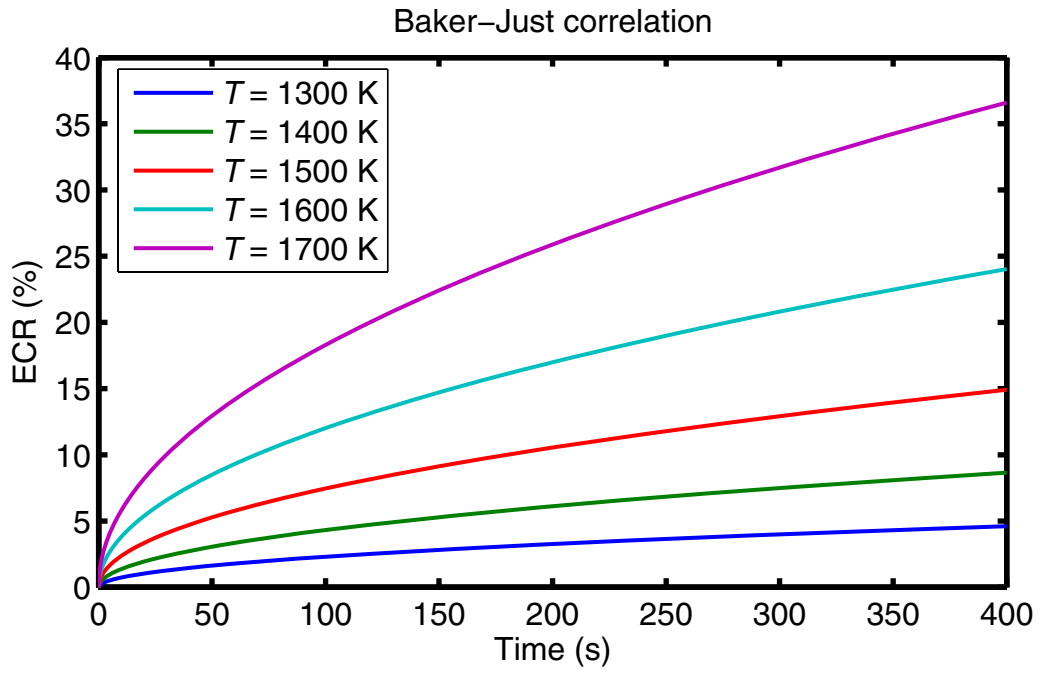


Figure A.4: The equivalent clad reacted (ECR) vs. time during Zircaloy oxidation process at several isothermal conditions. Upper panel: Calculations with the Baker-Just correlation. Lower panel: Predictions of the Cathcart-Pawel correlation.

Notes

ⁱ The clad material was 80% cold worked and stress relieved at 773 K for 4 h.

ⁱⁱ The equivalent stress is defined as $\sigma_{eq} = (\sqrt{2}/2)[(\sigma_r - \sigma_\theta)^2 + (\sigma_\theta - \sigma_z)^2 + (\sigma_z - \sigma_r)^2]^{1/2}$,

where $\sigma_r, \sigma_\theta, \sigma_z$ are the stress components in radial, circumferential, axial, respectively.

ⁱⁱⁱ The 18th-century researcher Johann Leidenfrost discovered that when a liquid is brought into contact with a surface significantly hotter than its boiling temperature, a cushion of vapour insulates and levitates it over the hot surface. In the Leidenfrost regime, the insulated droplets evaporate rather slowly without actually boiling.

^{iv} The NDT is the temperature at which fracture initiates with essentially no prior plastic deformation.

^v It is noted that 1477 K in Hobson's experiment was the furnace temperature; the true specimen temperature was estimated to be 1533 K.

^{vi} According to the assessed equilibrium phase diagram of the binary Zr-O system, this transition occurs at 1478 K (Liang et al., 2001), which is 205 K higher than the value suggested by Nagase et al. (2003) without any validation. There is, however, hysteresis in phase transition temperature, i.e., transition temperature on cooling vs. heating can differ by more than 200 K (Baun, 1963).

^{vii} A. N. Kolmogorov (1937, USSR), W. A. Johnson, R. F. Mehl (1939, USA), M. Avrami (1940, USA).

www.ski.se

STATENS KÄRNKRAFTINSPEKTION
Swedish Nuclear Power Inspectorate

POST/POSTAL ADDRESS SE-106 58 Stockholm

BESÖK/OFFICE Klarabergsviadukten 90

TELEFON/TELEPHONE +46 (0)8 698 84 00

TELEFAX +46 (0)8 661 90 86

E-POST/E-MAIL ski@ski.se

WEBBPLATS/WEB SITE www.ski.se